Advanced Lectures 1988

The atmospheric boundary layer

arters, Bracknell

Advanced Lectures
1988

The atmospheric boundary layer

P.J. Mason

M.K. MacVean

P. Hignett

F.B. Smith

R.H. Maryon

The atmospheric boundary layer

Errata for notes on lectures 1, 2 and 3 of the 1988 Advanced Lectures on the Atmospheric Boundary

In addition to some obvious typographic errors, the following more serious points should be noted.

Page 1.2 — 2nd line after equation (1) - add "and $\overline{p} = 0$".

Page 1.4 — line 2 - delete "density".

Pages 1.4 and 1.5 — note some "∇" imply "$\nabla\cdot$"

Lecture 2 — note all "log"s are natural logarithms, i.e. "ln".

Page 2.2 — equation (1) lower case u should be upper case U.

Page 3.1 — equations (3) and (4) add minus sign to stress.

Page 3.2 — equations (6) and (7) lower case u and v should be upper case U and V.

Page 3.4 — equation (11) ignore ...

Page 3.5 — sentence before equation (12) chosen coordinate frame has $V_g = 0$ not surface $\overline{vw} = 0$.

Page 3.8 — 2nd line after equation (13) 10 ms^{-1} should be $1ms^{-1}$.

Apologies.

12 September 1988.

P.J.Mason
AD Met O (BC)

Basic Equations and Ideas

P.J.Mason

27 July 1988

Turbulence is a common characteristic of many natural and engineering flows. The distinction between turbulent and laminar flows is fairly obvious but not easy to be precise about. In steady flows particles follow flow lines and there is no mixing of adjacent fluid layers. In unsteady flows the distinction is not straightforward and conceptual difficulties can arise in some flows such as those containing waves. The issue is not just semantic and has particular implications for the prediction and modelling of such flows. However, these are research issues and here we will limit attention to flows with 'unambiguous' turbulence. Definitions of turbulence are given through lists of properties and can be found in standard texts, e.g. Lumley and Panofsky (1964), Tennekes and Lumley (1972).

In addition to the irregularity an essential feature is the local importance of flow advection and vortex stretching. This vortex stretching mechanism is critical in leading to the cascade of energy to smaller and smaller scales and thus to the influence of molecular diffusion. Before attempting any description of such turbulence and its effects it is useful to introduce some simple, purely statistical, concepts.

If we consider a variable in a turbulent flow which is a function of time it is useful to introduce the concept of a mean and fluctuations, i.e. consider a variable $\phi(x, y, z, t)$ Then:

$$\overline{\phi} = \frac{1}{T}\int_0^T \phi dt \quad and \quad \phi' = \phi - \overline{\phi}$$

In engineering flows the time mean may be well defined but often in meteorology there are significant variations on many time-scales and some judgement is necessary for the concept to be of value. Although circumstances may vary considerably a typical averaging period for the planetary boundary layer is about 0.25 to 1 hour, this time scale is sufficient to include almost all purely three-dimensional fluctuations. The lack of any spectral gap

makes this division both arbitrary and imprecise, but it proves a useful distinction. In a practical evaluation of $\overline{\phi}$ and ϕ' time averaging may be replaced by space averaging and ϕ' may be defined relative, not to a constant mean, but to a linear variation with time over the averaging period. The use of spatial averaging is employed in the analysis of aircraft data. This supposes that $\overline{\phi}$ is function of time only and the method is subject to errors when there are spatial variations in $\overline{\phi}$ such as those due to variations in surface characteristics.

This distinction between mean and fluctuating variables can be applied to the equations of motion, e.g. considering an incompressible homogeneous flow

$$\frac{\partial \mathbf{u}}{\partial t} + \mathbf{u}\nabla\mathbf{u} = -\nabla p + \nu\nabla^2\mathbf{u} \tag{1}$$

(where p and ν are respectively the pressure and molecular viscosity divided by density) and substituting $\mathbf{u} = (U+u, V+v, W+w)$ and averaging such that $\overline{u} = \overline{v} = \overline{w} = 0$ we obtain in tensor notation

$$\frac{\partial U_i}{\partial t} + U_j\frac{\partial U_i}{\partial x_j} + \overline{u_j\frac{\partial u_i}{\partial u_j}} = -\frac{\partial P}{\partial x_i} + \nu\frac{\partial^2 U_i}{\partial x_j^2} \tag{2}$$

which with the aid of the continuity equation may be rewritten

$$\frac{\partial U_i}{\partial t} + U_j\frac{\partial U_i}{\partial x_j} = -\frac{\partial P}{\partial x_i} + \nu\frac{\partial^2 U_i}{\partial x_j^2} - \frac{\partial \overline{u_i u_j}}{\partial x_j} \tag{3}$$

The last term is an *exact* description of the effects of the flow fluctuations on the mean flow. Its features are most easily seen in the case of a flow with no horizontal variations, a boundary layer over a homogeneous surface. Then for a 1-D flow

$$\frac{\partial U}{\partial t} = -\frac{\partial P}{\partial x} + \nu\frac{\partial^2 U}{\partial z^2} - \frac{\partial \overline{uw}}{\partial z}$$

$$\frac{\partial U}{\partial t} = -\frac{\partial P}{\partial x} + \frac{\partial}{\partial z}\left\{\nu\frac{\partial U}{\partial z} - \overline{uw}\right\} \tag{4}$$

where $\overline{uw}$ is identified as a stress whose divergence changes the mean flow. This is called a Reynolds stress and arises from the correlation between the two components of flow. Thus $\overline{uw}$ negative implies that faster values of $U+u$ are correlated with downward (negative) w. The Reynolds number, defined as UL/ν, where L is a typical flow length scale, measures the relative magnitude of the viscous and non-linear terms in the equations of motion. In the high Reynolds numbers flows considered here the molecular diffusivity terms have a negligible effect on the mean flow remote from the boundary. However, as we shall see

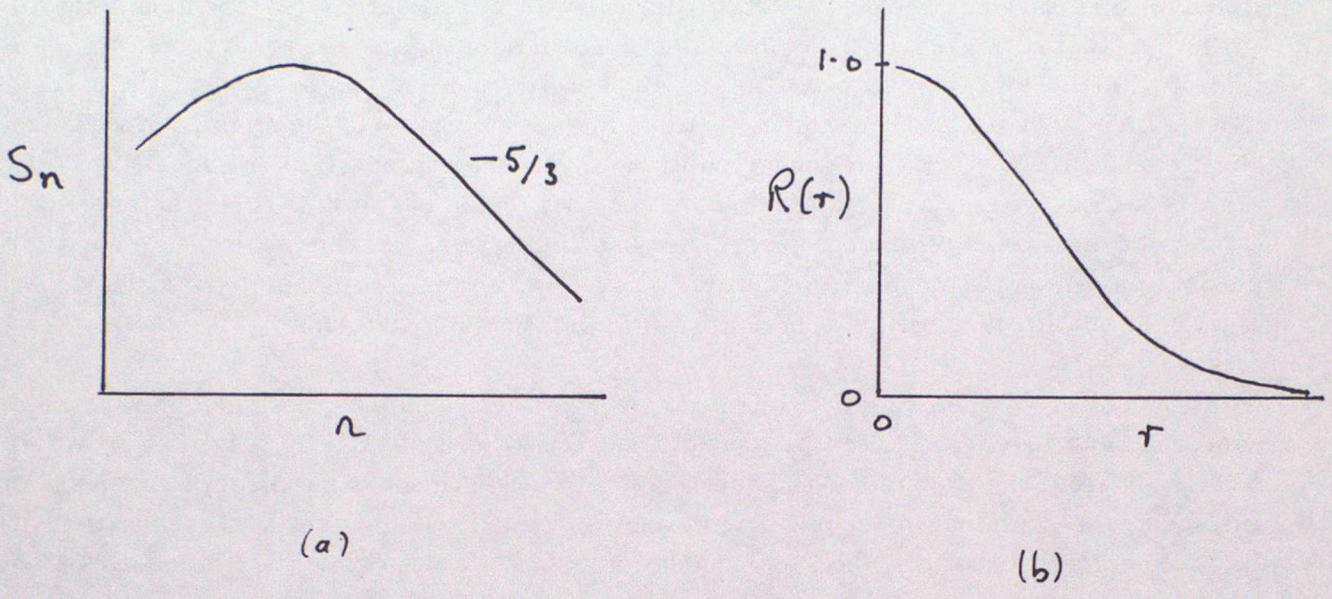

Figure 1: (a) a typical energy spectrum and (b) a typical autocorrelation function

below, molecular processes retain an important influence in allowing the dissipation of eddy motions, this influence does not depend on the magnitude of the viscosity but only on its non-zero value.

The 'Reynolds' averaging procedure can be applied to all the equations describing the flow and the prediction of the mean flow then *just* requires evaluation of the Reynolds stress tensor and the corresponding Reynolds scalar fluxes. As they arise from the non-linear terms these Reynolds averaging terms are not always easy to evaluate. Before considering the basis of the various methods of estimating these terms it is useful to return to the structure of the turbulent motions.

A precise description of the character of turbulence can be provided in idealised cases by a knowledge of the magnitude of the fluctuations and their correlations over varying spatial separations. In practice such full details are seldom available, and instead attention is usually given to the one-dimensional energy spectra derived either directly by measurement in space or by a 'Taylor' hypothesis where time variations at a point are translated through a mean velocity to a spatial variation. Figure 1a illustrates a typical energy spectrum which might be obtained by a Fourier transform of a time series of a turbulent velocity component. The energy spectrum is a plot a the square of the amplitude S_n at each frequency n (or wavenumber by Taylor hypothesis) against frequency n. The example shown is typical

but in some flows the shape of the low frequency part of the spectrum in particular will differ. For short length scales the spectrum shows a fall in energy ~~density~~ at a slope of -5/3. This region of the spectra is termed an inertial subrange and it is characteristic of a truly turbulent flow. It is common to plot the spectral density, the product of the energy and the frequency nS_n rather than S_n as this provides a measure of the amount of variance contributed in a particular frequency band. In such plots the inertial subrange has slope -2/3. Spectral theories of turbulence show that this region of the flow is characterised by a flow of kinetic energy down the spectrum to progressively smaller scales and eventual dissipation. In the atmosphere molecular dissipation becomes important on scales order 1mm. and its direct influence is seldom seen in practical observations.

If, as shown in the example, the spectrum has a well defined peak then the variable concerned can be characterised by a magnitude based on the variance, say $\overline{\phi'^2}$ (provided directly or from the area under the spectrum) and a length scale λ typical of the peak of the spectrum. The length scale λ is equivalently related to the decay with separation of the auto-correlation of ϕ. The auto-correlation of a variable ϕ which is homogeneous so that its mean and statistics do not depend on x is a function of separation r given by

$$R(\mathbf{r}) = \frac{\overline{\phi'(\mathbf{x})\phi'(\mathbf{x}+\mathbf{r})}}{\overline{\phi'^2}}$$

In practise the most computationally efficient way of deriving the auto-correlation function is by fourier transformation of the power spectrum. Figure 1b illustrates a typical auto-correlation. The integral of the area under the auto-correlation is termed the integral scale, and should also roughly equal λ. Problems defining in λ by any of these methods arise when the spectra do not fall off at low frequencies. Such difficult behaviour is common with most variables, but owing to the inhibiting influence of a rigid surface is not usual with the vertical component of velocity.

This discussion has dealt only with Eulerian statistics of the flow. Langrangian statistics are quite different and are important for some applications, in particular in dispersion problems. Brevity prevents a full discussion here.

To re-cap, we have introduced notions of a mean $\bar{\phi}$ a variance $\overline{\phi'^2}$ (or standard deviation $\sigma_\phi = \sqrt{\overline{\phi'^2}}$ and a characteristic length scale λ. We have also noted that the influence of the turbulence on the mean flow depends on the divergence of the Reynolds stresses $\nabla \overline{u_i u_j}$. Next, we consider possible methods of representing these stresses - i.e. a so-called turbulence closure.

The simplest approach was first proposed by Boussinesq (1877) who introduced the concept of a turbulent viscosity. The basis is simply the analogy of the large scale mixing

with small scale molecular mixing, i.e.

$$\overline{u_i u_j} = \nu_t \left\{ \frac{\partial U_i}{\partial x_j} + \frac{\partial U_j}{\partial x_i} \right\} \tag{5}$$

This tensor expression follows directly from the more general form of the Navier Stokes equations in which the viscous term is written as a divergence of the stress tensor (with continuity $\nu \nabla^2 \mathbf{u} = \nabla \nu (\partial u_i / \partial x_j + \partial u_j / \partial x_i)$). In a 1-D boundary layer

$$\overline{uw} = \nu_t \frac{\partial U}{\partial z}.$$

The turbulent viscosity ν_t can be expected to be a function of space and needs to be specified in each problem. Given some thought to the specification of the values involved, this method still finds applications. The most significant turbulence model proposed is Prandtl's (1928) mixing-length hypothesis which has its origin in the kinetic theory of gases. He proposed

$$\nu_t = l_m v_t \tag{6}$$

where l_m is a mixing length and v_t a turbulence velocity scale. He further noted (in 1-D)

$$v_t = l_m \left| \frac{\partial U}{\partial z} \right| \tag{7}$$

giving

$$\nu_t = l_m^2 \left| \frac{\partial U}{\partial z} \right| \tag{8}$$

This approach requires the specification of a length scale which in Prandtl's and many applications was taken as proportional to distance from the surface. Refinements to this method form the basis of many other models. For example, v_t may be related to an equation for the flow turbulence energy (see below) and l_m may be related to flow curvature or an equation. Although close to the surface the specification of l_m is easy, in general it is the correct specification of l_m elsewhere in a flow that causes the greatest difficulties. To go further in discussing the turbulence models it is useful to return to the equations obtained by supposing a mean with fluctuations. If we consider the Navier-Stokes equations again and multiply the equation for $U_i + u_i$ by u_j and add to the equation for $U_j + u_j$ multiplied by u_i and then average we obtain

$$\begin{aligned} \frac{\partial \overline{u_i u_j}}{\partial t} + U_l \frac{\partial \overline{u_i u_j}}{\partial x_l} = &- \left(\overline{u_i u_l} \frac{\partial U_j}{\partial x_l} + \overline{u_j u_l} \frac{\partial U_i}{\partial x_l} \right) + \overline{p \left(\frac{\partial u_i}{\partial x_j} + \frac{\partial u_j}{\partial x_i} \right)} \\ &- \frac{\partial \overline{u_i u_j u_l}}{\partial x_l} - \left(\frac{\partial \overline{p u_j}}{\partial x_i} + \frac{\partial \overline{p u_i}}{\partial x_j} \right) + \nu \left(u_i \frac{\partial^2 u_j}{\partial x_l^2} + u_j \frac{\partial^2 u_i}{\partial x_l^2} \right) \end{aligned} \tag{9}$$

This is an equation for each of the components of the Reynolds stress. It contains some terms which, are known but introduces third order correlations (correlations of pressure and velocity are third order) which are unknown. So-called second order closures attempt to model these third order terms and do achieve *some* impressive predictions in *some* complex flows. On the other hand such closures have not proved universally applicable and involve considerable complexity. They seem best reserved for flows in which fast time and space variations cause the turbulence to be out of equilibrium with the local flow gradient. In such cases simpler models may always fail. Given the equation for the Reynolds stresses, there is still a need to specify either a length scale or, equivalently, the local dissipation rate. This length scale is needed to evaluate higher order terms in the same way that a length scale was needed for the stress in the mixing length closure. To provide predictions of length scale an equation is usually formed but, in contrast to the stress equations, the theoretical basis is poor. The resulting equation, perhaps for dissipation, describes a number of useful features, such as the effect of flow curvature in realistic manner, but has many failings.

Models employed in practice adopt various levels of complexity between the basic mixing length and the full second order closure (or if equations for third order quantities are considered, third order closure). Significant models replace the velocity scale of the mixing length v_t by the square root of the turbulence energy E obtained by an energy equation. e.g.

$$\nu_t = l_m E^{\frac{1}{2}} \tag{10}$$

and

$$\frac{\partial E}{\partial t} + U_i \frac{\partial E}{\partial x_i} =$$

$$\underset{\text{shear production}}{-\overline{u_l u_i}\frac{\partial U_i}{\partial x_l}} \qquad \underset{\text{dissipation}}{-\epsilon} \qquad \underset{\text{turbulent transport}}{+\frac{\partial}{\partial x_i}\nu\frac{\partial E}{\partial x_i}} \tag{11}$$

where

$$\epsilon = c_E \frac{E^{\frac{3}{2}}}{l_m} \tag{12}$$

The value of the constant c_E is set by applying the relation near the surface in a boundary layer. Equation (12) follows from the spectral description of turbulence. Within the inertial subrange the dissipation is related to the energy at a particular wavlength. In keeping with this (12) describes the gross characteristics of the spectrum with l_m being typical of but not identical to the scale of the spectral peak. It relates the dissipation to the energy and scale of the the dominant eddies. An important further refinement is to predict l_m by an equation and the so-called $q - \epsilon$ models have equations for turbulence energy (called q by

engineers) and dissipation ϵ. The next level of refinement is usually to predict the stresses from E and ϵ on the assumption that for the individual stress components alone, the time dependent and diffusive terms are negligible. The approach is called an algebraic closure as the stress equations themselves then form algebraic relations for the stresses.

All of the above models can be generalised to include the influence of buoyancy effects and can be used to describe the behaviour of passive scalars as well as the flows themselves. The question remains as to how well all these models of varying complexity actually work. Without dwelling on the relative merits of the various models, all tend to perform well in certain types of flow and badly in others The successes occur in flows dominated by shear production of turbulence and especially in regions near the ground. The characteristic of these flows that leads to the success is the fact that the flow eddies are indeed then relatively small compared with the scales of the flow. In such cases the mixing length does fairly well and refined models add improvements. On the other hand, in flow with buoyant convection or turbulence behind bodies, the eddies are large and extend over the whole flow. In such cases the local flow gradient is not well related, if at all, to the local stresses and all the models can fail with a risk of more complex models suffering a more severe failure.

In such cases, where the physical basis for the parametrization breaks down, failure of the model must be expected but fortunately these are the very cases in which an alternative approach should work best. This alternative, called a Large-Eddy simulation, explicitly resolves the large scale eddies with a numerical model and only represents small scale motion with a closure. Although the technique can work well, at present it is too expensive in application for its general use. It can be applied to develop simpler models and examine particular single flows.

The Atmospheric Surface Layer

P.J.Mason

28 July 1988

A very large part of our understanding and empirical knowledge of turbulent flows concerns the behaviour of turbulence in the region of the boundary layer near the surface. This region of the boundary layer is studied not just because of its relative simplicity but also because of its practical importance. A full understanding of these flows is nevertheless complicated and it is best to proceed in stages. We will begin with high Reynolds number flow over a smooth surface.

Consider flow between two infinite plane smooth surfaces a distance 2δ apart under the action of a pressure gradient, $\partial P/\partial x$ parallel to the surfaces. This consideration of a bounded flow enables a boundary layer depth (equal to half the channel width) to be introduced without discussion of rotation or capping inversions. The equations describing this flow in a steady state are those introduced for a 1-D flow in the previous section, i.e.

$$0 = \frac{\partial P}{\partial x} + \frac{\partial}{\partial z}\left(\nu\frac{\partial U}{\partial z} - \overline{uw}\right)$$

Noting the centre plane of symmetry and the constant value of $\partial P/\partial x$, this implies that the total shear stress ($\nu\partial U/\partial z - \overline{uw}$) must have a linear gradient and range between zero at the zero plane and $\pm\delta\partial P/\partial x$ on the lower and upper surfaces respectively. We shall see that in general the total shear stress always shows this characteristic linear variation with height on scales of order the boundary layer depth.

Suppose that the Reynolds number $U\delta/\nu$ is arbitrarily large and consider the flow a distance $z \ll \delta$ but so that Uz/ν remains very large. If z is very much less than the boundary layer depth δ then the total shear stress from 0 to z will be close to the surface value. Such a region is termed a surface, or constant stress layer. The stress is not constant in the sense that it has a negligible gradient but rather that its magnitude remains virtually

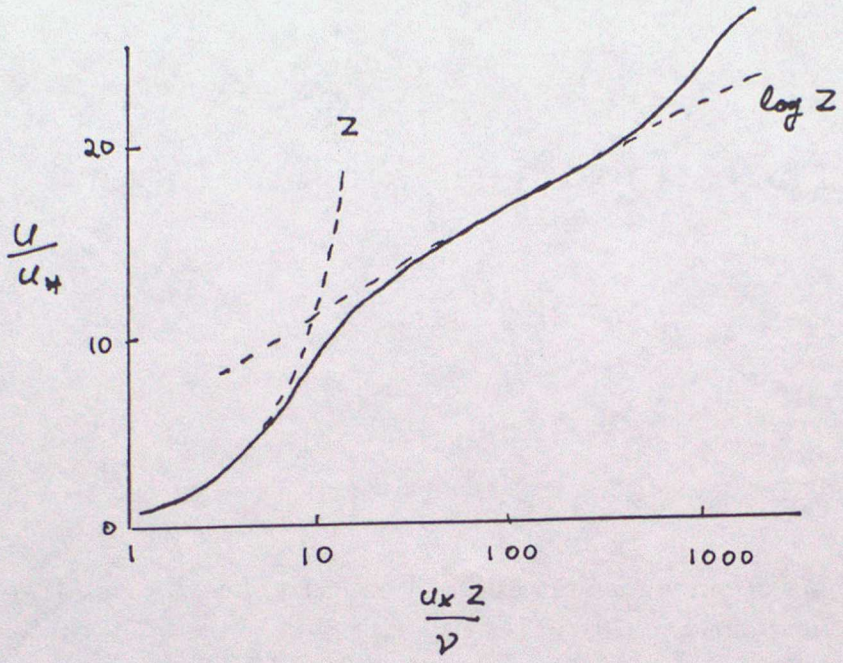

Figure 1: Flow profile observed over a smooth surface

constant. Now if Uz/ν is very large then the molecular term $\nu \partial U/\partial z$ will be negligible at this height z. A critical requirement in this case is that

$$\frac{\partial U}{\partial z} = f(u_*, z)$$

where u_* is the square root of the surface stress. This dimensional requirement follows solely from the high Reynolds number and the constant stress. Dimensional analysis then requires

$$\frac{\partial U}{\partial z} = \frac{u_*}{kz} \tag{1}$$

where k is constant for all comparable high Reynolds number flows. This constant is the von Karman constant. Note that whilst the *local* flow properties must be functions of u_* and z, in consequence of the behaviour very close to the surface, the mean flow U will remain a function of the viscosity . Integration of equation 1 over the region where it applies leads to the result that

$$U = \frac{u_*}{k} [\log z + C]$$

where C is a dimensional constant. Again dimensional analysis suggests

$$U = \frac{u_*}{k} \left[\log \left(\frac{z u_*}{\nu} \right) + A \right]$$

where A is a non-dimensional constant. Since there are no analytical theories of turbulence this key idea of the logarithmic velocity profile is of necessity based on dimensional analysis. The result also follows from the ideas in mixing length turbulence closures and, more important, as Figure 1 shows, observations. Observations find the constant A to be about 5.0 and the flow to become logarithmic at heights above $zu_*/\nu \sim 40$.

Smooth surfaces are not unknown in meteorology but usually surfaces, including the sea with waves, are rough. If the roughness features have a height scale h then we can form the 'Reynolds Number' hu_*/ν. With these roughness elements the shear stress near the surface is not just transfered by molecular stresses but by the pressure forces acting on the elements. For bluff bodies at high Reynolds numbers the pressure forces dominate. There is then an expectation on dimensional grounds that if hu_*/ν is very large (greater than about 50 in practice) that the mean flow will be completely independent of ν but will depend, for roughness elements of the same type or shape, on h.

Such conditions usually apply in meteorology and for such cases we can expect on dimensional grounds that

$$U = \frac{u_*}{k} \log\left(\frac{z}{z_0}\right) \tag{2}$$

where z_0 is a dimensional constant related to the height and character of the roughness elements. For bluff surface features with a high surface density of features z_0 is usually about $0.1h$. With this analysis molecular influences would be seen as z_0 depending on the wind speed. In fact such effects are weak and more often are not due to molecular influences but due to flexible roughness elements, such as vegetation, changing shape and orientation with wind speed. Equation 2 contains an assumption that U will equal zero at $z = z_0$. This is a definition of the origin of the z coordinate and although the issue may not always be of practical consequence the height at which $U = 0$ above any physical surface is unknown. For this reason it is usual to consider

$$U = \frac{u_*}{k} \log\left(\frac{z - D}{z_0}\right)$$

where just as z_0 is no more than a constant of integration, D is no more than the height needed (given what definition is adopted for the z co-ordinate) to satisfy $U = 0$ at $z = D + z_o$. The displacement height D has practical significance in flow over trees, urban areas and hilly terrain. There are no complete theories for estimating z_0 and D, and almost all of our knowledge of these quantities is based on observations.

Values of z_0 for different terrain types are available from past experiments and values range from $\sim 10^{-4}$m over the sea, $\sim 10^{-2}$m in short grass, $\sim 10^{-1}$m in fields with hedges or crops, ~ 1.0m in forests and urban areas and, as noted with some caution in subsequent

lectures, $\sim$ 10.0m for hilly regions. In boundary layer models, including those in weather prediction models, the influence of this near surface region is not given by an explicit representation of the flow profile but by relating the surface stress to the flow at some height z by a drag coefficient e.g.

$$u_*^2 = C_D.U(z)^2$$

where

$$C_D = \frac{k^2}{[\log(z/z_0)]^2}$$

The atmospheric boundary layer has important influences from heat and moisture. If we consider the equation for the turbulence energy we have the shear production term $-u_i u_l \partial U_i/\partial x_l$ or $\overline{uw}\partial U/\partial z$ for a 1-Dimensional flow. The addition of a bouyancy term B ($B = -g(T - T_0)/T_0$) to the vertical equation of motion, leads to an extra production term $\overline{wB}$ the bouyancy flux. If $\overline{wB}$ is significant compared with $\overline{uw}\partial U/\partial z$ then we can expect bouyancy forces to be significant. The bouyancy flux should, like the shear stress, have a fairly linear variation of the whole boundary layer depth and will be nearly a constant value in the surface layer. Using the above relations we can note that in the surface layer $\overline{uw}\partial U/\partial z$ will be $\sim u_*^3/kz$ so the ratio of shear to buoyant production (a flux Richardson number) will be $u_*^3/\overline{wB}kz$. This may be written as L/z where

$$L = \frac{u_*^3}{\overline{wB}k}$$

is the Monin-Obukhov Length. If we consider a surface layer with $L/z \gg 1$ then the bouyancy will have no influence on the flow. In such a case it follows, again from dimensional analysis, that for our rough surface

$$T = \frac{T_*}{k} \log\left(\frac{z - D_T}{z_{0T}}\right)$$

where $T_* = \overline{wT}/u_*$ and T is effectively just a passive scalar variable. In this case the surface value of T, T_s is very hard to be precise about. In an experiment it is the value of T deduced only by extrapolation to the height $z = D_T$ where D_T is determined again solely by the requirement that the profile is logarithmic. This value of T_s is just an extrapolated value and cannot, with any certainty, be related to any measured value of temperature, such as one on the skin of the roughness elements. In spite of this it is common in models to associate T_s with the radiative surface temperature and also the soil heat flux calculation. This is an area of errors where further work is needed. The value of z_{0T} is usually about one tenth of the value of z_0 and probably never exceeds values of $\sim$ 0.01m. This is because the transfer of heat is unaffected by pressure forces and only responds to the surface roughness in consequence of the changes in surface area and the enhanced near surface mixing.

Observation of the vertical velocity turbulence spectra in the surface layer show a spectral peak at a wavelength of about $3z$. With a knowledge of some of the constant correlation coefficients, and energy component ratios, the neutral stability surface layer is well described. Typically $\sigma_w = 1.3u_*, \sigma_v = 1.9u_*, \sigma_u = 2.4u_*$, and $\sigma_T = 1.6T_*$.

For the mixing length model to match the above description $l_m = kz$. The following relations then illustrate the consistency

$$\left|\frac{\partial u}{\partial z}\right| = \frac{u_*}{kz} \qquad u_*^2 = \nu_t \left|\frac{\partial u}{\partial z}\right| \qquad l_m = kz$$

$$u_t = l_m \left|\frac{\partial u}{\partial z}\right| = u_* \qquad \nu_t = l_m u_t = kzu_*$$

To complete a discussion of the atmospheric surface layer the case when L/z is of the order 1 needs to be considered. Monin-Obukhov similarity then recognises that we have the additional length scale L in our analysis. Dimensional analysis for the flux of a variable C gives

$$\frac{\partial C}{\partial z} = \frac{C_*}{kz}\phi_C(z/L)$$

where $C_* = \overline{WC_*}/u_*$ and ϕ_C is a universal function of z/L. These functions are empirical and various functional fits are considered by various authors. Such functions may diverge for large values of z/L but tend to match for $z/L <\sim 1$. Most data apply to the later region and so fortunately do most applications. A typical example is

$$\phi_m = (1 - 16z/L)^{-1/4} \qquad z/L < 0$$

$$\phi_H = (1 - 16z/L)^{-1/2} \qquad z/L < 0$$

and

$$\phi_m = (1 + 5.0z/L) \qquad z/L \geq 0$$

$$\phi_H = (1 + 5.0z/L) \qquad z/L \geq 0$$

where ϕ_m and ϕ_H are for momentum and temperature. The above expressions give a ratio of ϕ_H/ϕ_m of unity at at $z/L = 1.0$. Authors differ on the value of this ratio and others use expressions with $\phi_H/\phi_m = 0.74$ for $z/L = 1.0$. This introduction does not have the scope to give a critical review of the data and the reader is referred to texts, e.g. WMO Technical Note No.165, for details. These expressions for the gradients are integrated to specify the profiles and hence the transfer coefficients to the surface;e.g.

$$U(z) = \frac{u_*}{k}\left[\log(z/z_0) - \Phi_m(z/L)\right]$$

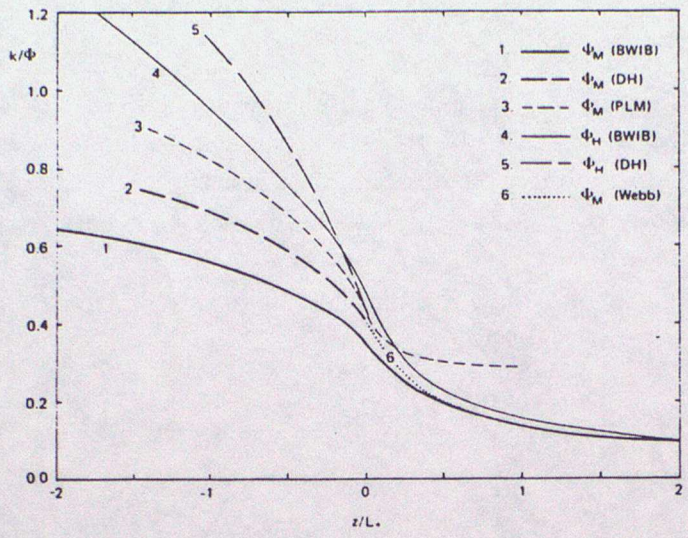

Figure 2: A comparison of various empirical fits for ϕ_m and ϕ_H

where Φ_m has been obtained by the integration. Analytical forms of Φ are available for most ϕ but since the ϕ are empirical there is no special advantage in the analytical rather than numerical calculation.

These Monin Obukov similarity functions can also be linked to the mixing length specification with $\nu_t = ku_*z\phi(z/L)^{-1}$ but more advanced turbulence models are needed to resolve the relative changes in ν_t or l_m implied by ϕ. They likewise are involved in converting a Gradient Richardson number

$$Ri = \frac{g}{T}\frac{\partial T}{\partial z}/(\partial U/\partial z)^2$$

into the flux Richardson number which relates the relative sizes of shear and bouyancy production of turbulent energy.

The Planetary Boundary Layer

P.J.Mason

27 July 1988

Having outlined the basic ideas of turbulence structure and some properties of the near surface part of the boundary layer, this section considers the overall problem of the planetary boundary layer. In essentially unbounded Engineering flows the boundary layer is the region of the flow near the surface into which the deceleration due to the non-slip condition has diffused. Such boundary layers grow for all time unless constrained by geometry. In the planetary boundary layer the region of direct influence is invariably confined. This confinement is usually due to stable stratification but as we shall note, in principle, the Earth's rotation alone could effect a limited scale.

The influence of the Earth's rotation is more profound in the coupling of the boundary layer to the free atmosphere. This coupling to the large scale flow occurs through the "Ekman" pumping mechanism. Consider flow of a turbulent planetary boundary layer with no horizontal variations apart from those of the basic pressure field, (taken to vary in the y-direction) i.e.

$$\frac{\partial U}{\partial t} = fV + \frac{\partial}{\partial z}(-\overline{uw}) \tag{1}$$

$$\frac{\partial V}{\partial t} = -\frac{\partial P}{\partial y} - fU + \frac{\partial}{\partial z}(-\overline{vw}) \tag{2}$$

Consider steady motion and assume that above a height h the turbulent stresses are zero. Integration from the surface to h leads to the result

$$\int_0^h fV \, dz = -\overline{uw}_s \tag{3}$$

$$\int_0^h \left(-\frac{\partial P}{\partial y} - fU\right) dz = -\overline{vw}_s \tag{4}$$

where $-\overline{uw}_s$ and $-\overline{vw}_s$ denote the surface vlaues of the stresses, i.e. $-\overline{uw}_s = u_*^2 \cos\alpha$ and $-\overline{vw}_s = u_*^2 \sin\alpha$ and α is angle of the surface stress to the geostrophic wind $U_g = -(1/f)\partial p/\partial y$. These equations relate the surface stress to the mass flux of the departures from geostrophic balance. Should the surface stress vary in space due to variations in the geostrophic wind or surface roughness then mass continuity demands a vertical velocity w_p at the top of the boundary layer. Specifically, this relates w_p to the curl of the surface stress, i.e.

$$w_p = \frac{1}{f} \nabla \times \tau_s \tag{5}$$

where $\tau_s = (-\overline{uw}_s, -\overline{vw}_s, 0)$, the surface stress vector. In a rotating planetary atmosphere these vertical motions act through vortex stretching and compression on the whole of the troposphere and tend to try to bring the atmosphere into a state of solid body rotation ("Ekman pumping"). With this Ekman pumping "spin up" mechanism momentum transfer to the bulk of the atmosphere is achieved without direct fluid mixing. The transfers of heat and moisture are of equal importance to the atmospheric circulation but their influence requires fluid exchange over the troposphere and usually involves either deep convection or frontal ascent. Heat and moisture thus enter the troposphere through regions of a small area whilst most of the rest of the boundary layer is subject to gradual descent. Without entrainment the boundary layer would collapse. Much of this entrainment is best described as encroachment and is simply due to buoyant overturning as the surface heating raises the boundary layer temperature. The shear driven entrainment is much harder to model as it occurs in the thin capping inversions and is not easy to describe over a larger finite difference mesh.

The term Ekman layer strictly refers to the description of a boundary layer with a constant viscosity in a rotating fluid. The equations

$$0 = +fV + \nu \frac{\partial^2 U}{\partial z^2} \tag{6}$$

$$0 = (U_g - U)f + \nu \frac{\partial^2 V}{\partial z^2} \tag{7}$$

can then be solved analytically with solution

$$\begin{aligned} U - U_g &= -U_g e^{-\varsigma} \cos\varsigma \\ V &= U_g e^{-\varsigma} \sin\varsigma \end{aligned} \tag{8}$$

where $\varsigma = \sqrt{(f/2\nu)}z$. The height scale $\delta = \sqrt{2\nu/f}$ is called the Ekman layer depth. Figure 1 illustrates this solution for a constant value of ν. It is instructive to examine the general balance of terms in this true "Ekman Layer". The height scale δ follows from a balance

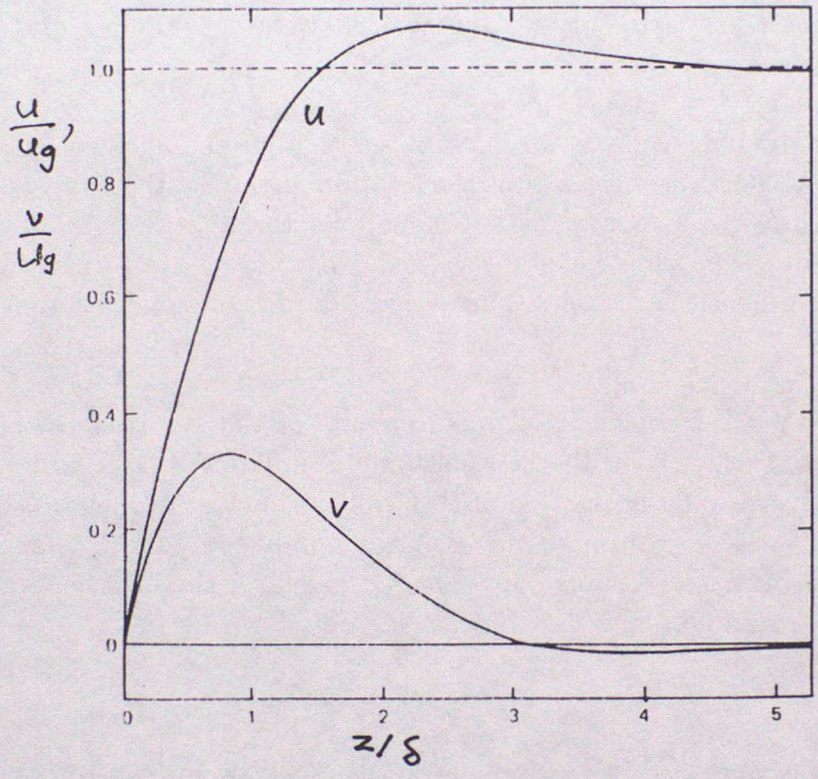

Figure 1: Illustrating a laminar Ekman boundary layer

between the coriolis term and the stress divergence, i.e.

$$fU \simeq \nu \frac{\partial^2 U}{\partial z^2} \quad \rightarrow \quad fU \simeq \nu \frac{U}{\delta^2}$$

$$\rightarrow \quad \delta^2 = \frac{\nu}{f} \tag{9}$$

The velocity gradients are $O(U_g/\delta)$ and the surface stress $\tau = \nu U_g/\delta$ and ageostrophic mass flux is $U_g\delta/2$.

For a turbulent boundary layer we have noted that in the surface layer $\nu \sim u_*\kappa z$. Such a variation with height continues up to a fraction of the depth of the boundary layer (~ 0.2) and then limits to a more constant value over the depth of the boundary layer. Some analytic solutions patch a constant viscosity boundary layer onto the top of the surface layer. These theories are usually linked with a further application of dimensional analysis.

In the surface layer the dimensional requirements of the variation with height were noted and within the surface layer the flow was only a function of z, L, and u_*. If the flow above the surface layer is only a function of U_g,f and the surface properties then, with the introduction of the variable f through the scale u_*/f universal functions should describe the flow above a height $z \gg z_0$. Thus above the surface layer the flow departure from the geostrophic will be a function of zf/u_* and Lf/u_* only. i.e.

$$(U - U_g)/u_* = F(zf/u_*, Lf/u_*) \tag{10}$$

If we assume that the validity of this function overlaps with the surface layer solution which is only valid for $z \ll u_*/f$ then by matching this flow with a surface layer the similarity relation between the geostrophic wind and the surface properties is obtained, e.g.

IGNORE THIS EQUATION

$$\frac{U_g^2}{u_*^2} = \frac{1}{\kappa^2}\left[\left(\ln\left(\frac{u_*}{fz_0}\right) - A\right)^2 + B^2\right] \ldots \tag{11}$$

and

$$\sin\alpha = -\frac{B}{\kappa}\frac{u_*}{U_g} \ldots$$

where α is the angle between the surface stress and the geostrophic wind and A and B are functions of u_*/fL. From observations with $L = \infty$, A is found to be about 1.0 and B about 5.0. Such formulations are essential to so-called "bulk" boundary layer parametrisations which, in simple cases, can allow empirical data to be used with effect. Considerations of dimensional analysis aside, it is useful to compare the scale involved in this analysis with

that in the laminar boundary layer. If we suppose viscosity of magnitude $\nu_t \simeq u_* \kappa \delta_t$ then the scale $\delta_t = (2\nu_t/f)^{\frac{1}{2}}$ gives $\delta_t = 2\kappa u_*/f$. consistent with the adopted scaling. In many observations the height scale of the capping inversion z_i is $< u_*/f$ and then z_i rather u_*/f is the appropriate scale for the analysis.

The formulations above, are termed Rossby number similarity and the parameter u_*/fz_0 which arises is termed the "surface Rossby number". This usage of a Rossby number is of course unrelated to the more usual dynamical definition. This approach, which tries to describe the whole boundary layer empirically fails when the boundary layer is not in a local or equilibrium state. Its value is in providing a framework for the analysis of data and theoretical results.

Owing to the lack of analytical theories for turbulent flow, observations and their unification through proper non-dimensionalisation, form a critical part of the study of the boundary layer. The final description is not usually just empirical but also employs dynamical models. This section concludes with an attempt to outline the features of some of the common types of boundary layer. The critical parameters determining the boundary layer type are its depth and the surface fluxes. The ratio the boundary layer depth z_i to the Monin Obukhov length $L = u_*^3/\kappa \overline{wB}$ determine the extent and sign of the main buoyancy effects. Some remarks on complicating influences are given below.

The Neutral Static Stability Boundary Layer

Although this type of boundary layer is a convenient reference point it seldom occurs. The most usual cases are either strong winds or near zero heat flux beneath a high level capping inversion. A typical depth is one to two kilometres. Figure 2 illustrates various profiles typical of neutral conditions. The mean flow profiles are logarithmic near the surface but at the top the boundary layer show a small Ekman oscillation and slightly super-geostrophic flow. The shear stress profiles indicate the chosen coordinate frame with the surface value of $V_g = 0$. In this frame, common for the analysis of observations it is clear from the equations of steady motion that:

$$\frac{\partial}{\partial z}(-\overline{uw}) = -f(V - V_g) \; ; \qquad \frac{\partial}{\partial z}(-\overline{vw}) = f(U - U_g) \tag{12}$$

Both $-\overline{uw}$ and $-\overline{vw}$ must decrease with height near the surface when U and V are less than U_g or V_g. At the top of the boundary layer U must be greater than U_g to allow $\overline{vw}$ to return to zero, and as with the laminar Ekman layer, a damped oscillation of wind

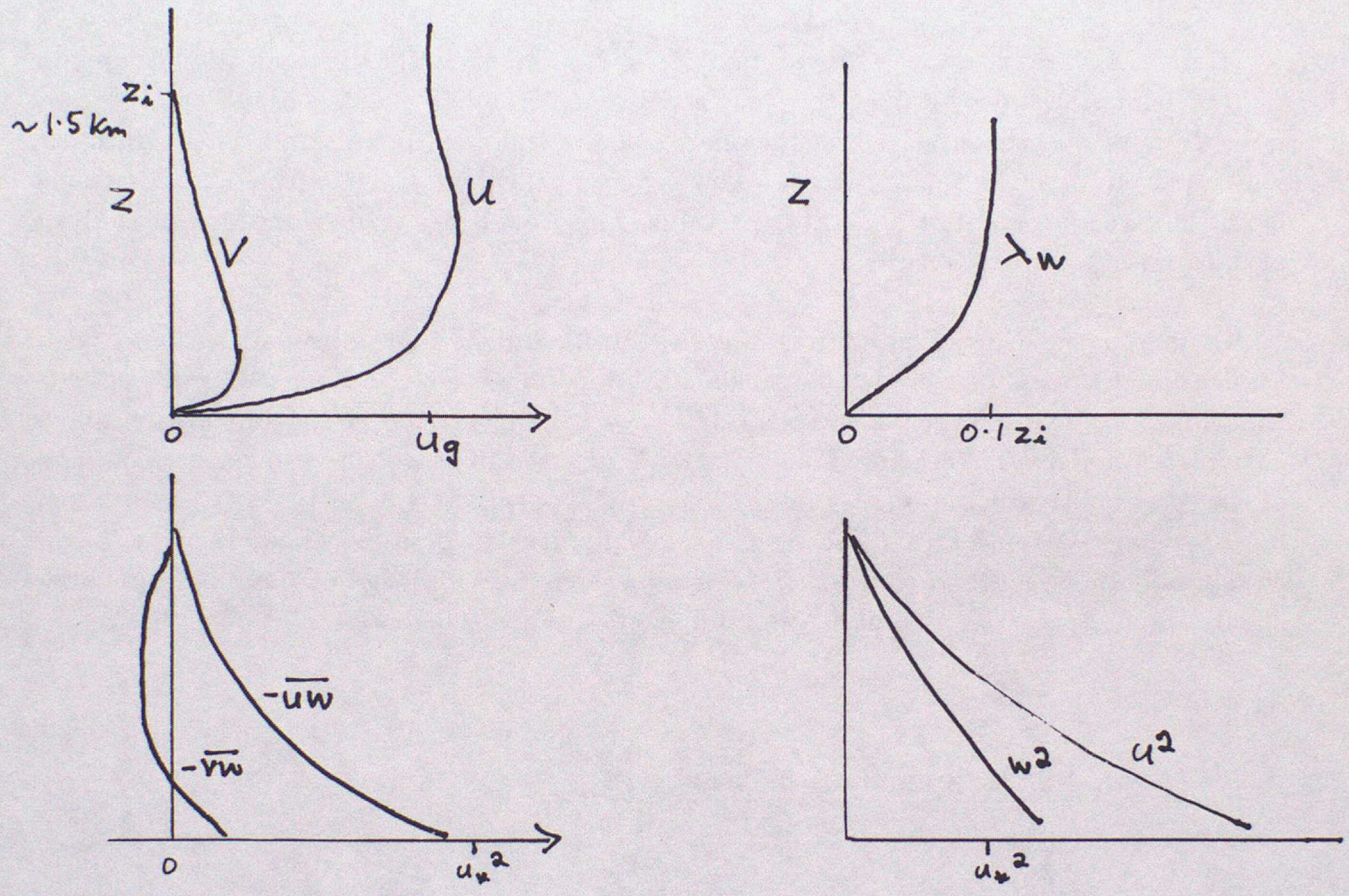

Figure 2: Illustrating some features of the neutral static stability boundary layer

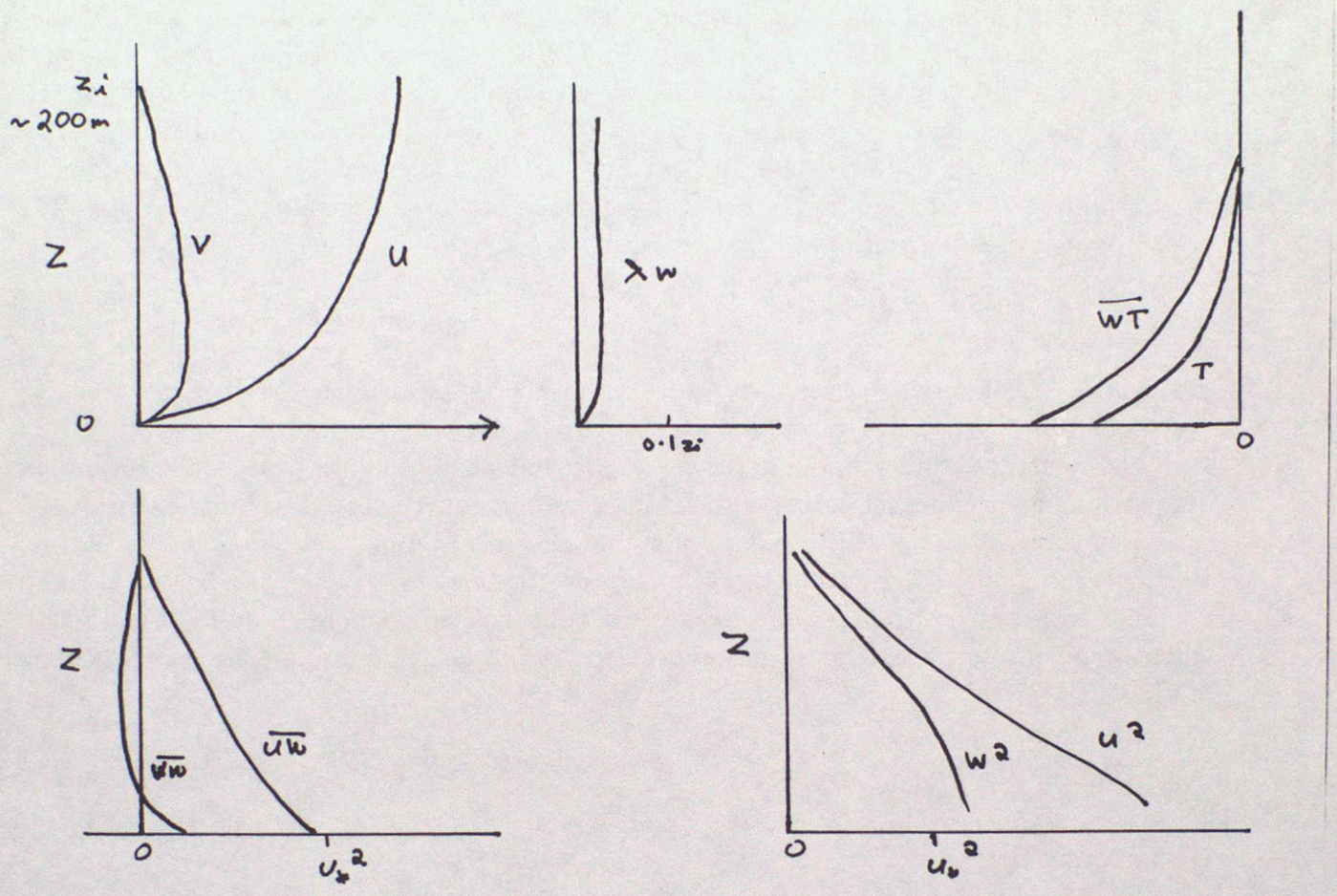

Figure 3: Illustrating some features of the stable nocturnal boundary layer

speed and direction occurs with height. The energy component profiles match the total shear stress profile in shape. Spectral analysis of this type of boundary shows eddies on all scales but the dominant motions are eddies with a scale a fraction of the boundary layer depth. As a result, for the greater part, the turbulence is in a local balance between energy production due to the mean shear and the energy dissipation. This is reflected in the match of the stress and energy profiles. In consequence of this local balance this flow is easy to model with mixing length turbulence closures:

The Stable Boundary Layer

Under the action of nocturnal cooling or passage over a cold sea a stable surface heat flux arises. Compared with the neutral boundary layer the magnitude of the turbulence intensity and the depth of the boundary layer reduce. The depth is typically between 10's and 100's of metres. Were equilibrium to prevail then Rossbly number similarity could provide a useful description. In fact most stable boundary layers are evolving due to the limited time of cooling and/or the influence of sloping terrain, e.g. consider the U-component of the equations of motion with a terrain slope α, i.e.

$$\frac{\partial U}{\partial t} + \frac{\partial}{\partial z}\overline{uw} = f(V - V_g) + g\frac{T - \overline{T}}{\overline{T}}\sin\alpha \qquad (13)$$

Then if $T - \overline{T}$ is only $3°C$ and $\alpha = 10^{-3}$ (1 in 1000) the drainage term is as great as a typical 1 ms^{-1} pressure gradient term. Figure 3 illustrates some typical profiles. As with the neutral stability boundary layer the turbulence is mainly in a local production dissipation balance and models of stable flow seem fairly successful. They do however need refinement for aspects of the influence of stable stratification on the turbulence structure. Particular difficulties arise from the influence of gravity waves generated by terrain and flow instabilities. Practical concern also arises from the strong cooling and light wind case when turbulence essentially vanishes and material may drift for some distance with little mixing.

The Convective Boundary Layer

Unless z_i/L is less than perhaps 0.5 convective dynamics dominate the flow; such conditions occur most of the time over the land during the day. Other convective situations can arise with cloud top cooling rather than surface heating. Figure 4 illustrates profiles for the case with surface heating. In contrast to the shear driven flows there is no longer a balance between local production and dissipation. The energy production is given by the heat flux profile and shows a near linear decrease with height with a negative region at the top of the boundary layer due to entrainment. In contrast the dissipation is fairly uniform with height. The vertical velocity variance shows a maximum at mid-boundary layer and the horizontal velocity variances show weak maxima near the surface and inversion. The turbulence is evidently no longer in a locally balanced state. The flow is dominated by eddy structures which occupy the whole of the depth of the boundary layer.

Unlike the neutral and stable static stability boundary layers in which the surface stress forms the velocity scale, and gives the typical magnitude of the velocity fluctuations, the relevant velocity scale for the convective boundary layer is determined by the heat flux.

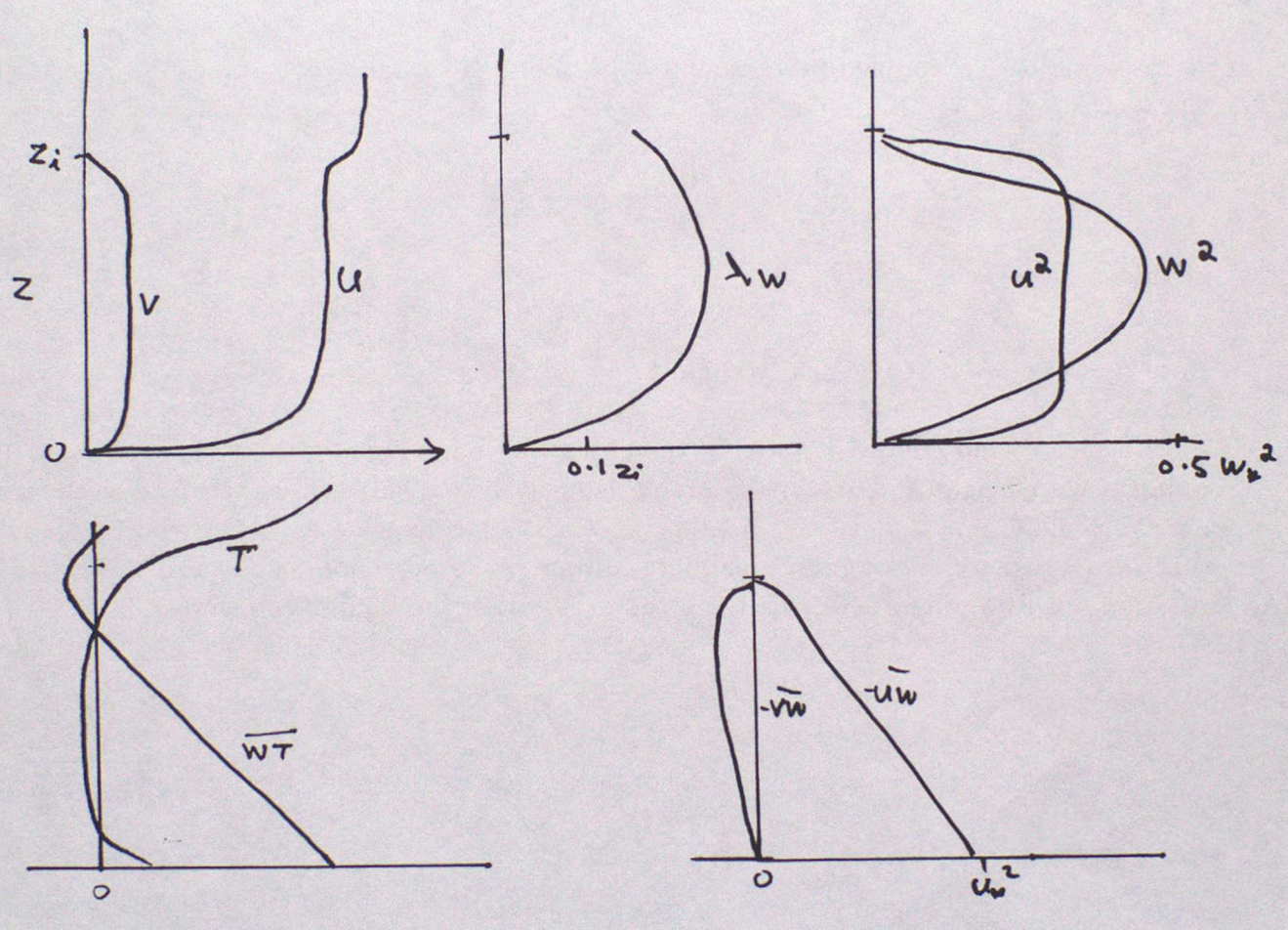

Figure 4: Illustrating some features of the convective boundary layer

This convective velocity scale w_* is given by $(\overline{wB}z_i)^{1/3}$ where $\overline{wB}$ is the surface value of the bouyancy flux and z_i is the boundary layer depth. This scale can be seen to follow from the turbulence energy equation with the bouyant energy production $\overline{wB}$ balancing the dissipation $E^{3/2}/l$ where E is the turbulence energy $\sim w_*^2$ and l is a length scale of order z_i. Alternatively if we note that the eddy viscosty should be of order $w_* z_i$ then

$$\overline{wB} \sim \nu \frac{\partial B}{\partial z} \sim w_* z_i \frac{\Delta B}{z_i}$$

If the value of ΔB implied by this relation is assumed to balance the non-linear term in the vertical equation of motion i.e.

$$w \frac{\partial w}{\partial z} \sim \frac{w_*^2}{z_i} \sim \frac{\overline{wB}}{w_*}$$

giving as before

$$w_* = (\overline{wB}z_i)^{1/3}$$

Note that the ratio L/z_i is nearly equal to u_*^3/w_*^3.

If a mean wind is present then, in the absence of baroclinicity, the mean flow is fairly uniform with height and the stress profile is fairly linear between the surface value and near zero aloft. For a convective boundary layer the height scale $(2\nu_t/f)^{\frac{1}{2}}$ where ν_t is the turbulent viscosity is generally much larger than z_i the inversion height and the Earth's rotation has little direct effect on the structures within the boundary layer.

Lecture 4

Models of the Planetary Boundary Layer

Dr M.K. MacVean

Met O 14

In this lecture, the major points that need to be considered in the design and implementation of a one-dimensional boundary layer model will be discussed. This encompasses most of the *boundary layer* considerations which enter into multi-dimensional models.

4.1 Analytic equations and turbulence closure

If molecular viscosity is neglected, the x-component of the Reynolds-averaged momentum equation given in Lecture 1 becomes

$$\frac{\partial U}{\partial t} = -\frac{\partial P}{\partial x} - \frac{\partial \overline{uw}}{\partial z} \tag{4.1}$$

Similarly we may obtain

$$\frac{\partial V}{\partial t} = -\frac{\partial P}{\partial y} - \frac{\partial \overline{vw}}{\partial z} \tag{4.2}$$

In the one-dimensional context, P is the pressure field supporting an externally determined geostrophic wind. In the case of dry air, the set of prognostic equations for the mean fields is completed by one for temperature which, in the absence of internal heat sources and sinks, is

$$\frac{\partial \Theta}{\partial t} = -\frac{\partial \overline{w\theta}}{\partial z} \tag{4.3}$$

A typical set of surface boundary conditions might be $U = V = 0$, together with either a specified heat flux ($\overline{w\theta} = H_s$) or a specified temperature ($\Theta = \Theta_s$). Difficulties associated with determining the appropriate height at which these boundary conditions should be applied over a rough surface, have been discussed in Lecture 2. Throughout this lecture, we will assume that they are applied at a distance z_o above the surface, where z_o is a length scale characterizing the size of roughness elements on the surface. The three equations above, together with the boundary conditions, do not, however, constitute a closed system, as they involve the correlations of fluctuating quantities. As discussed in Lecture 1, the turbulence closure problem is concerned with producing a closed set of equations from these. At the most straightforward level, the first-order closure, no further prognostic equations are involved and the second-order correlations are directly related to the mean fields. In principle, an infinite hierarchy of higher-order closures exists. In the general nth-order closure, additional prognostic equations are carried for all the correlations up to nth-order but, because of the non-linearity of the Navier-Stokes equations, the equations for the nth-order correlations will involve correlations of order $n+1$. The closure problem at the nth-order consists of finding a relationship between the $n+1$th-order correlations and the quantities for which prognostic equations are carried. A theoretical basis for such relationships is generally lacking, thus leaving only the option of empirical relationships,which become increasingly complex and questionable as n increases. Furthermore, the number of prognostic equations also increases rapidly with the order of the closure. The greatly increased computer resources necessary to carry out the additional calculations, severely limit the applicability of closures of second-order and higher. Therefore, we shall limit ourselves to a more detailed examination of a typical first-order closure.

In this case,by analogy with molecular mixing, the second-order correlations are related to the vertical gradients of the mean-field variables by

$$\begin{aligned} \tau_x = \overline{uw} &= -\nu_t \frac{\partial U}{\partial z} \\ \tau_y = \overline{vw} &= -\nu_t \frac{\partial V}{\partial z} \\ H = \overline{w\theta} &= -\kappa_t \frac{\partial \Theta}{\partial z} \end{aligned}$$

where ν_t and κ_t are the eddy diffusion coefficients for heat and momentum, respectively. For simplicity, the turbulent Prandtl Number ($Pr = \nu_t/\kappa_t$) is often regarded as a constant.

Since molecular mixing is neglected here, we may, for simplicity of notation and without ambiguity, omit the subscript t from the eddy diffusion coefficients We would now have a closed set of equations but for the fact that, in any realistic situation, the eddy diffusion coefficients will be functions of the flow field. Here, we will consider a mixing length closure of the form

$$\nu = \ell_o^2 \, S \, F(Ri)$$

where

$$S^2 = \left(\frac{\partial U}{\partial z}\right)^2 + \left(\frac{\partial V}{\partial z}\right)^2$$

ℓ_o is the mixing length in conditions of neutral stability, Ri is a Richardson Number defined as the ratio of buoyancy production to shear production in the equation for sub-grid turbulence energy and $F(Ri)$ is an empirical factor to allow for the effects of non-neutral stability on the turbulence. Typical choices of F are $(1 - 6Ri)^{1/2}$ in unstable conditions $(\partial\Theta/\partial z < 0)$ and $Max\{0, 1 - 3Ri\}$ in stable conditions $(\partial\Theta/\partial z > 0)$. Note that the second of these formulae implies a critical Richardson Number of $1/3$, at which turbulence is completely suppressed. It must be stressed that there is no general agreement on the optimal choice of F; a wide variety of different formulae are quoted in the literature. The Richardson Number may be expressed in terms of quantities appearing in the turbulence energy equation as

$$Ri = \frac{g}{\Theta_o}\overline{w\theta} \Big/ \left(\overline{uw}\frac{\partial U}{\partial z} + \overline{vw}\frac{\partial V}{\partial z}\right)$$

or,on substituting the first-order closure relations, as

$$Ri = \kappa \frac{g}{\Theta_o}\frac{\partial \Theta}{\partial z} \Big/ \nu S^2$$

Note that, in the case of constant Prandtl Number, Ri does not depend on the formulation used for the eddy diffusion coefficients. The only quantity which still needs to be specified, in order to produce a closed system, is the neutral stability mixing length (ℓ_o). A widely used formula for this (Blackadar, 1962) is

$$\frac{1}{\ell_o} = \frac{1}{\ell_{oo}} + \frac{1}{kz}$$

where k is von Karman's constant. Close to the surface, $\ell_o \sim kz$, that is, the scale of the eddies is determined by the proximity to the boundary. Such behaviour is reasonably well documented observationally. For large z (i.e. in the upper part of the boundary layer) $\ell_o \sim \ell_{oo}$. The appropriate choice of ℓ_{oo} will depend on the application; in convective conditions it will be related to the boundary layer depth. Observational support for any particular choice is much more limited at these greater heights than is the case close to the surface. Other factors limiting the scale of sub-grid motions, for example, the presence of a strong capping inversion, may also need to be taken into account in specifying ℓ_{oo}.

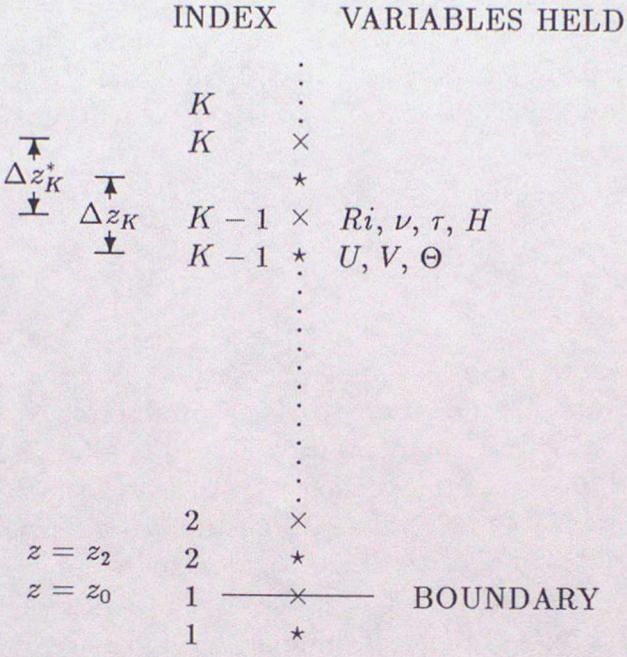

Figure 4.1: Distribution of variables on staggered grid. Boundary conditions are applied at $z = z_o$

4.2 Numerical Implementation

Here we give details of how the above equations and boundary conditions may be solved using a finite difference model. It is common in dynamical numerical models to use a staggered grid system, in which the different variables are held at different mesh points. Suitable choice of staggering minimizes the amount of interpolation necessary to calculate terms in an energetically consistent way. The natural choice in the present case is shown in Figure 4.1. Consider the vertical finite difference discretization of (4.1) at level m

$$\begin{aligned}\frac{\partial U_m}{\partial t} &= -\left(\frac{\partial P}{\partial x}\right)_m + \frac{\tau_{x\,m} - \tau_{x\,m-1}}{\Delta z_m^*} \\ &= -\left(\frac{\partial P}{\partial x}\right)_m + \frac{1}{\Delta z_m^*}\left\{\nu_m\left(\frac{U_{m+1} - U_m}{\Delta z_{m+1}}\right) - \nu_{m-1}\left(\frac{U_m - U_{m-1}}{\Delta z_m}\right)\right\}\end{aligned}$$

where derived quantities are calculated as follows

$$\begin{aligned}\nu_m &= \ell_o^2\, S_m\, F(Ri_m) \\ Ri_m &= \frac{g}{\Theta_o}\left(\frac{\Theta_{m+1} - \Theta_m}{\Delta z_{m+1}}\right) / Pr\, S_m^2\end{aligned}$$

$$S_m^2 = \left(\frac{U_{m+1} - U_m}{\Delta z_{m+1}}\right)^2 + \left(\frac{V_{m+1} - V_m}{\Delta z_{m+1}}\right)^2$$

Thus it may be seen that such a staggering of variables obviates the need to perform any averaging of variables between grid boxes. Energetic consistency is also particularly easy to demonstrate, using the control volume approach.

Turning now to the implementation of the boundary conditions, we first consider the velocity field. In particular, the U-momentum equation at the lowest interior level is

$$\frac{\partial U_2}{\partial t} = -\left(\frac{\partial P}{\partial x}\right)_2 + \frac{1}{\Delta z_2^*}\left\{\nu_2\left(\frac{U_3 - U_2}{\Delta z_3}\right) - \tau_{x1}\right\}$$

Thus, as a boundary condition for this equation we require the value of the x-component of the stress at $z = z_o$. This may be calculated from knowledge of the velocity at level 2 and the boundary condition $U = 0$ at $z = z_o$, if we assume that the Monin-Obukhov similarity laws hold between $z = z_o$ and the height of the first interior velocity grid point ($z = z_2$). For this procedure to be valid, the height of the first interior velocity grid point has to be chosen to be within the expected surface layer. It is assumed that the wind direction and, hence, the direction of the stress, do not change with height between $z = z_2$ and $z = z_o$. Thus

$$\tau_{x1} = |\boldsymbol{\tau}|_1 cos\vartheta$$

where ϑ is the angle between the velocity vector at $z = z_2$ and the x-axis. As discussed in Lecture 2, we expect, on dimensional grounds, the velocity within the surface layer in neutral conditions to satisfy

$$|\mathbf{U}| = \frac{u_*}{k} log\frac{z}{z_o} \tag{4.4}$$

Also

$$u_*^2 = \left(\overline{uw}^2 + \overline{vw}^2\right)^{1/2} = |\boldsymbol{\tau}|$$

Applying the above at $z = z_2$, remembering that the stress is constant within the surface layer, gives

$$\tau_{x1} = \left(k|\mathbf{U}|_2 / log\frac{z_2}{z_o}\right)^2 cos\vartheta$$

In non-neutral conditions, Monin-Obukhov similarity theory leads us to expect that the non-dimensionalized shear in the surface layer will be given by universal functions $\phi_m(z/L)$, as discussed in Lecture 2. The form of these functions can only be determined from observations and, although many observational experiments have been performed, there is still no general agreement as to the best choice. Much of the data can be fitted by analytic functions of the form $\phi_m = (1 - \beta_m z/L)^{-1/4}$ in unstable conditions and $\phi_m = 1 + \gamma_m z/L$ in

stable conditions. These functions may be integrated to give the velocity profile. In stable conditions, instead of (4.4) we have

$$|\mathbf{U}| = \frac{u_*}{k}\left\{log\frac{z}{z_o} + \gamma_m\frac{z}{L}\right\} \tag{4.5}$$

In unstable conditions we have

$$|\mathbf{U}| = \frac{u_*}{k}\left\{log\frac{z}{z_o} - \psi_m\left(\frac{z}{L}\right)\right\} \tag{4.6}$$

where

$$\psi_m = 2\,log\frac{1+\eta}{2} + log\frac{1+\eta^2}{2} - 2\,tan^{-1}\eta + \frac{\pi}{2}$$

and

$$\eta = \left(1 - \beta_m\frac{z}{L}\right)^{1/4}$$

In the above, the Monin-Obukhov length L is given by

$$L = -u_*^3/k\frac{g}{\Theta_o}\overline{w\theta}$$

and γ_m and β_m are empirical constants. In Lecture 2, specific typical values of the empirical constants were used, viz. $\gamma_m = 5, \beta_m = 16$.

The inversion of (4.5) or (4.6) to give u_* is not straightforward and, in general, must be carried out iteratively. A further potential complication is that the surface heat flux appears in L. If a constant heat flux boundary condition is imposed, this is trivial. If, however, the surface temperature is specified, then the surface heat flux itself depends on u_* in a complicated way (see below). If the model time step is short enough (less than $60s$, say), it may be accurate enough to use the value of L from the previous timestep. Otherwise it might be necessary to devise a complicated iterative method for obtaining a more accurate solution. Alternatively, an explicit method without iteration has been developed by Louis (1979), especially for application to operational forecast models with large timesteps.

A constant heat flux boundary condition may be straightforwardly implemented in the temperature equation as shown below, since H_s is known

$$\frac{\partial\Theta_2}{\partial t} = \frac{1}{\Delta z_2^*}\left\{\frac{\nu_2}{Pr}\left(\frac{\Theta_3 - \Theta_2}{\Delta z_3}\right) - H_s\right\}$$

If, instead, the surface temperature (Θ_s) is specified, then the implied surface heat flux H_s must be calculated for use in the temperature equation at level 2. Again using Monin-Obukhov similarity theory in conjunction with empirical fits to observational data, we may

obtain the relationships below. In stable conditions

$$\Theta_2 = \Theta_s + \frac{\theta_*}{k}\left\{\alpha_H \, log\frac{z_2}{z_o} + \gamma_H \frac{z_2}{L}\right\} \tag{4.7}$$

while, in unstable conditions

$$\Theta_2 = \Theta_s + \frac{\theta_*}{k}\alpha_H \left\{log\frac{z_2}{z_o} - \psi_H(\frac{z_2}{L})\right\} \tag{4.8}$$

where

$$\begin{aligned} \psi_H(\varrho) &= log\frac{1+\varrho}{2} \\ \varrho &= \left(1 - \beta_H \frac{z_2}{L}\right)^{1/2} \\ \theta_* &= -H_s/u_* \end{aligned}$$

and α_H, β_H, γ_H are empirical constants. In the formulae for the non-dimensional surface layer temperature gradient (ϕ_H) given in Lecture 2, specific typical values of these constants were used, viz. $\alpha_H = 1$, $\beta_H = 16$, $\gamma_H = 5$. Note that, strictly, the roughness length appropriate to temperature (z_{oT}) should appear in (4.7) and (4.8) rather than z_o, as discussed in Lecture 2. In most models, it is assumed that these quantities are identical. Given u_*, these equations can be inverted to give H_s in terms of Θ_2 and Θ_s. It is necessary, in general, to carry out the inversion using iterative methods. As mentioned earlier, there is the further complication that the determination of u_* itself depends on the surface heat flux.

So far, this section has considered only the *vertical* discretization of terms which are diffusive in nature. A final important remark is appropriate, concerning the time discretization of such terms. Consider, for simplicity, the equation

$$\frac{\partial U}{\partial t} = D$$

where D is a diffusive term. Using a leapfrog scheme, this may be discretized as

$$U(t+\Delta t) - U(t-\Delta t) = 2\Delta t D(t^*)$$

The time level t^* at which D is evaluated, is still to be specified. A linear numerical stability analysis shows that the most obvious choice ($t^* = t$) results in an unconditionally unstable scheme. It is important that the calculation of all diffusive terms is performed either at $t^* = t - \Delta t$, in which case an explicit, conditionally stable scheme results, or at $t^* = t + \Delta t$, in which case the numerical scheme will be implicit and unconditionally stable. In the latter case, although no restriction is placed on the timestep by considerations of numerical stability, the timestep will, in practice, be limited by the requirement to keep the discretization error acceptably small.

4.3 References

Blackadar, A.K., 1962. *J.Geophys. Res.*, **67**, 3095-3102.

Louis, J-F., 1979. *Bound.-Layer Meteor.*, **17**, 187-202.

4.4 Bibliography

Haugen, D.A. (ed.), 1973. *Workshop on Micro-meteorology.* Amer. Meteor. Soc., 392pp.

Haltiner, G.J. and R.T. Williams, 1980. *Numerical Prediction and Dynamical Meteorology*, Second Edition, Wiley, 477pp.

Boundary Layer Flow Over Hills

P.J.Mason
Meteorological Office, Bracknell

25 April 1988

1 Introduction

An understanding of flow in the atmospheric boundary layer is essential for wide range of applications. Estimates of the net momentum, heat and moisture fluxes are required for numerical weather prediction models whilst information on detailed flow structures is needed for applications such as pollution dispersion, wind power studies, agriculture and the siting and strength of buildings. Over level terrain our knowledge of these processes is incomplete but extensive studies have allowed a description and understanding which provides reasonable guidance. Over hills and complex terrain our knowledge is much more limited due to the absence of both theory and observations. Here an outline of current understanding of flow over hills and complex terrain is given. Attention will not be given to details of the complex models and theories which have developed but rather to the conceptual ideas which they embody. The reader is referred to the few papers cited for a more complete review and extensive bibliography.

In what follows, neutral static stability flow over a low hill is considered first. The dynamics which determine the changes in mean flow and turbulence are outlined and estimates of the changes made. The description then proceeds to the local and gross effects of steep orography with flow separation and vortex generation. The important gravity wave generation processes which occur for length scales greater than and of order about 6km are excluded from this discussion. Finally some attention is given to buoyancy effects in short length scale flows.

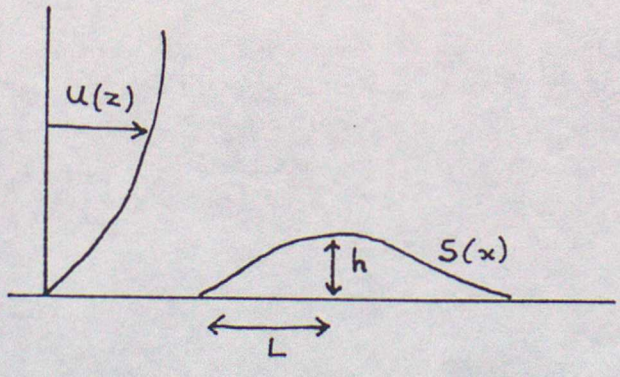

Figure 1: Schematic geometry of flow over a hill

2 The Mean Flow Over A Low Hill

The ideas in this and the next section are those usually invoked for predictions of flow and turbulence in neutral static stability flow (strong wind). A recent review, Taylor, Mason and Bradley 1987, provides further references and details. They prove successful for the regions of flow speed up but for reasons noted later are not reliable in regions where a flow sheltering is expected. Consider (see Figure 1) an undisturbed flow in the lower part of the atmospheric

boundary layer with a flow profile $U_o(z)$. Although the arguments can be applied for a general velocity profile we can, for example, consider the usual flow in the neutral atmospheric surface layer

$$U_o(z) = (u_*/\kappa) \ln z/z_o \tag{1}$$

where z_o is the roughness length, κ the von Karman constant and u_* the square root of the surface stress. We shall not be concerned here with steep orography and flow separation and it is easy to estimate the magnitude of key terms in the equations of motion

$$\frac{\partial \mathbf{u}}{\partial t} + \mathbf{u}\nabla\mathbf{u} = -\nabla p + \nabla\tau_{ij} \tag{2}$$

where $\mathbf{u}$ is the flow velocity, p the pressure divided by density and τ_{ij} a Reynolds stress tensor. With a large flow perturbation the non-linear term $\mathbf{u}\nabla\mathbf{u}$ will be of order U_o^2/L where L is typical scale of differentiation and U_o a typical flow speed. In contrast the turbulent stresses in the flow will be of order ${u_*}^2$ and $\nabla\tau_{ij}$ of order ${u_*}^2/l$ where l remains to be determined and is the scale over which the stresses vary. Now ${u_*}^2 = C_D U_o^2$ where C_D is a drag coefficient which might typically be 2.10^{-3} for a surface with low vegetation ($z_o \approx 0.1m$). Thus ${u_*}^2/l$ can only be large enough to influence the balance of the non-linear term over a small length scale $l \approx C_D L$. If L is order a few kilometres then l is only of order a few metres. Such a region does occur within a distance $\approx l$ of the surface but above l, in a steady flow, the non-linear term must balance the pressure gradient. i.e.

$$\mathbf{u}\nabla\mathbf{u} = -\nabla p \tag{3}$$

Further indications of the properties of this flow can be obtained by assuming the hill is so low that the flow perturbation is much smaller than U_o. Assuming for simplicity of analysis a two dimensional ridge we have $\mathbf{u} = (U_o(z) + u, w)$ which on substitution in 3 and with the neglect of second order terms gives

$$U_o(z)\frac{\partial u}{\partial x} + w\frac{\partial U_o(z)}{\partial z} = -\nabla p \tag{4}$$

together with a linearised boundary condition

$$w = U_o(l)\frac{\partial S}{\partial x} \quad \text{on} \quad z = l \tag{5}$$

where $h = S(x)$ is the hill height and l (assumed $\ll L$) is identified with the lowest height at which these equations apply. Since U_o is a function of z the solution of these equations involves some algebra but the form of the solution is essentially that obtained with U_o a constant, i.e.

$$U_o\frac{\partial u}{\partial x} = -\nabla p;\ w = U_o\frac{\partial S}{\partial x} \quad \text{on } z = l, \quad \text{and of course} \quad \frac{\partial u}{\partial x} + \frac{\partial w}{\partial z} = 0 \tag{6}$$

Taking

$$S = h_o e^{ikx},\ u = u_o e^{ikx},\ w = w_o e^{ikx}, \text{ and } p = p_o e^{ikx} \tag{7}$$

we obtain

$$p_o = U_o^2 h_o k e^{-zk},\ u = -U_o h_o k e^{-zk} \text{ etc.} \tag{8}$$

The disturbance decays with height on a vertical scale $k^{-1} = \lambda/2\pi$ where λ is the horizontal wavelength of the hill. The pressure perturbation shows a minimum over the crests of the wavy surface and maxima over the troughs. The pressure field reflects an integrated response of the flow to the surface perturbation and a detailed analysis of the problem posed in equations 4 and 5 with $U_o(z)$ gives the solution.

$$p \sim U_o(L)^2 h_o k e^{-zk} \tag{9}$$

where $U_o(L)$ is the basic flow at a height k^{-1} (the wavelength divided by 2π). The vertical advection term in equation 4 is of magnitude $u_*/U_o(z)$ less than the horizontal advection and

small in effect. To a good approximation the horizontal flow perturbation u is given by the balance

$$U_o(z)\frac{\partial u}{\partial x} = -\frac{\partial p}{\partial x} \tag{10}$$

so we obtain

$$u_o \sim \frac{p_o}{U_o(z)} \sim \frac{U_o(L)^2}{U_o(z)}\theta e^{-zk} \tag{11}$$

where $\theta = h_o k$ is the peak slope. This flow perturbation differs from that obtained with $U_o(z)$= constant, by the factor $(U_o(L)/U_o(z))$.

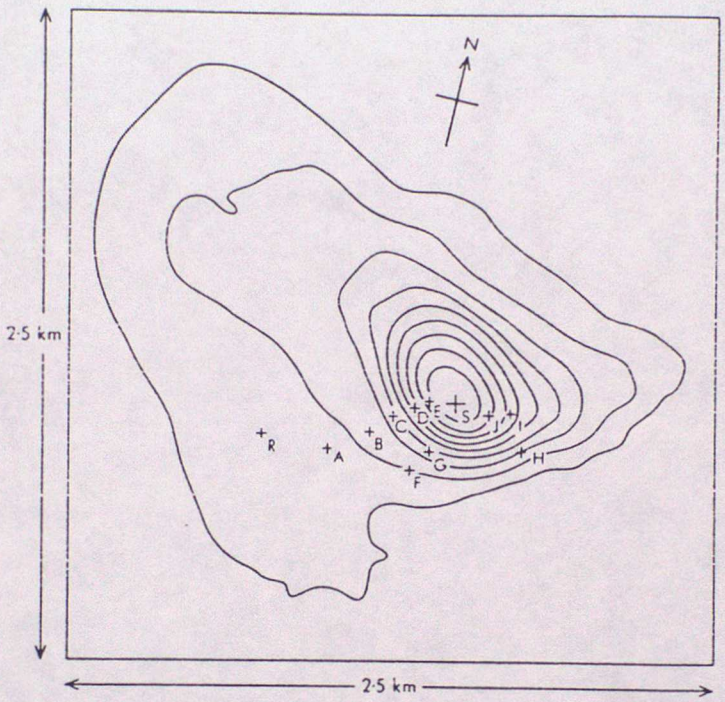

Figure 2: Contours of the digitized topography, as used in the numerical model, at 10m intervals. The positions of the sites at which 8m mean wind velocities were measured are marked. After Mason and King 1985.

With this flow perturbation we can make a more refined estimate of the height scale l. Consider the balance

$$U_o(z)\frac{\partial u}{\partial x} = -\frac{\partial p}{\partial x} + \frac{\partial \overline{uw}}{\partial z} \tag{12}$$

The pressure gradient $\partial p/\partial x$ derived as above is essentially independent height near the surface and $\overline{uw}$ is a linearised estimate obtained by a mixing length turbulence closure, i.e.

$$\overline{uw} + {u_*}^2 = l^2 \left|\frac{\partial(U_o(z)+u)}{\partial z}\right| \frac{\partial(U_o(z)+u)}{\partial z} \tag{13}$$

This leads to the estimate of l given by

$$l \sim 2\left(\frac{u_*}{U_o(l)}\right)^2 k^{-1} \tag{14}$$

or

$$l(\ln l/z_o)^2 \sim 2\kappa^2 k^{-1} \tag{15}$$

Note that a detailed analysis of flow over an isolated hill rather than a wavy surface shows that $2\pi k^{-1}$, the wavelength of the wavy variation, corresponds to length scale which when combined with the hill height gives a realistic value of peak hill slope, i.e. roughly the hill half width.

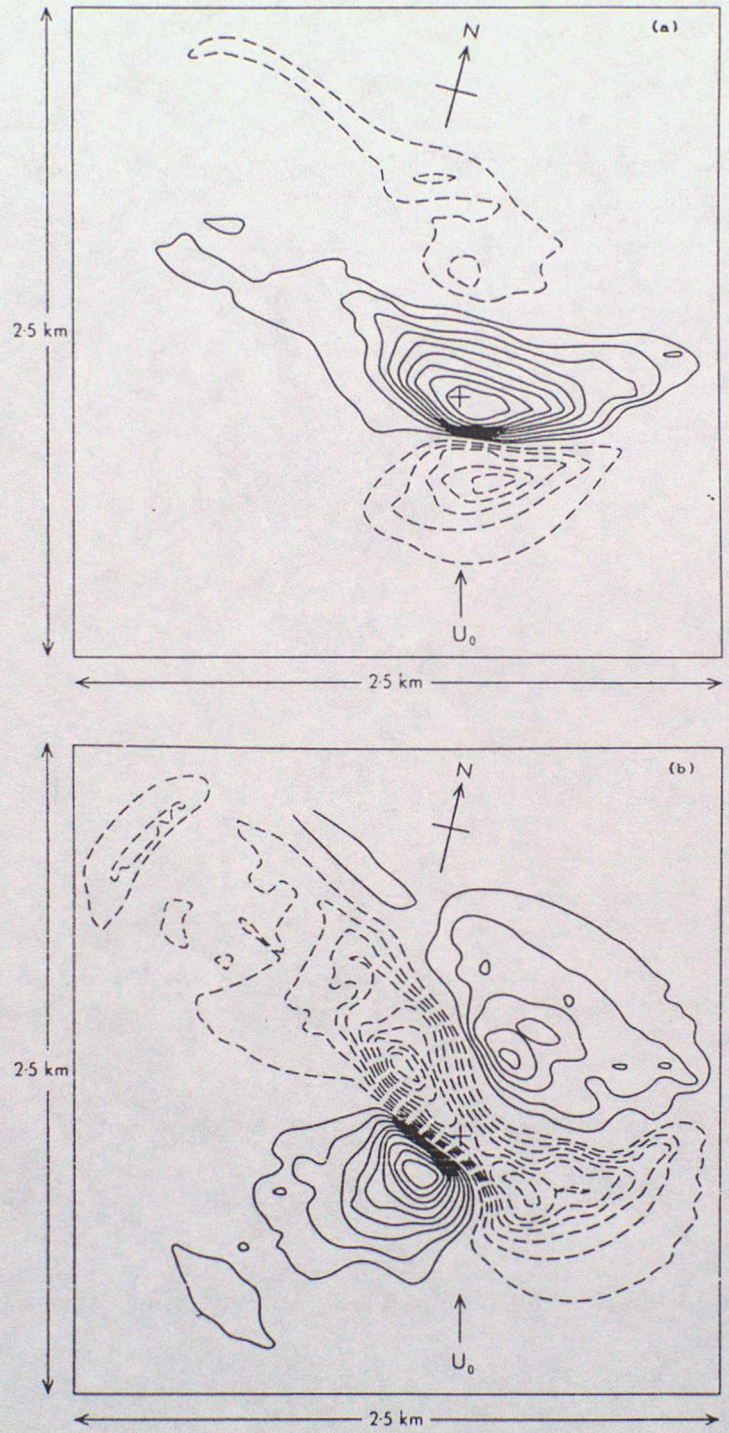

Figure 3: Contours of velocity perturbations at a height of 8m above the surface obtained by the application of model D (see Mason and King 1985) to the digitized terrain. (a) shows the streamwise component of the perturbations and (b) the transverse component. The contour intervals are 0.061 and 0.025 respectively where a value of unity corresponds to the undisturbed flow speed at 8m. Negative contours are shown dashed. The basic wind direction and map orientation are indicated. For clarity, contours are presented in a domain 2.5km square rather than the actual 6.7km square domain used for the calculation. After Mason and King 1985.

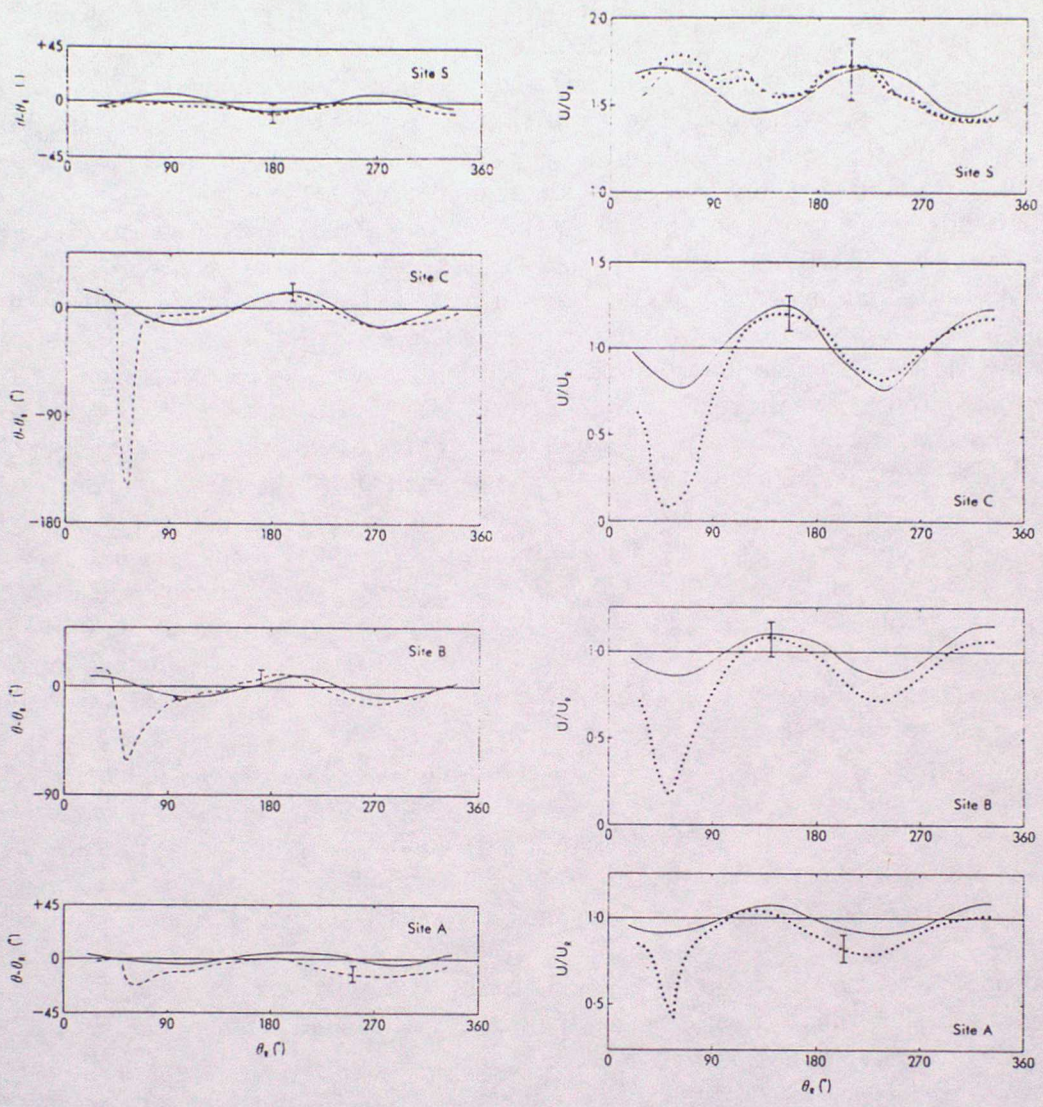

Figure 4: Measurements of 8m wind speed and direction at the summit site, S, and three other selected sites. Wind speeds have been scaled by that measured at the reference site, U_R, and directions are expressed as differences from that measured at site R. The solid lines are predictions from model D; broken lines are measurements, averaged over 10° intervals, of wind direction. Error bars show the typical scatter of the observations. On the plot for wind speed at site S, results are shown from both a Gill anemometer system (.....) and a cup anemometer system (- - -). After Mason and King 1985.

To summarise, above $z = l$ we obtain a fractional change in the flow of

$$\frac{\Delta u}{U_o(z)} = \left(\frac{U_o(L)}{U_o(z)}\right)^2 \theta e^{-z/L} \tag{16}$$

where θ is the peak hill slope. The factor $(U_o(L)/U_o(z))^2$ is introduced by the velocity profile and arises as the pressure field, dependent on $U_o(L)$ interacts with the local flow $U_o(z)$. As a result of this factor the flow speed up depends upon the surface roughness z_o, and as noted below, the basic flow static stability. Below a height l given by equations 14 and 15 the flow will be influenced by the turbulent stresses and the perturbation will reduce towards the surface. In many practical examples this height is below the region of interest.

For a 2-D ridge good results are obtained with θ evaluated as indicated, whilst for a circular hill the flow is partly diverted to either side and the value of θ should be reduced by about 0.75. The dynamics and equations described have been incorporated into models which can be applied to give complete flow predictions in complex terrain. These predictions have been verified by comparison with field experiments. Figures 2, 3 and 4 illustrate such a comparison. Figure 2 shows terrain contours of the Hill Blashaval on North Uist. Figure 3 shows predictions for the two flow components at 8m and Figure 4 shows individual site comparisons of the observations and the predictions. The height of Blashaval is about 100m above the surrounding terrain and the peak slope is about 0.4 rad giving a value of L of about 250m. The local value of roughness length z_o was measured to be 0.01m. It follows that l is about 6m and the expected flow speed up at 8m over the summit is $\Delta u/U \sim 2.2 \;\; 0.4 \;\; 0.75 \;\; = 0.68$ which corresponds well with values observed on the summit. Here the factor 2.2 is $(U(250)/U(8))^2$, 0.4 is the slope, and 0.75 the circular hill factor. It is evident in Figure 4 that there are some serious discrepancies occurring on the lee side of the hill. At site C with a wind direction of about 50° the predicted flow reduction is only about 25° yet the observations suggest a near zero reversed flow. This discrepancy arises as the observed flows separate in the lee of the hill at much smaller topographic slopes than these simple ideas would suggest. This flow separation has its origins in the near surface region close to the summit of the hill. Refined studies have found that complex turbulence closure methods are needed to describe this feature. Indeed, as noted below, the separated regions of all flows are also characterised by large turbulence intensities and are difficult to predict with accuracy.

A final note is that, except for the flows with direct stability influences which are noted below, a flow speed up much greater than a factor of 2 is unlikely. When the flow speed up reaches a value of this size the flow will be close to separating upstream as well as downstream and after upstream separation occurs the streamline paths over the upstream separation do not reach greater slopes than roughly this critical angle for flow separation.

3 Turbulence structure in flow over a low hill

The boundary layer turbulence which passes over the hill is subject to the changing velocity gradients on a time scale over order L/U (where L is scale of the hill and U a typical flow speed). The turbulence itself involves eddies of some length scale and typical internal velocity scale. The typical size of the flow eddies increases with distance from the surface and is of order that distance, z. The typical velocity scale is of order the square root of the surface stress u_*. Thus an eddy turnover time is $\sim z/u_*$. It follows that for heights $z > Lu_*/U$ $(u_*/U \sim \sqrt{C_D} \sim 0.05)$ the flow gradients are changing faster than the response time of the eddies. This situation corresponds to so-called rapid distortion and the influences are often described in terms of the way in which the flow distortions change the length of vortex filaments and hence alter velocity components. It is possible to make analytic calculations of these responses but the calculations are complex and even the sign of changes can depend on the upstream values of the different turbulent stress components. The nature of the changes also alter between two and three dimensional flows. The general effect of these changes in both theory and observations

is to tend to increase the vertical turbulence fluctuations $\overline{ww}$ and to give a smaller decrease in the horizontal component fluctuations $\overline{uu}$. Typically the expected fractional increase in $\overline{ww}$ is of order $(\Delta u/U)^2$ the speed up increase squared.

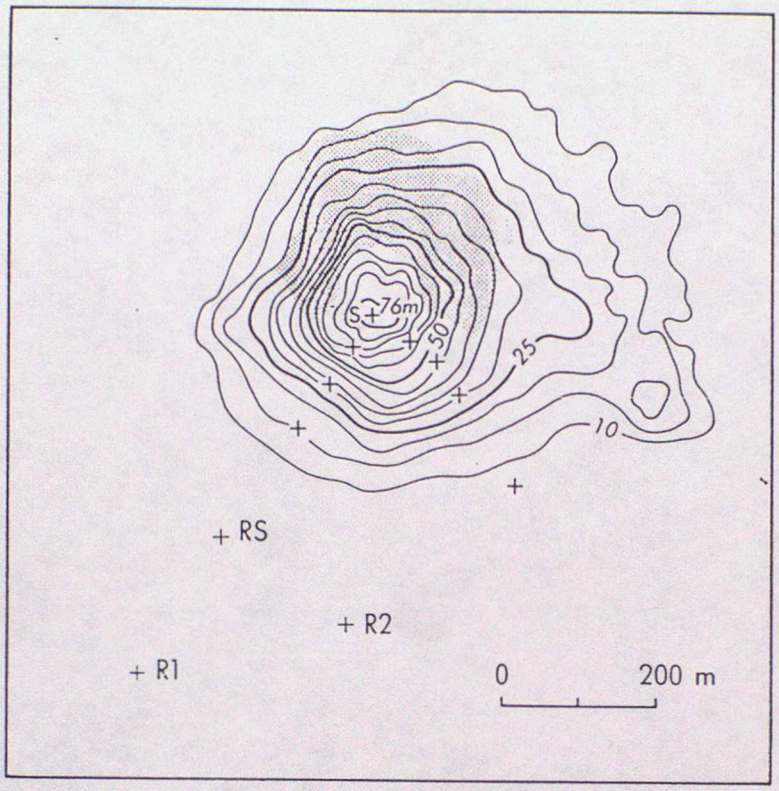

Figure 5: A topographic map of Nyland hill. The contour interval is 5m. The hatched area is covered with low trees and bushes. The sites marked R1 and R2 are the upstream reference sites, the site RS is the ultrasonic anemometer site, S is the summit site and the mean flow measurement sites are shown by unlabelled crosses. After Mason 1986.

The height scale l_t above which these rapid distortion effects should dominate can be found from a formal analysis involving high order turbulence closures. It is found to be given by

$$l_t \ln l_t/z_o \sim 2\kappa L \tag{17}$$

and thus matches the rough estimates already made. If we consider the case of a hill with scale $L = 250$m and $z_o = 0.01$m we obtain a value of l_t of about 30m. In contrast to heights above l_t, at heights well below l_t, the turbulence time scale is very fast compared with the rate at which the velocity gradients change. In these regions very near to the surface the turbulence achieves "local equilibrium" with the velocity gradients. The turbulence then simply matches the values expected with the local flow speeds and surface roughness. In between these two regions the changes are complex and involve challenging dynamics. The changes, however, are no more extreme than those in the surrounding regions of the flow.

From these considerations it is clear that, apart from effects involving flow separation, the influence on dispersion processes will occur mainly through the mean flow changes. Estimates of gusts in the wind are harder to make but are important for regions of flow where further speed increases may have implications for the design of structures. The above theoretical arguments suggest that above the near surface, the turbulence energy (especially $\overline{uu}$) will not be much greater than upstream and the relative size of the gusts thus less. In fact this assertion can be misleading as the above section has only considered the fluctuations due to small scale eddies. In the atmospheric boundary layer there will usually be energy in horizontal flow fluctuations on larger scales than the scale of many hills. For example, with a 250m hill eddies on scales greater than 250m will behave as part of the mean flow and any u fluctuations on this scale will

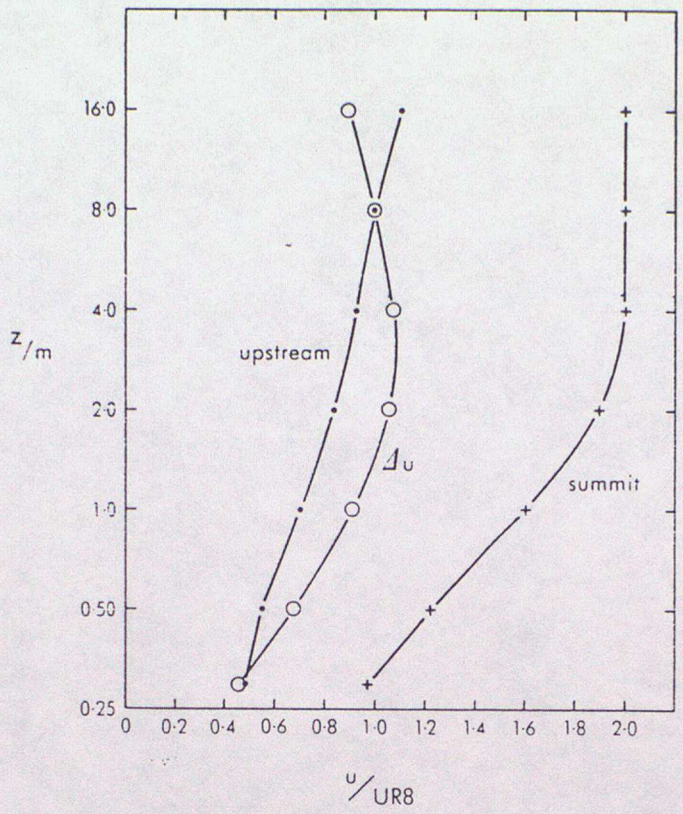

Figure 6: Vertical profiles of wind speed at the upstream and summit sites. The ordinate shows height above the ground on a logarithmic scale and the abscissa gives the speed relative to the reference speed UR8. The dots show upstream data, the crosses summit data and the open circles the difference of these two: the speed-up. After Mason 1986.

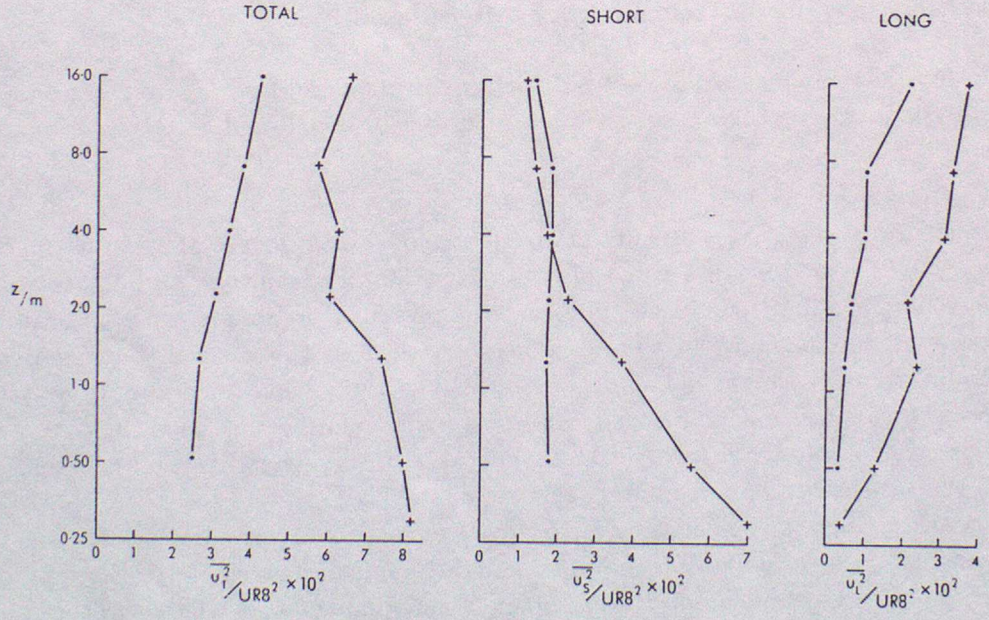

Figure 7: Illustrating statistics of $\overline{uu}$ at the upstream and summit sites. (a), (b) and (c) show the variance of the 'total' (all measured scales up to 5km), 'short' (all measured scales up to 200m) and 'long' (scales between 500m and 5km) contributions to $\overline{uu}$ respectively. Dots denote data values for the upstream site and crosses those above the summit. Each symbol is derived as the mean of about 6 measurements and the values are scaled by UR8. The ordinate is height on a logarithmic scale. The u-direction is defined as streamwise. After Mason 1986.

be subject to the mean flow speed up. Thus low frequency gusts will speed up in proportion to the flow speed up.

These various effects can be well illustrated by data from a field experiment. Figure 5 shows contours of Nyland hill in Somerset. This is a small scale feature with $L = 100$m but has the smooth surface characteristic essential for representative field measurements at single points. Figure 6 shows the upstream and summit mean velocity profiles and Figure 7 shows measurements of the streamwise energy component. The energy component has been displayed as total, short scale and long scale contributions. Since the hill scale is small the importance of the long scale components is especially marked. Application of the flow speed up rules to this site agree well with the observed speed up of about 2.0 ($\Delta u/U \sim 1$). l has a value of about 2m and the flow increase Δu is a maximum at this low height. The height scale l_t has a value of 11m and the rapid distortion expectation of a decrease in the short scale contibution to $\overline{uu}$ at these heights is borne out. Below 2m the short scale energy increases towards values matching the local flow speeds. The low frequency components, like the mean flow, show a near logarithmic increase with height and are seen to increase by factor of nearly four over the values found upstream.

4 Separated Flows

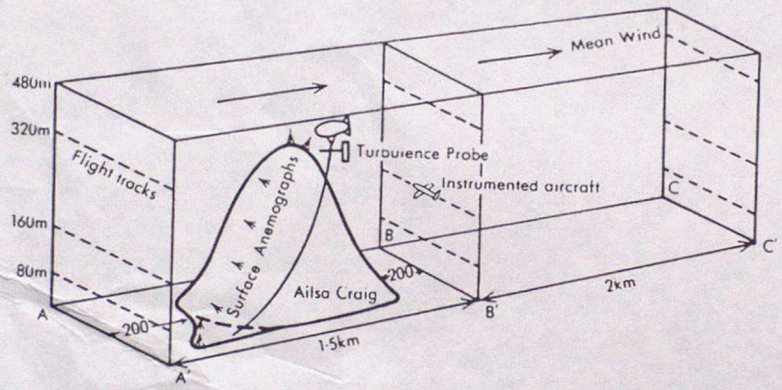

Figure 8: Sketch showing the general arrangement on and around the island, including aircraft flight tracks perpendicular to the mean wind. After Jenkins et.al. 1981.

When the orography is sufficiently steep flow separation will occur. With separation the adverse pressure gradient between the lee of the hill and the summit decelerates the flow faster than it can be accelerated by the transfer of momentum towards the surface by the diffusion. Accurate estimates of the critical angle of slope for flow separation require complex turbulence closure models and simple closures tend to underestimate the tendency to separate. This was seen in the example presented above (Figure 4). The observed flow reduction in the lee of the hill was greater than that predicted. A rough guide to the critical angle is obtained by considering a unity flow perturbation at a height l, i.e. from equation 16

$$\theta_{crit} \sim \left(\frac{U_o(l)}{U_o(L)} \right)^2 \tag{18}$$

In forested terrain a typical angle for flow separation is about 20° whilst in short grass terrain a typical angle is about 30°.

In flow over ridges the separated mean flow takes the form of a characteristic recirculating bubble. However, in contrast to the steady separations which occur in low Reynolds number laminar flows, turbulent separations are highly unsteady with the instantaneous velocities taking all directions. The main impact is often thus due to the very high turbulence intensity and the mean flow itself may be too weak to have much consequence.

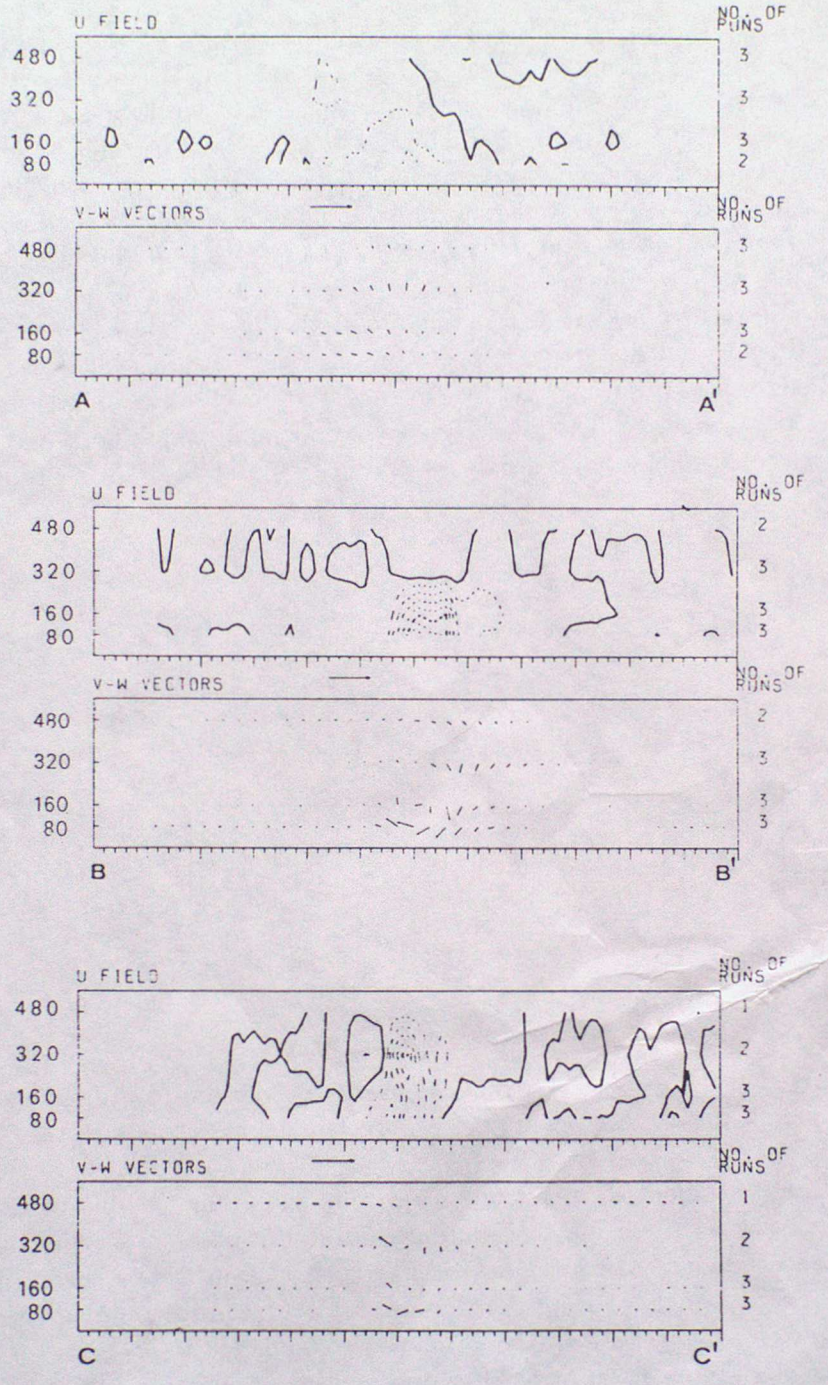

Figure 9: Mean velocity fields in vertical sections from aircraft observations. The three sections (a) AA', (b) BB', (c) CC' are defined in Figure 8 and are viewed looking in the downstream direction. In each figure the upper field is a contour plot of the dimensionless streamwise velocity component, i.e. normal to the section. The contour interval is 0.1, and dashed contours denote values less than 1. The lower field shows the secondary flow vectors in the transverse section, and the length of the arrow is proportional to the velocity. The arrow at the top of the box shows the length of the arrow corresponding to unit speed, i.e. the mean streamwise wind speed remote from the hill. The numbers to the right of the box indicate the number of runs used to obtain the average, and the heights are on the left. Tick marks on the bottom of the box indicate a horizontal spacing of approximately 100m. After Jenkins et.al. 1981.

In flows past three dimensional bodies the flow in the separated region is of similar low mean value and high turbulence intensity. However the three dimensionality allows the important influence of vortex turning and stretching. The wakes of three dimensional bodies usually contain significant mean streamwise vortical circulations (Mason and Morton 1987). These circulations can persist some distance down wind and give mean vertical winds and enhanced wind gusts, both of which may have practical importance. The mechanism for generating these trailing circulations is complex but the turning of the transverse vorticity shed from the body is usually the dominant cause. This transverse vorticity is just the region of strong vertical and lateral shear which leaves the surface of body at separation. It can then be turned according to relative advection around the separation region. Cross-stream-symmetrical obstacles generate one or more nested vortex pairs, of which one pair is normally dominant. Tall objects tend to generate a pair with central down-wash, while squat objects tend to generate central up-wash. A more powerful circulation of a single sign is generated by a skew body. The tendency for flow to pass faster round one side of the body provides the inertial turning of the shed vorticity. Such vortices can be very powerful. Space prevents illustrations of all the various ideas raised in this section. An example of a fairly two-dimensional flow with separation is given below in section 6. Figure 8 shows a plan of flight tracks relative to the island of Ailsa Craig. This island has an elliptic section and the flow in the wake (Figure 9) reveals a powerful single trailing vortex.

5 Turbulence in complex terrain with flow separation

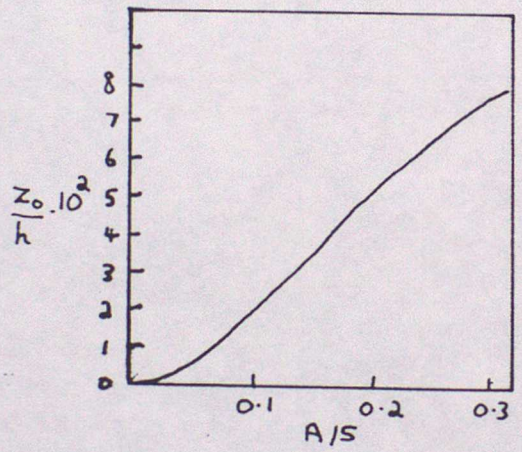

Figure 10: Values of z_o/h as a function of A/S where A is the sum of the frontal areas of the obstacles occupying a surface area S and values of $C_d = 0.3$ and $C_n = 0$ are assumed. The curve shows the relation given by equation 23.

Observations show that unless flow separation occurs the changes to turbulence intensity values relative to flat terrain values are usually modest. When separation occurs the turbulence intensity increases and some estimates of the changes can be made. As noted below these estimates are borne out by observations. The basis for these estimates is the remarkable way in which large-scale hills produce an influence greater in magnitude but similar in scaling to smaller scale roughness features. No formal theoretical justification exists but the results are borne out by numerical simulations and observations.

Consider a statistical distribution of steep hills with flow separation. The drag force on each of these hills will be of order $0.5\rho C_d A(U(h/2))^2$ where A is a frontal area $U(h/2)$ a typical flow, say that at half the object height, ρ the fluid density and C_d the body drag coefficient. For a separated flow C_d will be of order unity but its exact value will depend on the precise object shape and may be hard to determine. Typical values for orography seem to be about 0.3 (see Mason 1986b). If the boundary layer containing these steep hills follows its usual non-dimensional behaviour then the knowledge of this force allows us to infer the boundary layer

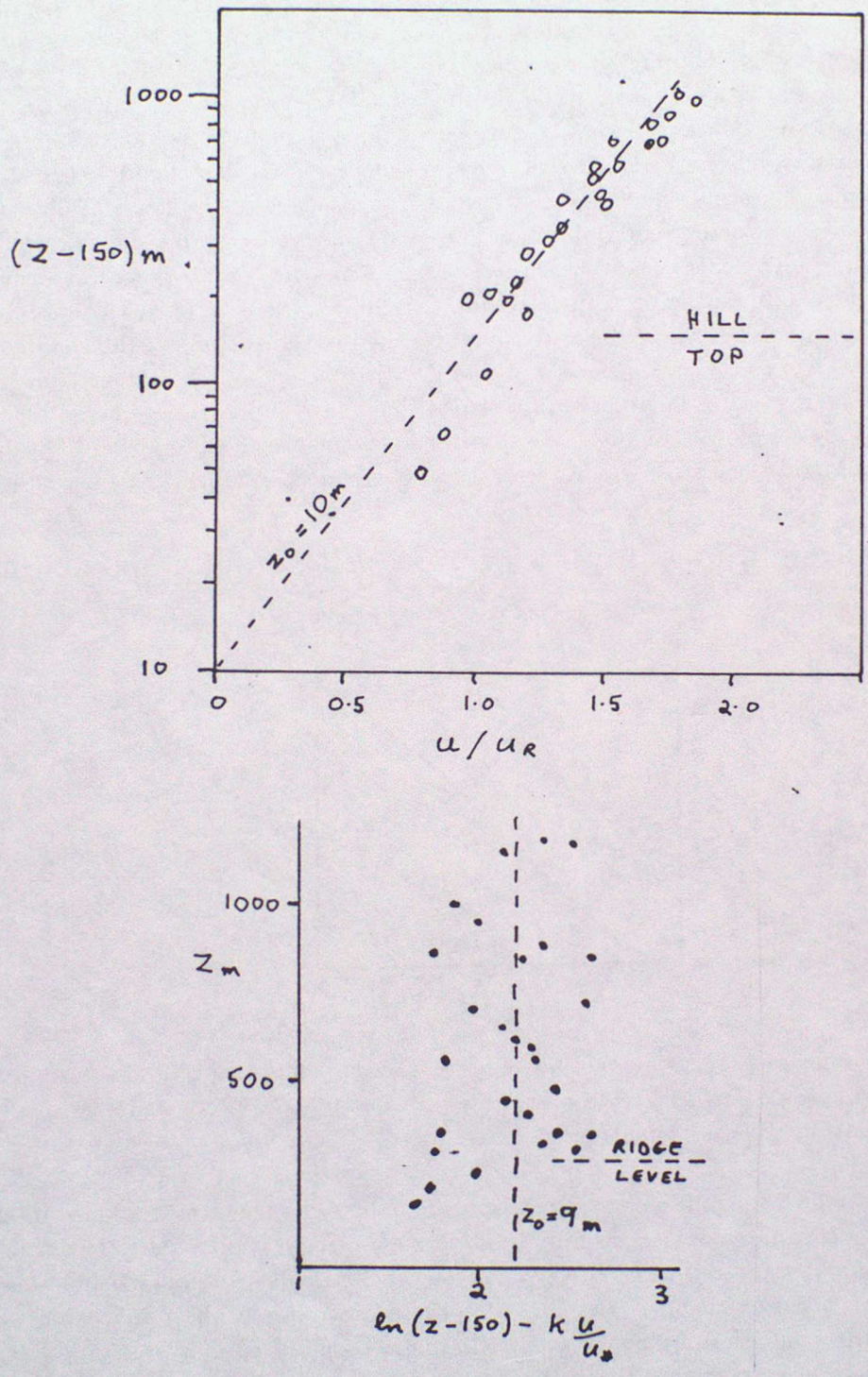

Figure 11: Measurements made by instruments on a tethered balloon cable at heights above complex terrain. Heights are measured above the level of the valleys and the summits extend to about 300m. (a) shows measurements of the velocity profile and how it matches a logarithmic variation with $z_o \sim 10$m. (b) shows values of the local ratio of $U/\sqrt{\overline{uw}}$ and how they are consistent with a value of $z_o \sim 9$m.

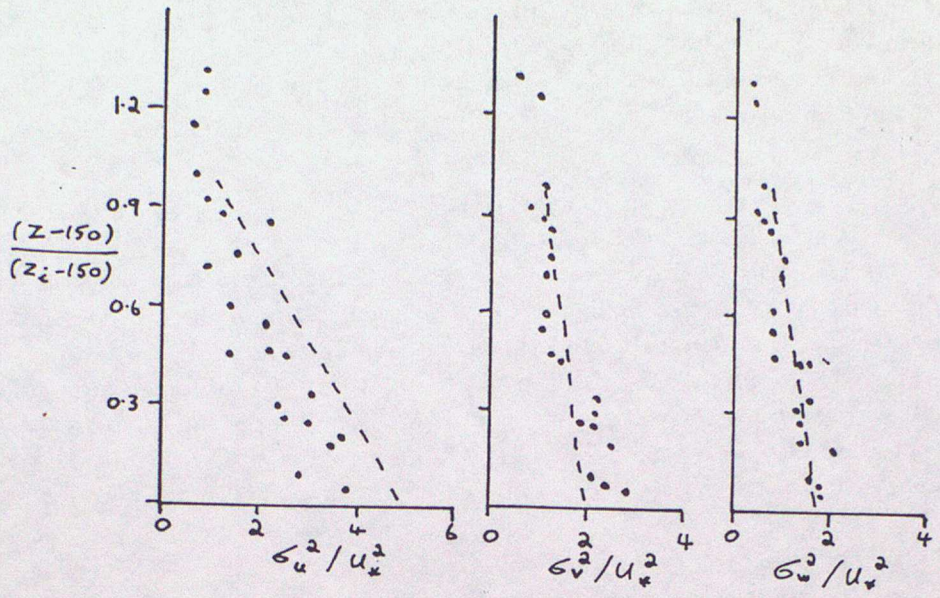

Figure 12: Measurements made by instruments on a tethered balloon cable at heights above complex terrain. Heights are measured above the level of the valleys and the summits extend to about 300m. the plots show the ratio of the 3 energy components to the estimated surface stress value. The ordinate has been normalised by the estimated boundary layer depth z_i. The dashed line denotes predictions from a standard boundary layer model.

statistics. We argue that the hills are sufficiently separate so that they experience a velocity derived from the final velocity profile, i.e.

$$U(h/2) = (u_*/\kappa)\ln(h/(2z_o)) \tag{19}$$

where h is the body height and z_o and u_* the effective values of z_o and u_* which we seek. The force on a body is then

$$F = 0.5\rho C_d A(U(h/2))^2. \tag{20}$$

In order to derive a relation with no singular behaviour we assume a stress u_{*1}^2 due to the undisturbed, say vegetative value of z_o i.e. z_{o1} so

$$U(h/2) = (u_{*1}/\kappa)\ln(h/2z_{o1}) \tag{21}$$

It follows that the area average of the effective stress equals the sum of the forces on the bodies and the background stress i.e.

$$Su_*^2 = \sum 0.5C_d A(U(h/2))^2 + SC_n(U(h/2))^2 \tag{22}$$

where S is the surface area considered, $C_n = \kappa^2/(\ln(h/2z_{o1}))^2$ and the summation includes all bodies in the area. From these equations we obtain

$$(\ln(h/2z_o))^2 = \kappa^2/(\sum 0.5C_d A/S + C_n) \tag{23}$$

which allows z_o the effective value of the roughness length to be estimated. From z_o the mean flow profile and shear stress can be estimated. Figure 10 shows the resulting values of z_o which arise with C_n and z_{o1} equal to a negligible value. The evidence is that the components of turbulence energy retain their usual ratios to these enhanced values of surface stress. This seems to apply even in separated regions of the flow where although the mean flow is very low the turbulence energy retains values typical of the overall value of surface stress u_*^2. Note that the value of z_o appropriate for heat and moisture transfer will not be influenced by pressure forces and will remain at a vegetative value.

Figures 11 and 12 show observations of turbulence made with a tethered balloon in complex terrain in South Wales. Application to this area of equation 23 above, gives an overall value of z_o about 8m and accords well with the observations. The mean flow profile above the hills matches this value whilst the turbulence, even into the region of valleys, also matches it well.

6 The influence of static stability

As has already been noted, the important effects which can occur in flows with gravity waves will not be discussed here. Such effects can be of particular importance in the estimation of wind speeds over large scale mountains and the generation of severe downslope winds in the lee of such mountains. The objective here is only to highlight the main influences on smaller scale flows and to indicate the relevant parameters. Unfortunately, observations able to give measures of these parameters are few and predictions of the flows are thus often difficult. Descriptions of the various types of flow, and drainage flows in particular, have an extensive literature (see e.g. Scorer 1968).

One significant influence of the static stability is indirect. The mean velocity profile is strongly influenced by the surface heat flux; with an unstable flux the wind shear is reduced and with a stable flux it is increased. The section on mean flows showed the importance of the shear $(U_o(L)/U_o(z))$ in determining the speed up and it follows that speed up will be increased when the flows are stable. Note has already been made that the turbulent stress divergence only influences the very near surface flow and buoyancy effects do not alter this situation. To proceed further we need to consider when buoyancy forces will be able to have a direct influence on the local flow.

An estimate of the direct influence of buoyancy forces on the flow is complex as it depends on the relevant scales of both the orography and the basic buoyancy gradients. The size of the influence will depend primarily upon the ratio of the perturbation of the hydrostatic pressure gradients to the dynamic pressure gradients. The magnitude of the dynamic pressure perturbation can be easily estimated as given above. For gentle orography of slope θ the flow perturbations will be of the order of $U\theta$, where U is a typical flow speed, and the linearised value of the dynamic pressure perturbation will be $\sim 2U^2\theta$. For large slopes this linearisation will fail but it should be noted that the pressure perturbation will not exceed $\sim U^2$. The hydrostatic pressure perturbation will be of order $\Delta B h^*$ where ΔB is the perturbation buoyancy contrast and h^* the vertical scale of this buoyancy perturbation. The ratio of the dynamic and hydrostatic pressure perturbations is the square of a Froude number

$$F^2 = 2U^2\theta/\Delta B h^* \tag{24}$$

To estimate this Froude number requires careful consideration of the appropriate values of ΔB and h^*.

In the case a stably stratified flow with a uniform vertical buoyancy gradient of $N^2 = \partial B/\partial z$ we can suppose that ΔB will be about hN^2 where h is the hill height and h^* will be about L where L is the hill length. This estimate of $h^* \sim L$ will only be strictly correct when gravity waves do not occur and the flow is close to inviscid potential flow. Noting that $\theta \sim h/L$ we obtain

$$F^2 \sim 2U^2/N^2L^2 \tag{25}$$

This is the usual Froude number obtained in the theory of linearised internal gravity waves. For values of F less than about unity internal gravity waves will be generated.

The main purpose of this section is simply to recognise the importance of an appropriately defined Froude number. The Froude number has been introduced as the ratio of the hydrostatic and dynamic pressure gradients. The Froude number given by equation 25 can also be seen as the ratio of the Brunt Vaisala period N^{-1}, the natural restoring period of the stable fluid, to the time for flow over the hill L/U. To generate gravity waves L/U must be greater than N^{-1}.

Taking typical values of $N \sim 10^{-2}\text{s}^{-1}$ and $U \sim 10\text{ms}^{-1}$, gravity waves will be generated if the hill wavelength λ is greater than $\sim 2\pi 10^3\text{m}$. The value of L denotes the scale of differentiation $\lambda/2\pi$.

If we consider a steep hill with a dynamic pressure perturbation U^2 and suppose that the buoyancy disturbance only extends to the height of the hill so $h^* = h$. Then we obtain

$$F^2 \sim U^2/N^2h^2 \tag{26}$$

This Froude number based on the vertical scale expresses the ratio of the flow kinetic energy to the potential energy needed to raise fluid a height h in the stable environment. When this Froude number is less than unity the flow over obstacle will be reduced and the flow will tend to pass around the obstacle. These various flow regimes can have important influences on plume dispersal in complex terrain.

A case worth further consideration arises with the stable nocturnal boundary layer when the depth of the stable boundary layer may be limited to a height scale h_b of order a few hundred metres or less. Taking $h^* = h_b$ and a sufficiently high hill so that $h > h_b$ then $\Delta B = \Delta B_b$ the buoyancy contrast across the stable layer and

$$F^2 \sim 2U^2/\Delta B_b L \tag{27}$$

When this Froude number is less than unity the dominance of the hydrostatic pressure gradient leads to drainage flows.

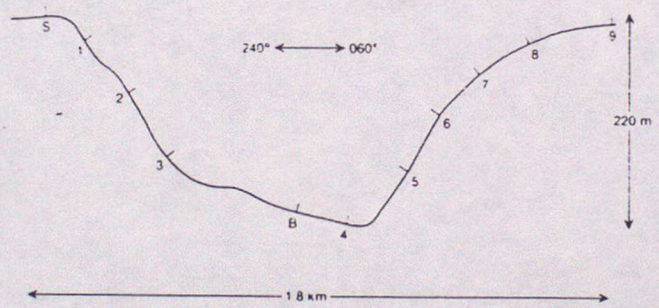

Figure 13: A topographic section in a roughly West-East line following the locations of the anemometer masts. The positions of the masts are indicated; the tethered balloon was flown from point 'B' and 'S' is the summit mast. After Mason 1987.

It is also possible to estimate the importance of buoyancy effects in the daytime convective boundary layer. In this case the magnitude of ΔB depends on the efficiency of the turbulent transfers within the boundary layer. To estimate ΔB it is necessary to utilise a turbulence closure. The key variable in a turbulence closure is the turbulence length scale l_o. With a buoyancy flux H_o a typical diffusivity is $\nu \sim w_b l_o$ where the velocity scale $w_b \sim (H_o l_o)^{1/3}$. The buoyancy difference ΔB over a scale h can then be estimated from

$$\nu \Delta B/h \sim H_o \tag{28}$$

i.e.

$$\Delta B \sim h H_o^{2/3} l_o^{-4/3} \tag{29}$$

With the assumption that the height h involved in this unstable buoyancy contrast is a small fraction of the boundary layer depth and less than L, it follows that

$$F^2 \sim 2U^2 \theta l_o^{4/3}/H_o^{2/3}h^2 \tag{30}$$

Observations of convective boundary layers show that the largest temperature gradients are confined to a shallow layer near the surface and that the minimum potential temperature occurs

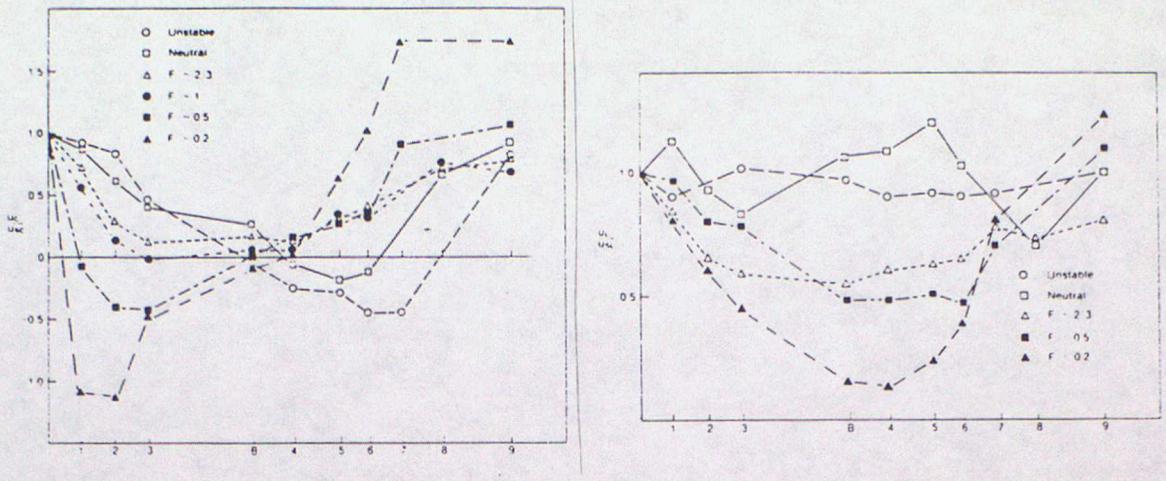

Figure 14: Illustrating the variation of wind velocity at 8m above the surface. (a) shows the across valley component of motion u_C and (b) the along valley component u_L. The horizontal axis corresponds to distance across the valley and the values shown are scaled by the components (U_{sC}, U_{sL}) measured at summit. The results are for a North Easterly flow with an across valley component from the right to the left of the figure. The symbols denoting various values and ranges of Froude number are given on the figure the wind speeds U_s corresponding to the Froude numbers "unstable","neutral",2-3,1,0.5,and 0.2 are 4.4,7.4,5.3,4.3,4.3,and 3.6 ms^{-1} respectively. After Mason 1987.

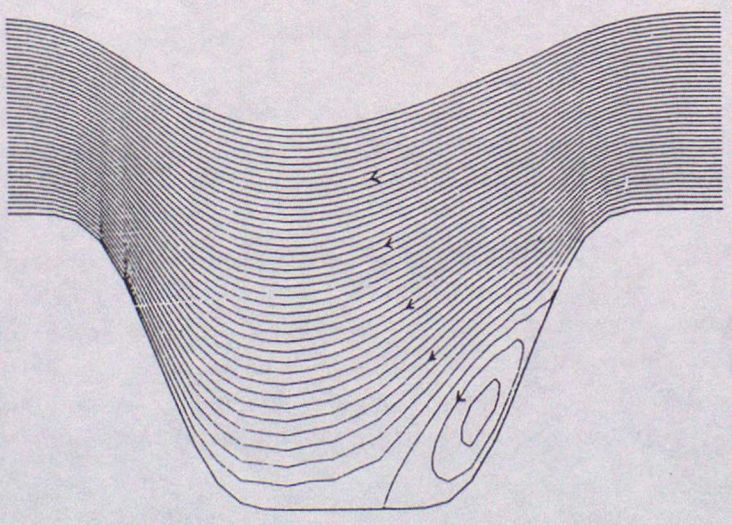

Figure 15: Numerical simulation of streamfunction contours at 15.00 G.M.T. obtained with an "Easterly" wind. The vertical exaggeration is a factor of 2.5. After Mason 1987.

Table 1: Values of Froude number obtained with steady wind speeds and clear skies.

U at 200m	F at 22:00 GMT	F at 03:00 GMT
10	>10	>10
8	5	3
6	2	1
2	0.4	0.2

in the middle part of the boundary layer. The present simple analysis will only be realistic when the pressure perturbations arise from the gradients above the shallow layer close to the surface. With realistic estimates of l_o (and h) equation 30 allows us to anticipate the importance of the buoyancy effects. If we take $\theta = 0.5$, $h = 300$m and $l_o = 300$m so as to correspond roughly with a 1km deep boundary layer

$$F^2 \sim 0.02U^2/H_o^{2/3} \quad \text{numerically} \tag{31}$$

and with $H_o \sim 3.0\ 10^{-3}\text{m}^2\text{s}^{-3}$ and roughly corresponding to a typical heat flux of $100\text{Jm}^{-2}\text{s}^{-1}$

$$F = U \quad \text{numerically} \tag{32}$$

which suggests that unstable buoyancy effects should only be important for wind speeds of order and less than a few metres per second. In practise the local winds within a valley with steep sides will be less than the flow above the valley and a more local criteria may be important.

Although the details of the buoyancy effects vary from case to case it is useful to consider an example. Figure 13 illustrates a topographic section of a valley located within a sequence of such valleys. The peak slope of the terrain is 30° and further details can be found in Mason (1987). Table 1 shows values of a Froude number obtained at night with clear skies. This Froude number is based on the hill height. The values obtained for various times and wind speeds are typical but of course depend on the meteorological and surface conditions. Figure 14 shows observations of the wind field 8m above the surface for a range of Froude numbers. The neutral stability flow shows a small flow separation near the valley floor. In the unstable case the surface heat flux was about $100\text{Js}^{-1}\text{m}^{-2}$ and the wind speed at the summit was 4.4ms^{-1}. This summit wind is subject to a flow speed up and consistent with arguments above there is a moderate change in the flow with the separation increasing under the influence of the up-slope winds. Figure 15 shows a numerical simulation of the streamline pattern for this case. For lighter mean winds the up-slope winds took a value of about 2ms^{-1}. The stable Froude numbers show two distinct effects. With a Froude number, based on the height, of about 2 the Froude number based on the length matches that required for a gravity wave and the flow through the valley does not separate. With Froude numbers less than unity drainage flows occur and with light winds and clear skies reached peak velocities of 4 ms^{-1}. The peak velocities in the up and down slope winds are difficult to predict without a comprehensive description of the turbulent boundary layers which these currents comprise. They do however always increase with the scale of the orography.

7 References

Jenkins,G.J., Mason,P.J., Moores,W.H. and Sykes,R.I., 1981: 'Measurements of the flow structure around Ailsa Craig a steep, three-dimensional, isolated hill'. *Quart.J.R.Met.Soc.*, **107**, pp 833-851.

Mason,P.J., 1986: 'Flow over the summit of an isolated hill'. *Boundary-Layer Meteorology*, **37**, pp 385-405.

Mason,P.J., 1986b: 'On the parametrization of orographic drag'. *Met.O.14 TDN No.177,*

Met.Office, Bracknell.

Mason,P.J., 1987: 'Diurnal variations in flow over a succession of ridges and valleys'. *Quart.J.R.Met.Soc.*, **113**, pp 1117-1140.

Mason,P.J., King,J.C., 1985: 'Measurements and predictions of flow and turbulence over an isolated hill of moderate slope'. *Quart.J.R.Met.Soc.*, **11**, pp 617-640.

Mason,P.J., Morton,B.R., 1987: 'Trailing vortices in the wakes of surface-mounted obstacles'. *J.Fluid Mech.*, **175**, pp 247-293.

Scorer,R.S., 1968: 'Air Pollution Meteorology'. *Pergamon.*

Taylor,P.A., Mason,P.J. and Bradley,E.F., 1987: 'Boundary-Layer Flow over low hills'. *Boundary-Layer Meteorology*, **39**, pp 107-132.

BOUNDARY LAYER INSTRUMENTATION

P HIGNETT

METEOROLOGICAL OFFICE RESEARCH UNIT

CARDINGTON

6.1. FLUX MEASUREMENTS

Frequently in boundary layer meteorology a firm knowledge of the vertical fluxes of heat, momentum, water vapour and gases is required, whether this be through the surface or in the upper part of the boundary layer. Measurement of fluxes directly through the surface is very difficult and often, for practical reasons, use is made of the 'constant flux' or 'surface layer' approximation. Here use is made of the assumption of zero flux divergence between the surface and the measurement level, which may be up to a few tens of metres.

6.1.1. Eddy Correlation Technique

The vertical turbulence flux of a property S is

$$F = \overline{\rho s' w'}$$

where the prime denotes a fluctuation about a suitably defined mean, and w is the vertical velocity component. The density is normally taken as constant and removed from the average. For measurements in the surface layer an indication of the instrumental frequency response required can be judged from the observation that contributions to the flux can be expected at frequencies in the range $0{\cdot}005 \leq f \leq 10$, where $f = nz/u$ (n is the 'natural' frequency, z the height and u the mean

wind speed). So if z = 10m, u = 10m s^{-1} and f = 10, then n = 10Hz. At greater heights, above the surface layer, the main contributions to the flux will tend to be at lower frequencies, and the requirements of the instrument frequency response are correspondingly less severe.

6.1.2. Profile Method

Turbulent fluxes can often be related to the mean gradient of a quantity, particularly close to a boundary. Perhaps the best known flux-gradient relationship is the logarithmic velocity profile introduced in lecture 2. Limitations are placed on the usefulness of this method by the accuracy and stability of the instruments used. For example the difference in wind speed between 2m and 10m will, over the sea, be only about 15% of the total difference between the surface and 10m, and perhaps 30% over an open land site.

6.2. ANEMOMETERS

6.2.1. Cup Anemometers

Cup anemometers are simple, reliable instruments that are extremely widely used and have been so for many years. They do not require any alignment into wind and can be made relatively sturdy. Leaving aside the problems of overspeeding and angular response discussed below they can be made typically accurate to ± 1% of reading, above 5m s^{-1} and to 5cm s^{-1} below.

A simple linear calibration function of the following form is usually sufficient.

$$U = U_s + CR\Omega$$

where U_s is the starting or threshold speed, R is the cup-arm radius and Ω the angular velocity. The starting speed arises from the need to overcome friction in the bearings. This linear relationship masks the complex aerodynamic interactions between individual cups and does not apply when $U \approx U_s$, particularly if the rotation of the cups is intermittent.

In terms of its dynamic response a cup anemometer can be treated as a simple, linear first-order system with a power transfer function of the form,

$$H(k) = \frac{1}{1 + (2\pi l k)^2}$$

where k is the wavenumber, and l is the length or distance constant, which may be defined as the length of the air column which must pass the anemometer to give 63% of the change towards the new equilibrium. An instrument with very lightweight polystyrene cups may have a length constant of about 0·5m, while the small anemometers with plastic cups typically used in boundary layer work have length constants of a few metres. The larger, heavier instruments intended for continuous, unattended operation may well have length constants significantly in excess of 10m. Principally, the length constant is related to the inertia of the cups, and can be reduced substanially only by the use of very lightweight materials; hence the difficulty in constructing short length constant instruments that are also physically robust.

Cup anemometers respond more quickly to an increase in the wind speed than to a decrease of the same magnitude. Consequently an anemometer calibrated in a laminar flow will overestimate the wind speed in a turbulent flow; this characteristic is usually known as

'overspeeding'. As a simple guide the relative overspeeding, $\delta U/U$, can be taken as approximately equal to the square of the turbulence intensity, $\overline{u'^2}/u^2$, a typical value of which may be 0·05.

An ideal cup anemometer would have a cosine angular response, ie. the angular velocity would be independent of the velocity component parallel to the anemometer axis. In practice the actual response, particularly for large inclinations to the wind may be significantly from ideal, and may be asymmetric to positive and negative angles of attack, because of wake effects from the anemometer body.

6.2.2. Wind Vanes

A cup anemometer will frequently be deployed in conjunction with a wind vane to provide directional information. The characteristics of a particular vane will depend largely on the area and mass of the vane and its distance from the centre of rotation; there can be considerable variations in the design of vanes to suit particular applications.

Broadly a vane can be considered to be a second-order system; the transfer function will rise (for an underdamped system) from a value of unity at low frequencies to reach a peak at a characteristic equivalent wavelength, falling again thereafter. Variations on the basic theme are bivanes, which are free to rotate about two axes, and trivanes, which are bivanes with a propeller mounted to give information about all three velocity components.

6.2.3. Propeller Anemometers

In recent years propeller anemometers have become a practical alternative to cup anemometer-vane combinations. An orthogonal set of propellers allows the measurement of three velocity components. A popular commercially available design is the 'Gill' propeller anemometer; this is made from polystyrene, or in a more robust version polypropylene, with usually four blades of helicoidal shape. The calibration can be taken as a linear function,

$$U = U_s + \gamma C R \Omega$$

where U_s is the threshold speed, γ is the pitch factor (= 0·43 for Gill propellers), R is the length of the blades, Ω the rotation speed and C is a constant.

Threshold speeds can be as low as 0·1m s^{-1} with length constants of about one metre for the polystyrene versions and about 3 metres for the polypropylene. Unlike a cup anemometer a propeller will tend to 'underspeed' in a turbulent flow, although the magnitude of the effect can be expected to be less.

For small angles of attack (up to $\approx 10°$) the Gill propeller has an almost ideal cosine response. However, as the angle of attack increases there is a substantial deviation from a cosine response, the actual speed of rotation being now smaller than would be expected. With the propeller mounted perpendicular to the mean wind there is a small range of angles ($\approx 2°$ to $4°$) about the horizontal over which the propeller stalls and stops completely.

6.2.4. Hot Wire/Film Anemometers

For very high frequency response measurements (up to $\approx$ 10 KHz) resort must be made to hot wire/hot film sensors. The principle of operation is very simple; the cooling of a heated wire or film depends on the velocity and density of the flow past the sensor. Hot wire sensors are made typically from wire of $\sim 10\ \mu m$ diameter, and therefore tend to be fragile. Hot film sensors use a platinum or nickel film ($\sim 0{\cdot}1\ \mu m$ thickness) laid onto an insulating substrate and then in turn covered with an insulating layer; these are more robust than hot wires.

There are two normal modes of operation; constant current or constant temperature. Constant current is the easiest to arrange but results in a nonlinear calibration; constant temperature is more complicated to arrange but results in an extended high frequency response. There is now a vast literature on the construction, configuration and use of hot wire and hot film sensors, the range of which is well beyond the scope of this lecture.

6.2.5. Sonic Anemometers

Sonic anemometers measure wind velocity components from the arrival times (or phases) of acoustic signals transmitted along a fixed path. This results in a good high frequency response limited by the implied averaging along the acoustic path, and the capabilities of the subsequent signal processing. The calibration is determined essentially by the characteristics of the transducers and the geometry of the instrument, and is very stable. Sonic anemometers are now established as prime research instruments in atmospheric boundary layer work. A typical commercially available instrument has an accuracy of

$\pm 1\%$ over its operating range of 0 to 30m s^{-1}, with a resolution of 0·5cm s^{-1}.

6.3. TEMPERATURE AND HUMIDITY MEASUREMENTS

This is a very extensive subject that can only be touched upon briefly here. Broadly, instruments can be separated into two categories, fast response and slow response.

6.3.1. Slow Response Measurements

The determination of surface fluxes via the profile method may typically require temperature differences between the various levels to be measured to 0·01K. If the air-surface (land or sea) difference can be measured the requirement can be relaxed to perhaps 0·1K. The most common sensors used are thermocouples, thermistors and resistance thermometers (particularly platinum). For the highest absolute accuracy careful attention must be paid to adequate ventilation and shielding from radiation (short and long wave). Humidity measurements are still frequently made from a combination of wet and dry bulb temperatures, although increasing use is being made of humidity sensitive capacitative sensors.

6.3.2. Fast Response Measuremnts

For the measurement of variances and eddy fluxes the same basic sensors are available, although absolute accuracy is much less important and any radiation errors are frequently ignored. For platinum resistance wires of 1μm in diameter extreme time constants of

10^{-5} seconds can be achieved. For humidity measurements from wet and dry bulb temperatures time constants of about 0·1 seconds can be achieved, although particular attention must be given to ensuring the close matching of the responses of the two sensors. If this is not done spurious results, under conditions of varying humidity, can easily be generated.

A quite different technique of humidity measurement is based on the absorption of radiation by water vapour. Instruments employing absorption at both Lyman-α and infrared wavelengths are available; although both offer fast response measurements they tend to suffer from long-term calibration drifts and require reference to a slower-response detector. The calibration will also be degraded at high relative humidities when hygroscopic growth of aerosol particles increases the measured extinction by introducing light scattering.

ATMOSPHERIC DIFFUSION

by F.B.Smith Met O 14

Dispersion is caused by a very wide range of turbulent motions whose scales vary from millimetres to thousands of kilometres. Usually the smaller turbulent motions are 3-dimensional whereas larger turbulent motions are essentially 2-dimensional. Various techniques have been developed over the years to describe dispersion. At this stage we will assume the material is passive, i.e. acts like "neutral" air particles. These techniques will be described briefly:

1. K Theory. An analogy is drawn with the conduction of heat in a metal bar in which the flux of heat is assumed proportional to the local gradient of temperature. This theory, when applied to diffusion in the atmosphere, effectively assumes the turbulence consists only of very small "eddies" with very large turbulent velocities associated with them. The coefficient of proportionality K is called the eddy diffusivity and can be made a function of position (and, if required, of time). When K is a constant, and the wind speed is also constant, a Gaussian concentration distribution results acrosswind at positions downwind of the source. The width of the resulting plume grows like $\text{time}^{\frac{1}{2}}$ (or $x^{\frac{1}{2}}$). This behaviour is known to be unrealistic at short range.

Other Difficulties: Eddies are not all very small. Transfer may thus not depend on the local gradient alone. Application in unstable convective conditions is consequently very suspect. Counter-gradient transfer of material is not unknown.

Advantages: The method is relatively simple and can produce both analytic or numerical solutions which are enlightening.

2. **Higher-Order Closure Schemes.** Equations of conservation can be taken to higher order in concentration, so that, for example, the time variation of the flux can be explicitly described in terms of other more complex terms rather than empirically expressed in terms of the concentration-gradient as in the K-theory. However, no closed set of equations can ever be obtained which can be solved.

Always at least one (and usually several) higher order terms are included which cannot be inferred except by "dimensional" empiricism. The expectation is that by making the empiricism at higher order smaller errors will result in the solution. To some extent this has proved to be the case, but at the expense of a much more complex numerical process.

This approach is not universally popular.

3. **Similarity Theories.** Rather like the Monin-Obukhov approach to describe the wind speed and temperature profiles in the lower boundary layer, dimensional arguments can be used to describe the growth of a plume from a source at ground level.

For example:

$$\frac{d\bar{z}}{dt} = b u_* \phi\left(\frac{\bar{z}}{L}\right)$$

where $\bar{z}$ is the mean height of the "particles" in the plume, u_* is the friction height velocity. This equation can be combined with the wind speed equation

$$\frac{d\bar{x}}{dt} = \bar{u}(c\bar{z})$$

when $\bar{x}$ is the mean along-wind displacement of the particles released at time $t = o$, $\bar{u}$ is the mean wind at a height $c\bar{z}$. (c is another constant.) In neutral stability conditions it has been shown that $b = k \simeq 0.4$ (k = von Karman's constant) and $c \simeq 0.6$. These can be solved (in neutral conditions) to give

$$\bar{x} = \frac{\bar{z}}{k^2}\left[\ln 0.6\frac{\bar{z}}{z_o} - 1 + \frac{z_o}{\bar{z}}(1 - \ln 0.6)\right]$$

Note however that this does not give $\bar{z} = \bar{z}(x)$ since the particles released at time t = o have a range of values of x and are not all at $\bar{x}$.

The method becomes much more complicated when two or more length-scales are involved. (e.g. in non-neutral conditions well above the surface layer.)

However, some progress has been made even in convective conditions (Yaglom 1972, Deardorff and Willis 1974). The latter authors give the following similarity form

$$\frac{\sigma_z(t)}{z_i} = f\left(\frac{w_* t}{z_i}\right)$$

where z_i is the convective boundary layer depth

w_* is the convective velocity

$\sigma_z(t)$ is the r.m.s. vertical displacement of the particles at time t.

(the source is at the ground.)

Figure 1 shows the result of this scaling for concentrations downwind of elevated sources within a convective boundary layer.

4. Statistical Theories. This approach, based on G.I.Taylor's (1925) classical work, has proved very productive.

In homogeneous turbulence, for a single particle

$$\frac{dz}{dt} = w(t)$$

Integrating $z(t) = \int_o^t w(s)\,ds$

Multiplying them together gives

$$\frac{d}{dt}\left(z^2(t)\right) = 2\int_o^t w(t)\,w(s)\,ds$$

Averaging over the whole ensemble of "particles" coming from the source gives

$$\frac{d}{dt}\sigma_z^2(t) = 2\,\overline{w^2}\int_o^t R(t-s)\,ds$$

or

or $$\sigma_z^2(t) = 2\sigma_w^2 \int_0^t \int_0^\xi R(\xi - s)\, ds\, d\xi$$

where R is the correlation between turbulent velocities, taken in a Lagrangian sense, of the same particle at times t and s.

At small times t, $R \simeq 1$

so that

$$\sigma_z^2(t) = 2\sigma_w^2 \frac{t^2}{2} = \sigma_w^2 t^2$$

i.e. $$\underline{\sigma_z(t) = \sigma_w t}$$

This is the result one would get if all particles followed straight paths during the short time interval t.

At large times t, $R \to 0$ but $\int R\, dt \to$ constant τ, τ has the dimensions of time and is called the Lagrangian time-scale of the turbulence.

Then $$\sigma_z^2(t) = 2\sigma_w^2 \tau t$$

ie. $$\sigma_z(t) \propto \sqrt{t}$$

in accord with the K-theory result. These results specifically apply to homogeneous turbulence but the technique has been extended to cover

(i) diffusion in the inhomogeneous boundary layer (see Pasquill and Smith (1984))

(ii) the growth of puffs (or instantaneous releases)

(iii) "conditioned" diffusion of particles with some other aspect pre-defined, e.g. those that pass through a second downwind point, or those that have a prescribed initial velocity.

5. Stochastic Models. The simplest form of this class is the Markovian random walk in which the diffusion process is represented by the movement of an ensemble of independent particles released from the source in which each particle has a motion governed by a continuous but gradual exchange of "momentum" with the environment of the particle. In the

simplest case of one-dimensional homogeneous stationary turbulence, this means its velocity at any time is governed by:

$$w(t+\delta t) = \left(1 - \frac{\delta t}{\tau}\right) w(t) + 2\sigma_w \left(\frac{\delta t}{\tau}\right)^{1/2} \varepsilon$$

where τ is the Lagrangian time scale

Δt is a small time interval

σ_w is the r.m.s. value of w

ε is a random quantity derived from a Gaussian probability-distribution with zero mean and s.d = 1.

The first term on the r.h.s. corresponds to the gradual "decay" in the particles momentum, the second term represents the "gain" in momentum from the surrounding environment.

The concentration distribution is built up by summing the contribution from very many particles whose motion is prescribed by the above equation. A computer is needed for this purpose of course, since the tracks of several thousand particles are normally required.

In inhomogeneous turbulence where σ_w is varying with z, the above equation has to be modified to

$$w(t+\delta t) = \left(1 - \frac{\delta t}{\tau}\right) w(t) + \frac{\partial}{\partial z}\sigma_w^2 . \delta t + 2\sigma_w \left(\frac{\delta t}{\tau}\right)^{1/2} \varepsilon$$

The justification for this has been given by Thomson (1984).

Concentration Fluctuations: Thomson (1986) has also extended the technique to study the problem of concentration fluctuations within a plume by considering the probability that two adjacent particles within a plume could have originated from the same source. The techniques uses the random walk equation, applied in a linked way, to the two particles to determine this probability.

Large-Scale Diffusion: The random walk approach is becoming increasingly popular for simulating the dispersion of material on a very large scale. To give an example, which will be returned to

in more detail in Mr.Maryon's lecture, the technique has been applied to the dispersion of radioactive debris across Europe originating from the damaged nuclear reactor at Chernobyl on April 26th 1986. Figure 2 shows the results for May 2nd.

6. Empirical Techniques. In a "field" situation it is often difficult to use the above methods because they involve parameters that can only be estimated using instrumentation.

To meet this need, Pasquill (1959) developed a simple approach which has proved very popular both in its original and developed states. He recognised that vertical dispersion takes place through the action of turbulence which has two major sources of energy: dynamic (through the action of wind over a rough surface) and thermal (through the difference in temperature between the ground and the air).

Pasquill therefore attempted to categorise the rate of vertical plume-growth in terms of the 10 metre wind-speed and the amount of incoming solar radiation. Later developments included other appropriate parameters like surface roughness and the moisture-state of the ground.

These methods are described in Pasquill (1974).

Advantages: Very simple requiring little instrumentation.
Easy to see the influence of and sensitivity to the input parameters.
Easy to use for the "layman".

Disadvantages: Should not be used for - (i) elevated sources
(ii) very convective conditions
(iii) in complex terrain especially in stable conditions.

Figure 3 shows one popular form of the method.

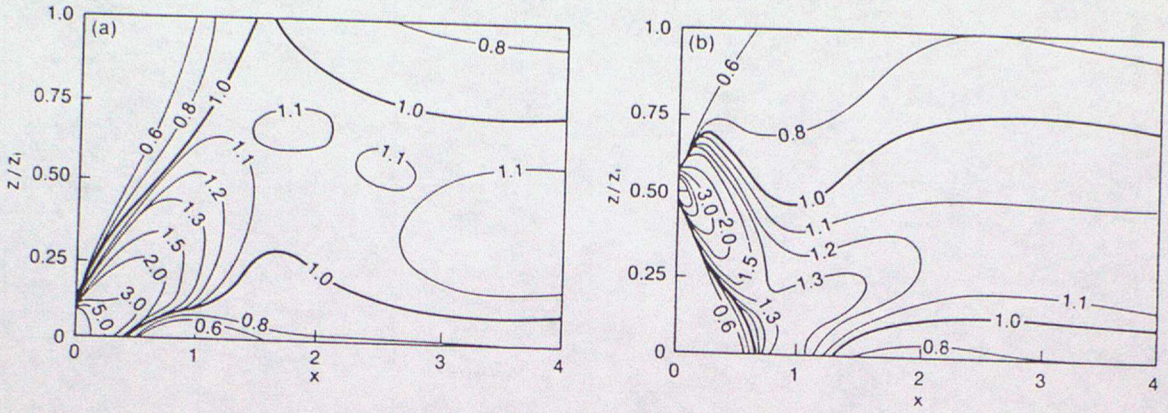

Figure 1 Model contours of concentration downwind of a source in a convective boundary layer for two source heights (a) $z/z_i = 0.067$ and (b) $z/z_i = 0.49$ (taken from de Baas *et al.* 1986). z is the height above ground and x is the downwind distance, non-dimensionalized by $z_i U/w_*$ where z_i is the inversion height, U is the mean boundary-layer wind and w_* is the convective velocity scale.

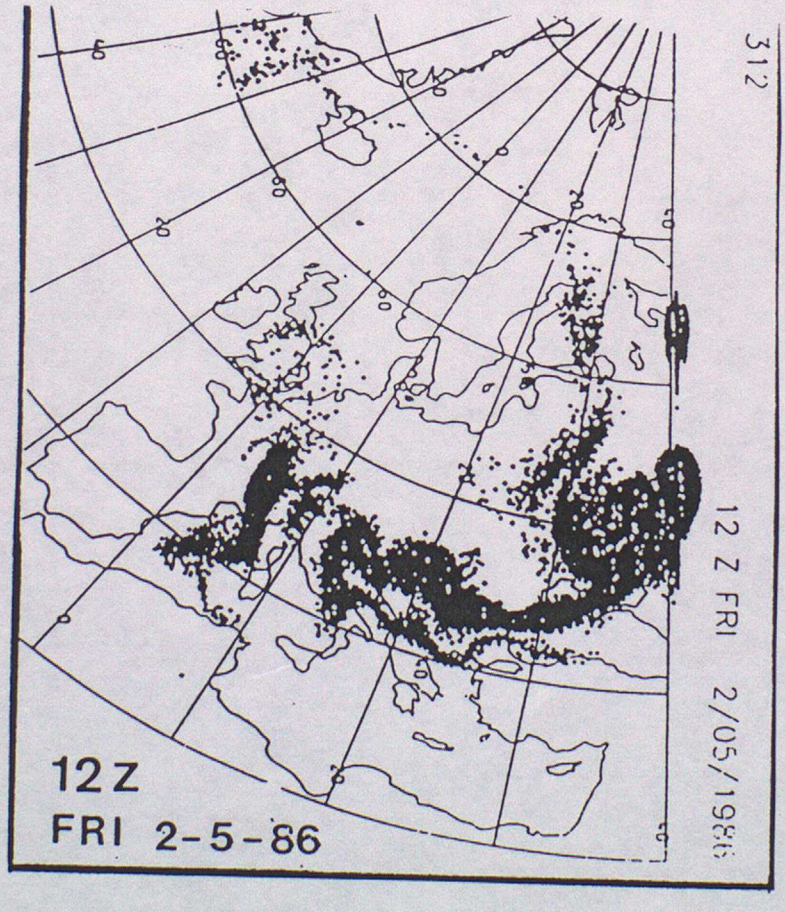

Figure 2. Monte-Carlo simulation of the dispersion of the radioactive debris from Chernobyl on Friday May 2nd, 1986. The accident occurred on the previous Saturday, April 26th and emission of activity had continued into the atmosphere up to the time of this picture.

THE REVISED SCHEME FOR P (PASQUILL STABILITY VALUES)

Roughness length (z_0) = 0·1 m

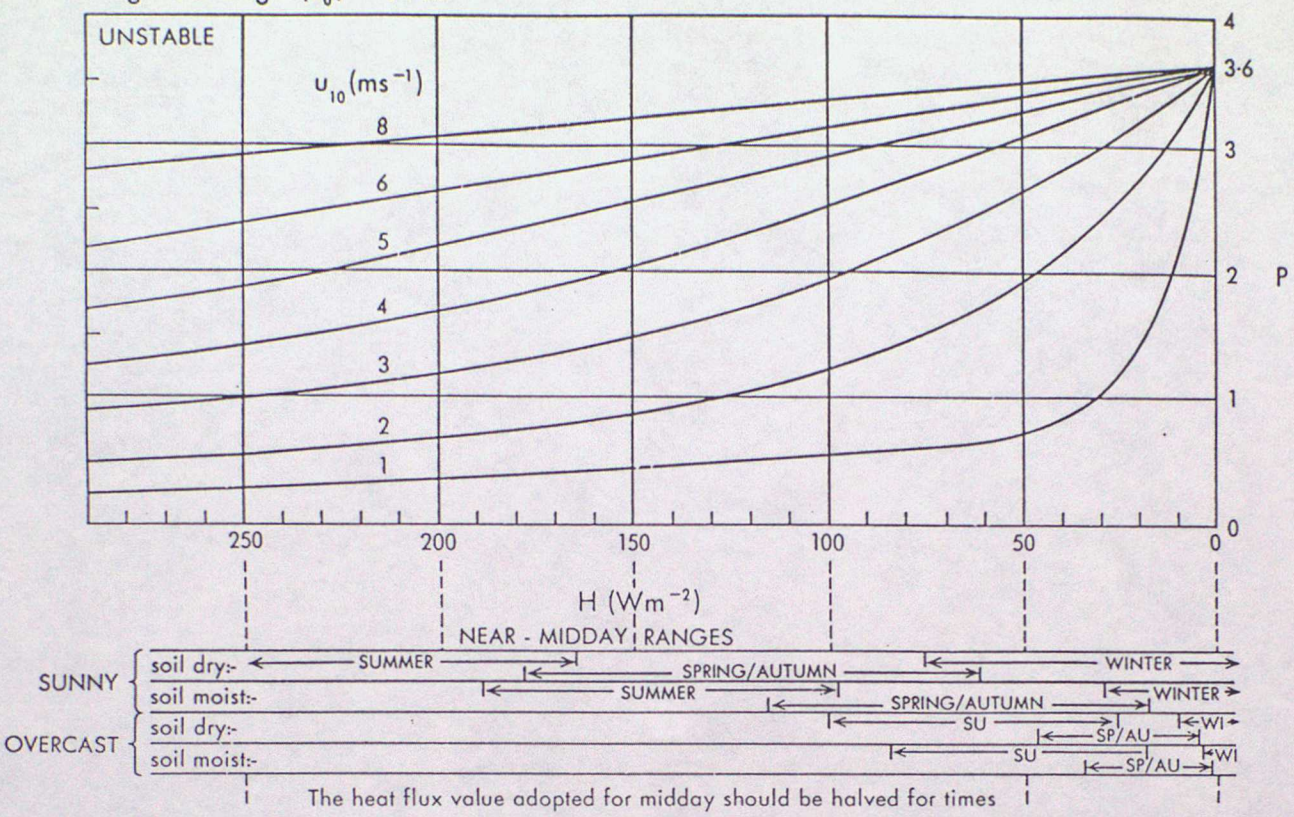

The heat flux value adopted for midday should be halved for times halfway between dawn and noon or noon and sunset

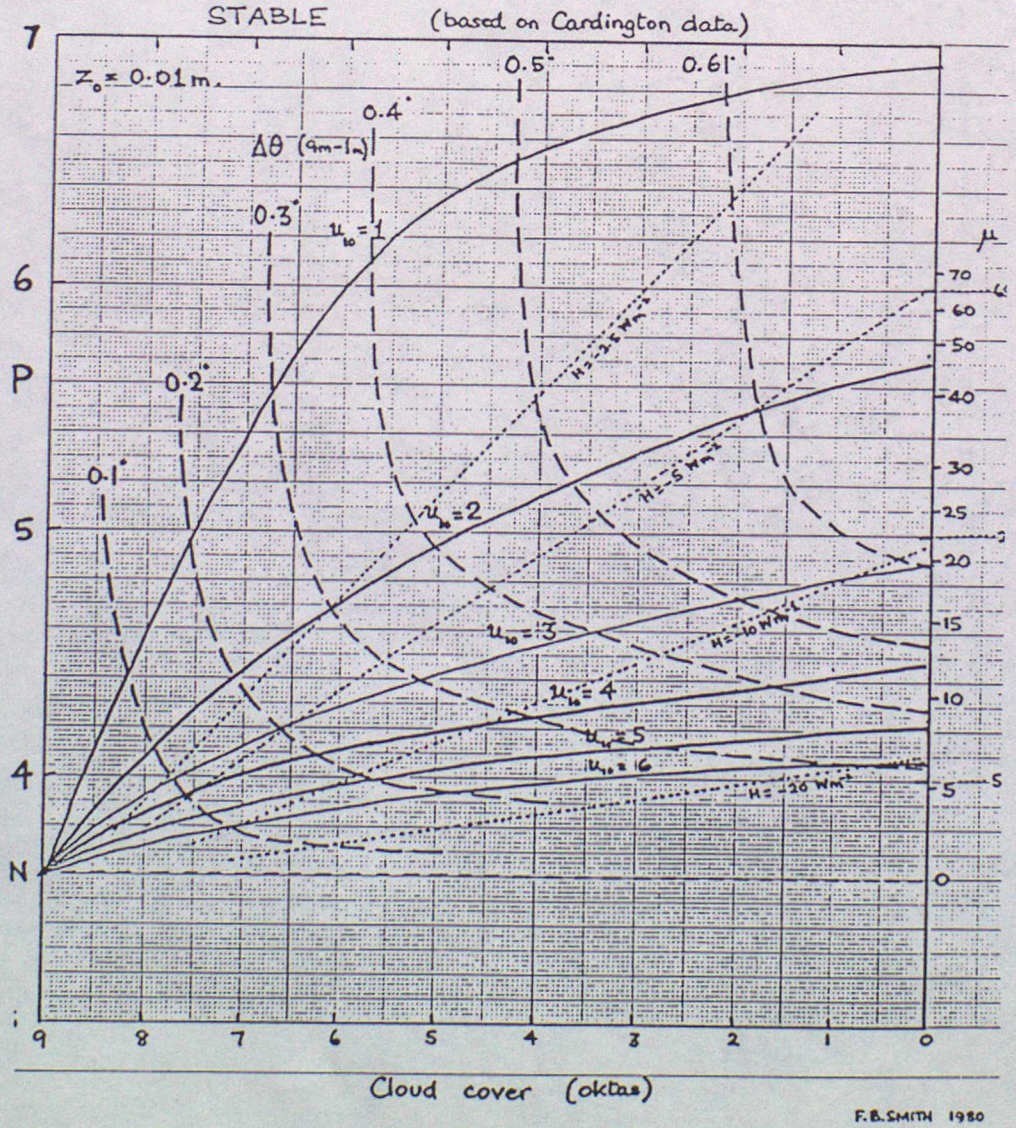

Figure 3

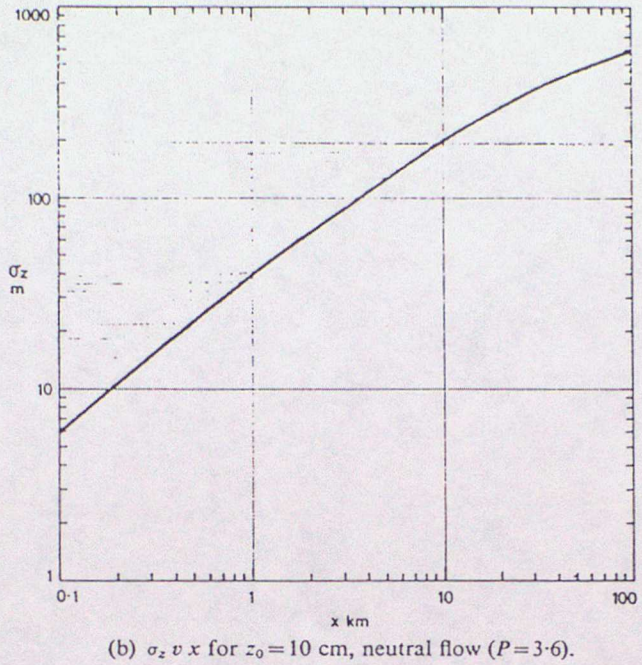

(b) σ_z *v* x for $z_0 = 10$ cm, neutral flow ($P = 3{\cdot}6$).

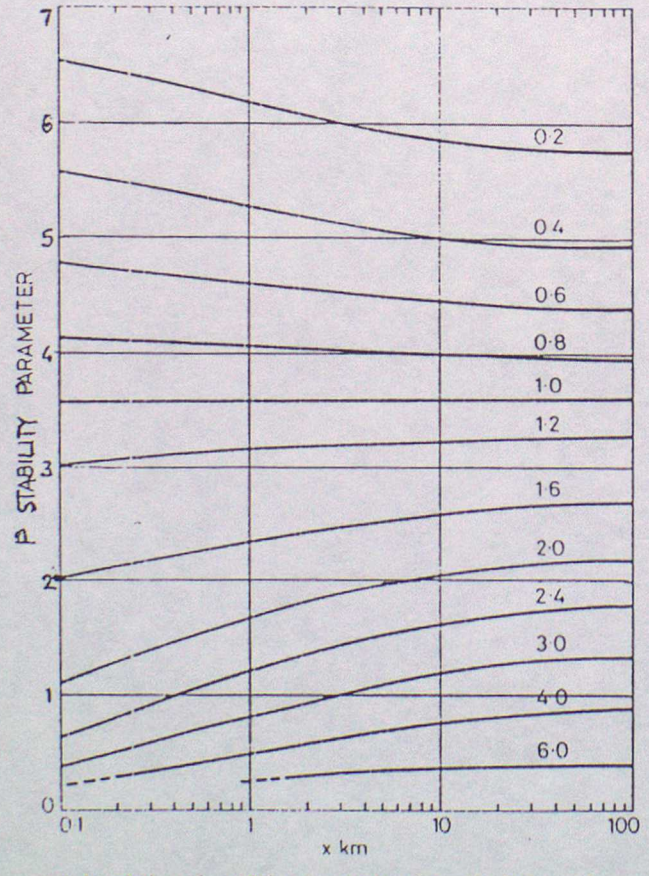

(c) Isopleths of $\sigma_z(P)/\sigma_z$ (neutral), virtually independent of roughness.

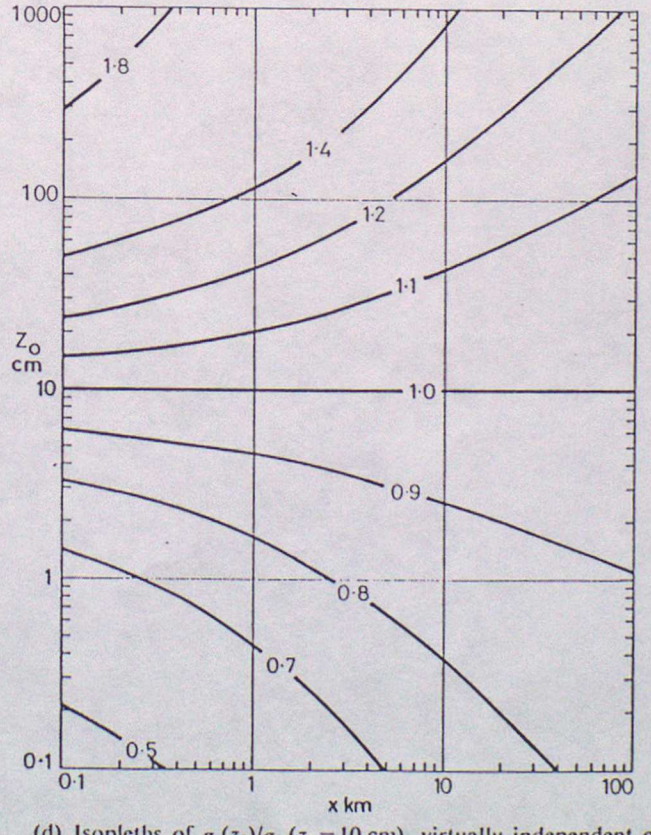

(d) Isopleths of $\sigma_z(z_0)/\sigma_z$ ($z_0 = 10$ cm), virtually independent of heat flux.

ATMOSPHERIC DIFFUSION: COMPLICATING ISSUES

by F.B.Smith, Met O 14

Dispersion near hills

As already described in earlier lectures, the flow of the air over hills and other complex terrain can be very complicated and it is difficult to come forward with simple rules. Indeed, this is still an area of continuing research and controversy.

Consequently we will limit ourselves to a number of qualitative observations:

(i) The first question that has to be posed is how does the terrain affect the flow field, taking into account the stability of the air ? Will there be drainage flows, recirculating eddies, flow separation, different levels of surface heating due to slopes of different orientation relative to the sun, sea or land breezes, etc. ? This question often dominates over all others in regard to plume behaviour.

(ii) In gently-sloping terrain, where flow separation is absent, then plume behaviour and ground-level concentrations in neutral and unstable conditions will be little affected by the terrain.

(iii) When a source is immediately upwind of a hill, the hill will tend to magnify the natural acrosswind fluctuations in the airstream and this will result in an enhancement of the width of the plume over the hill, thereby lowering the time-averaged ground-level concentrations.

In contrast, a plume originating from a source that is more "off-centre" may actually be narrowed as it passes round the side of the hill thereby increasing its time-averaged concentrations.

These changes in width modify ground-level concentrations in inverse proportion compared to those concentrations that would be experienced without the hill.

(iv) In stable conditions the plume may impinge on the upwind side of the hill if the hill-Froude number is less than 1, since the flow has insufficient energy to rise against gravity over the hill. Concentrations then are approximately equal to the peak concentration within the elevated plume in the absence of the hill.

(v) In unstable or neutral conditions when separation occurs (implying slopes $> 30^0$) the peak ground-level concentration may occur on the lee-slope of the hill. Pollution from sources within a recirculating eddy will tend to give relatively high concentrations within the eddy. Note, however, that these eddies tend to be very transient in their structure, varying in size and position quite rapidly with time.

Effect of buildings on dispersion

Many sources are either on buildings or very close to them. The pollution-concentration is then often considerably affected by the presence of the building for quite some distance downwind. This is especially true if the plume gets incorporated into the wake behind the building.

The following simple formulae give a feel for the effect on plume dimensions. The easiest way to use them is in conjunction with the Pasquill/Smith scheme outlined in section 6 of my first lecture.

(a) Barker's Model

This is a so-called "virtual source" model. By this is meant, the effect of the building on the plume is essentially to make it appear as if the source were in reality some distance upwind so that at the lee face of the building the plume already has width and depth.

If h = the height of the building

w = the acrosswind width of the building

then the plume dimensions downwind of the building are inferred from assuming at the lee face of the building

$$\sigma_y' = \frac{W}{3} \quad , \quad \sigma_z' = \frac{h}{3}$$

and the source height is $h_s' = \frac{h}{3}$

(b) Ferrara and Cagnetti Model

This is very similar in concept, but is rather simpler to use:

$$\sigma_y'(x) = \sigma_y(x) + \frac{W}{2{\cdot}5} \quad , \qquad \sigma_z'(x) = \sigma_z(x) + \frac{h}{2{\cdot}5}$$

(c) Huber and Snyder Model

For $3h < x < 10h$

$$\sigma_y'(x) = 0{\cdot}35W + (x-3h)/15$$

$$\sigma_z'(x) = 0{\cdot}7h + (x-3h)/15$$

and for $x \geq 10h$ apply a virtual source model matching of

σ_y' and σ_z' at $x = 10h$

Use the actual stack height in calculating concentrations.

In all these models, Gaussian concentration profiles are assumed, although these are modified by the addition of an extra contribution from a virtual source of identical magnitude at a depth h_s below the ground (to allow for the reflection of the plume by the ground). h_s = the real source height.

If the material coming from the source is either hotter or colder than the ambient airstream then proper allowance has to be made. Discussion of this can be found in NRPB Reports on Atmospheric Dispersion Modelling, but is too complex to discuss here.

Hot Plumes

Hot plumes result in significant ascent and hence lower ground-level concentrations. A doubling of the effective source height decreases g.l. concentrations by about 4. Moreover, since chimney height positively affects the rise of the plume, an increase in chimney height by a factor F results in more than an F^2 decrease in g.l. concentration. However, should the plume interact with an elevated inversion, which it has insufficient buoyancy to penetrate, the g.l. concentrations will decrease by a smaller factor.

Equating the rate of change of upward momentum per unit length of the plume (along the wind) to the buoyancy force

$$\frac{d}{dt}(\rho w \pi r^2) = \pi r^2 g \rho \frac{\Delta T}{T}$$

where ρ = density

w = upward velocity

r = plume radius

T = temperature

$t = x/u_0$ = time

Assuming no loss of heat from the plume

$$\frac{d}{dz}(\pi r^2 \rho c_p \Delta T) = 0$$

and that the plume width grows linearly with height, then

$$z(x) \propto Q_H^{1/3} x^{2/3} / \bar{u}$$

(the coefficient of proportionality is about 15).

Writing the stack parameter $F = g Q_H / (\pi \rho c_p T_c)$

and the stability parameter $S = \frac{g}{T} \frac{d\theta}{dz}$

Then the plume rise ΔH is given by:

incomplete rise in neutral windy conditions $\Delta H \propto F^{1/3} x^{2/3} / \bar{u}$

final rise in stable windy conditions $\Delta H \propto F^{1/3} / (\bar{u} S)^{1/3}$

final rise in stable calm conditions $\Delta H \propto F^{1/4} / S^{3/8}$

Very many formulae have been suggested for final plume rise in neutral conditions. A good source for a discussion of these is Chapter 8 by G.A.Briggs in "Atmospheric Science and Power Production", edited by D.Randerson, to be found in the Met.Office Library. In practice, what is most often required is the maximum downwind g.l. concentration and where it occurs.

Moore (1974) has supplied formulae for these which are largely based on measurements made around power stations in the U.K.

$$C_{max} = Q\left(\frac{A}{H^3} + \frac{C}{H^2 u^2} k^{1/3}\right) \quad \left\{ \begin{array}{l} \text{in neutral and stable, and} \\ \text{all stability conditions} \end{array} \right.$$

$$= Q\left(\frac{A^2}{H^6} + \frac{C^2}{H^4 u^4} k^{2/3}\right)^{1/2} \quad \text{in unstable conditions}$$

where $H = h_s + (275 + 2h_s) Q_H^{1/4} / \bar{u} = h_s + \Delta h$

h_s = chimney height

Q_H = heat output in MW

Q = pollutant output

$\bar{u}$ = mean wind speed at chimney height

k = min (1, 0.002H)

A and C are given as follows:

	A	C
All stabilities	1.63×10^6	2.55×10^5
Unstable	1.57×10^6	5.43×10^5
Slightly stable	1.76×10^6	2.06×10^5
Stable	1.76×10^6	1.76×10^5

This maximum occurs at about $x = x_{max}$ where

$$x_{max} = f_1 + k_3(H - 250) + k_4\left\{\left(\frac{275 + 2h}{2.4}\right)^{4/3} - \frac{f_1 (u\Delta h)^2}{H^2 (1+u)^2}\right\} \quad \text{(in metres)}$$

where $f_1 = 5.81 \times 10^5 \frac{k_2 (1+u) Q}{u^{3/2} H C_{max}}$

$k_2 = \begin{cases} 0.67 & \text{stable} \\ 1 & \text{otherwise} \end{cases}$ $\qquad$ $k_3 = \begin{cases} 5 & \text{unstable, } H > 250\text{m} \\ 0 & \text{otherwise} \end{cases}$

$k_4 = \begin{cases} 1 & \text{if } \{\} < 0 \\ 0 & \text{if } \{\} > 0 \end{cases}$

LONG RANGE TRANSPORT AND DISPERSION.

R.H.MARYON.

1.The nature of dispersion in the Earth's atmosphere.

The transport and diffusion of a passive scalar released into the atmosphere reflect the whole range of scales of motion. These can be summarised using a variance power spectrum, for example that of Gage and Nastrom (1986), Fig.1, which was derived from GASP aircraft observations of winds and temperatures. These curves may be divided into two zones: for wavelengths above about 1000 km all the spectra have a slope proportional to the wave-number (k) raised to the power -3, while below about 500 km the slope is proportional to $k^{-5/3}$. The long wavelengths are on the scale of synoptic motion systems, and the k^{-3} spectrum reflects the quasi-2-dimensional transfer of eddy enstrophy (root-mean-square vorticity) to higher wave numbers by the relative motions of the velocity field - for vorticity, the constraints on geostrophic flow are dynamically similar to those of purely 2-dimensional systems (Charney, 1971). Absolute vorticity is conserved (strictly, in frictionless, adiabatic, barotropic flows) so that the vorticity field becomes ever more convoluted as variations are driven towards smaller scales of motion. Fig.2, from a 'dishpan' simulation, illustrates this phenomenon. The enstrophy is dissipated at the high wave-number end of the k^{-3} region of the spectrum.

From dimensional analysis, the velocity v and rate of transfer of enstrophy, η, are related by

$$v \propto \eta^{1/3} l,$$

where l is an eddy length scale. Hence the kinetic energy may be expressed

$$\text{K.E.} \propto \eta^{2/3} l^2.$$

Writing $kl = 1$, for wavenumber,

$$\text{K.E.} \propto \eta^{2/3} k^{-2}$$

so that energy per unit wave-number, defining spectral density, is proportional to k^{-3}. In this region of the spectrum the fluctuations of vorticity, ζ, are independent of the eddy length scales and it is easily shown (Tennekes, 1978)

$$\zeta(l) \simeq \eta^{1/3}$$

and the characteristic time scale of the motion τ_L is

$$\eta^{-1/3} \simeq 2\pi/f$$

(of the order of a day) where f is the Coriolis parameter.

In 3-dimensional (and strictly, isotropic) turbulence chaotic motion is produced by the stretching of much smaller scale eddy vortices, in the first instance by the mean wind shear in the planetary boundary layer, but instabilities develop and Richardson's well-known cascade of energy to smaller and smaller motions occurs until ultimately the energy is dissipated (converted to heat) at and below the so-called micro-scales. The energy cascade region of the spectrum is called the inertial subrange. A similar argument to the above, but using energy rather than enstrophy, shows that the K.E. per unit wave number is proportional to $k^{-5/3}$: proportionality with $\varepsilon^{2/3} k^{-5/3}$ (where ε is the rate of dissipation of turbulent kinetic energy) was proposed by Kolmogorov as long ago as 1941.

3-dimensional turbulence in the boundary layer, however, is largely confined to scales below about 1 km - we are left with the problem of the large range of meso-scales between, say, 2 and several hundred km. Gage (1979) put forward the suggestion that the -5/3 law extended to lower wavenumbers through a 2-dimensional inertial range in which energy is 'reverse cascaded' from high to low wave numbers. Thus motions initiated by thunderstorms, orography, breaking waves and other mesoscale features could cascade energy in both directions, 3-D to high wavenumbers, 2-D to low. Lilly (1983) analyses the reverse cascade in terms of the decay of 3-dimensional turbulence into stratified 2-dimensional turbulence and gravity wave modes. Whether, between the enstrophy and energy cascades an energy/enstrophy sink exists, or the meso-scale spectrum is generally as free from gaps as Fig.1 suggests, are matters as yet unresolved.

The characteristic time-scale of the $k^{-5/3}$ cascade is $\tau_M = \overline{v^2}/\varepsilon \simeq 1/f$, - i.e. about 2 - 3 hours (Barr and Gifford, 1987). This scale is often estimated from the lag correlation function derived from time series of velocity measurements:

$$\tau_m = \int_0^\infty R(t+s)ds$$

where s is a time interval.

The foregoing discussion is necessary to illustrate the mechanics of atmospheric dispersion. Pollutants are DIFFUSED in the 3-D energy cascade range, although it has been suggested that diffusion can occur throughout a good part of the $k^{-5/3}$ region - perhaps due to the presence of vertical components. The inertial subrange has been much studied, and we talk of material 'spreading' or 'mixing'. In the enstrophy cascade region, as we have noted, the dynamics require the transfer of eddy enstrophy to higher wavenumbers by quasi-2-dimensional vortex motions generated on a large scale. The effect upon a patch of material is to DISTORT or DEFORM it, kinematically, (or as some say, stir it!). This large scale deformation,

which is area conserving, does not of itself cause diffusion, as there is no 3-D eddy vortex stretching necessary for the energy cascade. However, as will be seen from Fig.3, chaotic behaviour does not require high Reynold's number turbulence effects - simply a modulation in time of the stream function. Indeed, for 3-dimensional flows chaotic orbits are possible even in steady conditions. These effects are termed 'chaotic advection'. Chaiken et al (1986,1987) following Berry et al (1979) diagnose the typical morphologies of 2-dimensional deformation as WHORLS and TENDRILS, the former tight, curling structures which develops when a line element wraps around the neighbourhood of a stable circulation, the latter exponentially growing oscillations where a line element evolves in a more variable region of the flow. Their dye-streak experiments with concentric, rotating cylinders (Fig.3) feature these effects. Analogous features can be demonstrated as occurring in the atmosphere - e.g. Fig 4 which reproduces the simulation of a single level (2-dimensional) plume from a source in Cumbria, 'released' in Feb 1988. A whorl is associated with a complex low over Scandinavia in Fig 4(a), and tendrils appear to be in evidence in Figs. 4(b), (c) and (d). These plots also show diffusive effects, as the component trajectories were randomly perturbed to take into account sub-grid scale motions.

In summary, over long time scales a plume is distorted by the evolving synoptic pattern and, as a result of the stretching and thinning of the polluted air, the area of contact with clear air is increased, allowing the energy cascade diffusion processes to continue to operate on individual elements of the cloud. Distortion will generally take over from turbulent diffusion as the main mechanism for dispersing material in the atmosphere when a plume is about 2 to 3 days old.

2. Plume growth on regional scales.

The growth of plumes over scales of hundreds of km poses considerable difficulties for the experimental scientist, but studies have been made using releases of tracer or, in favourable conditions, plumes from industrial sources, such as the Mt. Isa smelter in Australia (Carras and Williams, 1981). Adventitious sources, such as radioactive clouds from nuclear weapon tests, have also been used. Such experimental results as are available have been studied in great detail in the light of theoretical predictions. It is necessary to contrast the spreading of a puff about its centroid (or an instantaneous plume about its centreline), RELATIVE DIFFUSION, with that of the time-averaged plume (which reflects the meandering of the plume). Batchelor (1952) investigated puff-spread by considering the separation of pairs of particles. He concluded that where the time elapsed was sufficiently large for the distance between the particles to have 'forgotten' the initial value, but not large in relation to the scale of turbulence, then the variance of the separation

$$\sigma^2(t) \propto \varepsilon t^3. \qquad (1)$$

The time-averaged plume does not expand at the same rate as a puff (whose expansion increases with puff size as progressively larger scale motions become engaged). Taylor's classical (1921) statistical theory, which assumes that the absolute velocities of individual particles are independent (clearly inappropriate for a puff, but applicable to a time-averaged plume) gives the well-known asymptotic result for large t:

$$\sigma^2(t) = 2\overline{v^2}\tau_M t = 2Kt, \qquad (2)$$

the 'parabolic' plume. In (2), $\overline{v^2}$ is averaged over the time of travel and K is an eddy diffusivity. Gifford (1982,1984) has obtained both these results as limiting cases of his 'random force' theory for relative diffusion. He solves the standard Langevin equation

$$\frac{dv}{dt} = -\frac{1 - R(\tau)}{\tau} v(t) + n(t) \qquad (3)$$

(taken from the theory of Brownian motion, and extensively utilised in dispersion modelling) which expresses an instantaneous change in velocity as the sum of a correlated component $R(\tau)v(t)$ and a random impulse $n(t)$, to give

$$\sigma_2(t) - \sigma^2(0) = 2\overline{v^2}\tau_M^2[T - (1-e^{-T}) - \tfrac{1}{2}(1-e^{-T})^2] \qquad (4)$$

where $T = t/\tau_M$. There are certain conceptual difficulties attached to Gifford's specification but for large t (4) reduces to (2), implying that at large times relative and absolute diffusion approach a similar value: the instantaneous puff and time averaged plume both, presumably, have engaged the bulk of the scales of diffusive motion. For t small but not too near the source, (4) reduces to

$$\sigma^2(t) = 2/3.\overline{v^2}/\tau_M.t^3 \qquad (5)$$

which is similar to (1). An identical result to (5) was, incidentally, obtained by Smith (1968) using his more stringent theory of conditioned particle motion which considers the release of puffs with the same initial velocity v(0) and an exponential shape for the autocorrelation, $R(\tau)$. Gifford deduces that $t^{3/2}$ plume growth (5) begins at about $t = 0.1\tau_M$ and that a transition to $t^{1/2}$ growth (2) occurs for t around 5 - 10 times τ_M.

Fig.5 shows a range of estimates of plume spread, σ, (from Hage and Church, 1967), with an empirical fit (solid line); in fact equation (4) is very close to the fitted line. However, Gifford's analysis of the Mt. Isa data (Fig.6) showing a region of accelerating ($t^{3/2}$) diffusion from 2 to 10 or more hours may not convince everybody.

For the enstrophy cascade range Lin (1972) has argued from similarity reasoning that particle pairs will separate in an exponential fashion, i.e.

$$\sigma(t) = \exp[2t/\tau] \qquad (6)$$

where τ is a time constant for diffusion in this range. However, (6) must be taken as an extreme simplification for the highly irregular deformations that occur in the k^{-3} region. It may, perhaps, be applicable in some ensemble average sense, as Morel and Larcheveque (1974) found from the separation of series of balloons released at 200mb. This is not, of course, a strictly diffusive process. At low wavenumbers, beyond the enstrophy cascade region, the spectra (Fig.1) depart from the k^{-3} slope. Morel and Larcheveque (1974) found that on these very large scales balloon pairs separated at $t^{1/2}$, at a rate governed by a global-scale diffusivity, $K_H = 2\times10^6\ m^2s^{-1}$. This compares with representative values for K in the energy cascade (where $K \simeq \overline{v^2}\tau_M = \varepsilon\tau_M^2$) of about $2\times10^4\ m^2s^{-1}$.

Long range plume spread over the sea seems to be less than that over the land - see Crabtree'S (1982) results in Fig 7 from Pasquill and Smith (1983). This may be attributed to the uniform surface (meso-scale motions are less in evidence) and perhaps to a greater incidence of stable stratification.

3. Practical difficulties in simulating the transport and dispersion of pollutants.

An accurate representation of the mean wind is, of course, of first importance when simulating plume transport. Either observations or the wind as resolved on the grid of a Numerical Weather Prediction (NWP) model can be used. Observations may be sparse in space and/or time, while modelled winds, strictly grid-volume means, subject to the smoothing and inaccuracies of the analysis process and perhaps less representative of

real terrain and conditions. In either case a good deal of interpolation is usually required. The advecting wind may be single-level (e.g. on a pressure surface or a mean boundary layer wind), or trajectories in 3 dimensions, or on isentropic surfaces. Trajectories derived from NWP's can be subject to error of various kinds, including systematic errors associated with the particular model or resulting from the choice of level used to simulate the trajectory. Comparisons of model trajectories with those of low-level tetroons (Hoecker, 1977) and with tracers (Haagensen et al, 1987) suggest a mean divergence of about 12° from validation. If forecast wind fields are used, further inaccuracies are involved - these are discussed and quantified in Maryon and Heasman (1988). Most NWP's of course, fail to represent properly the mesoscale motion systems which can be generated, for example, by land/sea juxtapositions or orography, or other changes in surface topography, type and roughness, which can influence the transports or the diffusive process. One advantage enjoyed by the long range modeller, however, is that the effects of the ensemble of small scale motion systems encountered over a track of hundreds or thousands of km will tend to undergo considerable blurring and smoothing, with individually little impact on the mature plume.

The mean vertical motion of the air can have a critical effect upon a trajectory, particularly near a region of marked mass ascent, such as a front. A 2-dimensional trajectory entering a region of horizontal convergence, such as this, can 'stagnate' and the apparent concentration of a pollutant in the boundary layer (which might, for example, have been computed using the area of a simulated plume segment) show a spurious increase. The conservation of area can only apply with strictly 2-dimensional motion systems.

Plumes can be laterally spread by wind shears in the vertical. Within the boundary layer the turbulent motions will convey parcels up and down so that they experience the wind at all levels - the plume centreline responds to a mean boundary layer wind. Above the boundary layer material extended in the vertical can be fanned out, as illustrated in the plume simulation in Fig.9(b). Should a developing convective boundary layer extend into such a region, material is quickly brought down to what might be a previously unaffected surface - a process analogous to plume 'fumigation'. Material can also be vented out of the boundary layer by convection - e.g. in cumulus clouds, which can 'vacuum up' pollutants, carrying them up into the free troposphere and releasing them in the dissipation stage. Frontal cloud may do this on a large scale.

It is clear from the foregoing that the static stability of the atmosphere, the diurnal changes in the boundary layer depth, and associated shears (including the 'nocturnal jet' which can develop above the stable night-time boundary layer), all influence the transport and spread of pollutants, and their treatment requires careful consideration.

There remains the problem of accurately estimating the strength (and sometimes position!) of the source of the pollutant, and its profiles in time and space. Loss processes also have to be parametrized. The latter include the flux of material to the surface in dry air (dry deposition) which may or may not involve gravitational settling, and the removal of pollutants in rainfall. Wet deposition processes are of profound importance, witness the acid rain problem and the washout of radioactive species following the Chernobyl release. Radioactive decay can be treated as a loss process.

4. Long range transport models.

Space permits only a brief summary of the methods used in the multitude of models developed to simulate the transport and dispersion of pollutants.

Eulerian models:

An obvious approach is the diffusion equation

$$\frac{\delta c}{\delta t} + \bar{u}\frac{\delta c}{\delta x} + \bar{v}\frac{\delta c}{\delta y} + \bar{w}\frac{\delta c}{\delta z} = \frac{\delta}{\delta x}[K_x \frac{\delta c}{\delta x}] + \frac{\delta}{\delta y}[K_y \frac{\delta c}{\delta y}] + \frac{\delta}{\delta z}[K_z \frac{\delta c}{\delta z}] \qquad (7)$$

(standard notation, c is concentration) which can be incorporated in operational NWP models. These can, in principle, hold all the evolving 3-dimensional motion fields and meteorology (including a more or less crude representation of the boundary layer). However, a model with a grid spacing of many km cannot be satisfactorily employed around a source region and early plume of perhaps a few tens of metres in width - there is an inevitable spurious diffusion. In addition, it is not easy to specify the vertical exchange coefficients, while it can be difficult to follow material emanating from specific source locations. There are variations on the Eulerian theme which to some extent surmount the computational difficulties: Fourier transforming the concentration equation into spectral space (e.g., Prahm and Christensen, 1977) can control the grid diffusion. Other workers (Egan and Mahoney, 1972) have developed models which conserve the low order moments of the concentration distribution.

Higher order closure models have also been applied in the solution of (7) (Enger, 1983).

Lagrangian models:

One alternative is to compute Lagrangian trajectories using observed or modelled winds, either by simply integrating

$$\frac{\delta x_i}{\delta t} = u_i$$

or by using more sophisticated integration schemes (some Met Office

trajectory routines employ a 5th order Runge-Kutta technique). The u_i generally require interpolation in time and space. The trajectories can be used to advect consecutive 'puff' centroids, or used to develop a plume centreline - in either case an empirical spread must be parametrized to allow the puffs or plume to expand, e.g. as $t^{1/2}$ or $x^{0.875}$ (the latter an empirical but consistent result over land - see Fig.7). Plume meandering and the relative diffusion are sometimes (e.g. for the meso-scales) dealt with as separate components. These models are very economical for computation and storage.

The Met Office 'Basic Model' developed for the national response in the event of another nuclear release such as Windscale or Chernobyl, is a 2-dimensional centreline model (using Fine Mesh winds) in which the plume is empirically expanded and divided into hourly segments (Fig.8). The segments are sub-divided across the width of the plume and, after a day or two, the segment vertices are advected individually as deformation takes over from turbulent spread as the key mechanism of dispersal. The 'Main Model', currently being developed for the same purpose, is multi-layered (to allow for macroscopic shear) and of 'Monte Carlo' type - the plume is represented by large numbers of particles which are released from the model 'source' and advected in the 3-dimensional wind field. Sub-grid scale motions in the boundary layer are accounted for by the addition at each timestep of a random contribution (from a formulation similar to (3)) to the horizontal wind components, and then random re-assignment in the vertical so that winds are sampled at all levels within the boundary layer. A mass of pollutant or measure of radioactivity is associated with each particle, which is progressively reduced by the processes of deposition and radio-active decay. Air concentrations are computed each hour, due weight being given to the position of the particles at each intervening timestep. Examples of the output are given in Fig.9.

A wide range of Lagrangian models is described in Chapter 7 of Pasquill and Smith (1983).

Particle in cell (PIC) models:

First formulated by Sklarew(1971), these also represent a plume by Lagrangian mass particles, which are advected through a network of grid-cells. Each particle contributes to the mass and hence concentration in a cell either by its location within the cell or, by treating the particles as puff centroids, computing the overlap of puffs with cells. A 'fictitious total velocity' is used for advection:

$$v = \bar{v} + (K.\nabla c)/c$$

where $\bar{v}$ is the mean velocity and the right-hand term a turbulent flux velocity which depends upon the concentration gradient (or equivalently, the change in density of the particles).

Mass-consistent models:

These models are perhaps most applicable to moderate sized regions. They attempt to obtain a realistic wind field over realistically defined orography. Assuming incompressible flow they conserve mass within the volume of integration - the wind components are adjusted using variational analysis to ensure non-divergence of the 3-dimensional wind field. The typical integral for minimization (using the standard Euler-Lagrange formulation) is

$$I = \int_v [\alpha_1^2(u-u^0)^2 + \alpha_1^2(v-v^0)^2 + \alpha_2^2(w-w^0)^2 +$$

$$+ \lambda(\frac{\delta u}{\delta x} + \frac{\delta v}{\delta y} + \frac{\delta w}{\delta z})]dxdydz$$

where u^0 etc are first guesses obtained by interpolation from the observations, and the α_i relative weightings for the horizontal and vertical components. The wind is calculated throughout the model domain and the method is considered economical in comparison with NWP integrations. (Sherman (1978), Barnard and Wegley (1987)).

Statistical models:

Many models are not event orientated, but are designed to produce long-term concentration patterns or regional emission/wet and dry deposition budgets. These may utilise climatological wind-roses and straight trajectories combined with a probabilistic or stochastic description of rainfall. Many kinds have been developed; examples are Fisher (1978), Smith (1982).

REFERENCES:

Barnard J.C. and Wegley H.L. 1987, J. Clim Appl. Met., p675.

Barr S and Gifford F.A. 1987,Atmos. Environ. 21, 8, p1737.

Batchelor G.K. 1952, Proc. Camb. Phil. Soc. 48, p345.

Berry M.V. and co-workers, 1979, Ann. Phys. 122 p26.

Carras J.N. and Williams D.J. 1981, Atmos. Environ. 15, p2205.

Chaiken J and co-workers, 1986, Proc. Roy. Soc. London, A408, p165.

Charney J.G. 1971, J. Atmos. Sc., 28, p1087.

Crabtree J. 1982, Proc. 13th NATO/CCMS Conf. on Air Pollution Modelling and its Applications, Plenum Press, New York.

Egan B.A. and Mahoney J.R., 1972, J. Appl. Met. 11, p312.

Enger L. 1983, Uppsala, K. Univ. Met. Inst. Rep. Nos 70, 71.

Fisher B.E.A. 1978, Atmos. Environ. 12, p489.

Gage K.S. 1979, J. Atmos. Sc. 36,10, p1950.

Gage K.S. and Nastrom G.D. 1986, J. Atmos. Sc. 43, p729.

Gifford F.A. 1982, Atmos. Environ.,16, 3, p505.

Gifford F.A. 1984, Boundary Layer Met., 30, 1-4, p159.

Haagensen and co-workers, 1987, J. Clim. Appl. Met., 26, p410.

Hoecker W.H. 1977, J. Appl. Met., 16, p347.

Lilly D.K. 1983, J. Atmos. Sc., 40, 3, p749.

Lin J-T, 1972, J. Atmos. Sc., 29, p394.

Maryon R.H. and Heasman C.C. 1988, Atmos. Environ., 22, 2, p259.

Morel P. and Larcheveque M. 1974, J. Atmos. Sc., p2189.

Pasquill F. and Smith F.B. 1983, 'Atmospheric Diffusion', 3rd Ed'n., Ellis Horwood Ltd. Chichester.

Prahm L.P. and Christensen O. 1977, J. Appl. Met., 16, p896.

Sherman C.A. 1978, J. Appl. Met., p312.

Sklarew R.C. and co-workers, 1971, 'Systems Science Software', California, Rep. 3SR.844 Vol 1, EPA contr. 68-02-0006.

Smith F.B. 1968, Atmos. Environ. 2, p491.

Smith F.B. 1982, Proc 13th NATO/CCMS conf. on Air Pollution Modelling and its Applications, Plenum Press, New York.

Taylor, G.I. 1921, Proc. London Math. Soc., Ser. 2, 20, p196.

Tennekes H. 1978, Bull. Amer. Met. Soc., 59, 1, p22.

FIGURES:

1. Diagram and caption from Gage and Nastrom (1986).

2. Diagram and caption from Tennekes (1978) after Welander.

3(a) Whorls and 3(b) tendrils demonstrated by Chaiken et al (1986) - streamlines developed in a fluid between two rotating cylinders.

4. 2-dimensional simulation by particles of a plume 'released' 1200z 4th Feb., 1988 (continuing source). 4(a) 1200z, 7th Feb; 4(b) 1200z 8th Feb; 4(c) 00z 9th Feb., 4(d) 1200z 9th Feb., 4(e) Corresponding synoptic situation 1200z 6th Feb to 1200z 9th Feb from Weather magazine Monthly Summary.

5. Diagram and caption from Gifford (1982) (after Hage and Church).

6. Diagram and caption from Gifford (1984).

7. Diagram and caption from Pasquill and Smith (1983), incorporating Crabtree's (1982) results obtained over the North Sea.

8. The Met Office 'Basic' nuclear response model output for a plume release 1200z 22nd Dec, 1987: 24 hr forecast.

9. Samples of 'hindcast' output from the Met Office 'Main' nuclear response model, currently under development. Plume release 00z 15th July, 1988 and continuing - 9(a) boundary layer plume at 00z 17th July; 9(b) plume between top of boundary layer and 850 mb, 00z, 17th July; 9(c) significant concentrations-in-air (Bq m^{-3}) 1200z, 19th July.

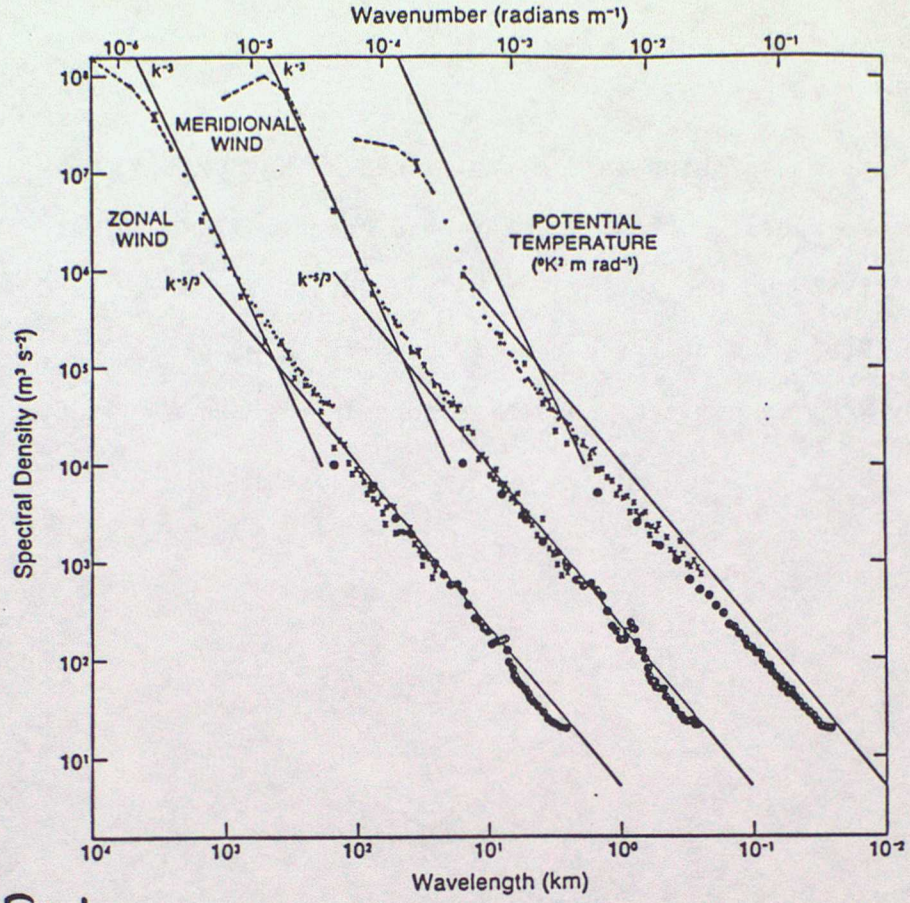

Fig. 1 Variance power spectra of wind and potential temperature near the tropopause from GASP aircraft data. The spectra for meridional wind and temperature are shifted one and two decades to the right, respectively; lines with slopes -3 and $-5/3$ are entered at the same relative coordinates for each variable for comparison.

Fig. 2 Successive stages in the evolution of a patch of dye being advected around on the surface of a pan filled with liquid (after Welander, 1955). The original pictures were redrawn with a fairly wide Leroy pen in order to simulate the effects of a small, but finite, diffusivity.

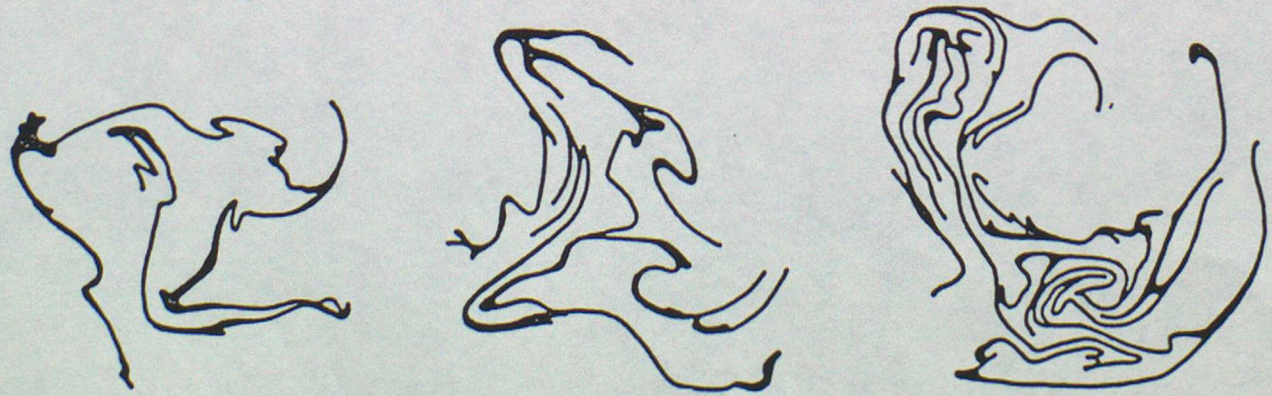

Fig. 3(a)

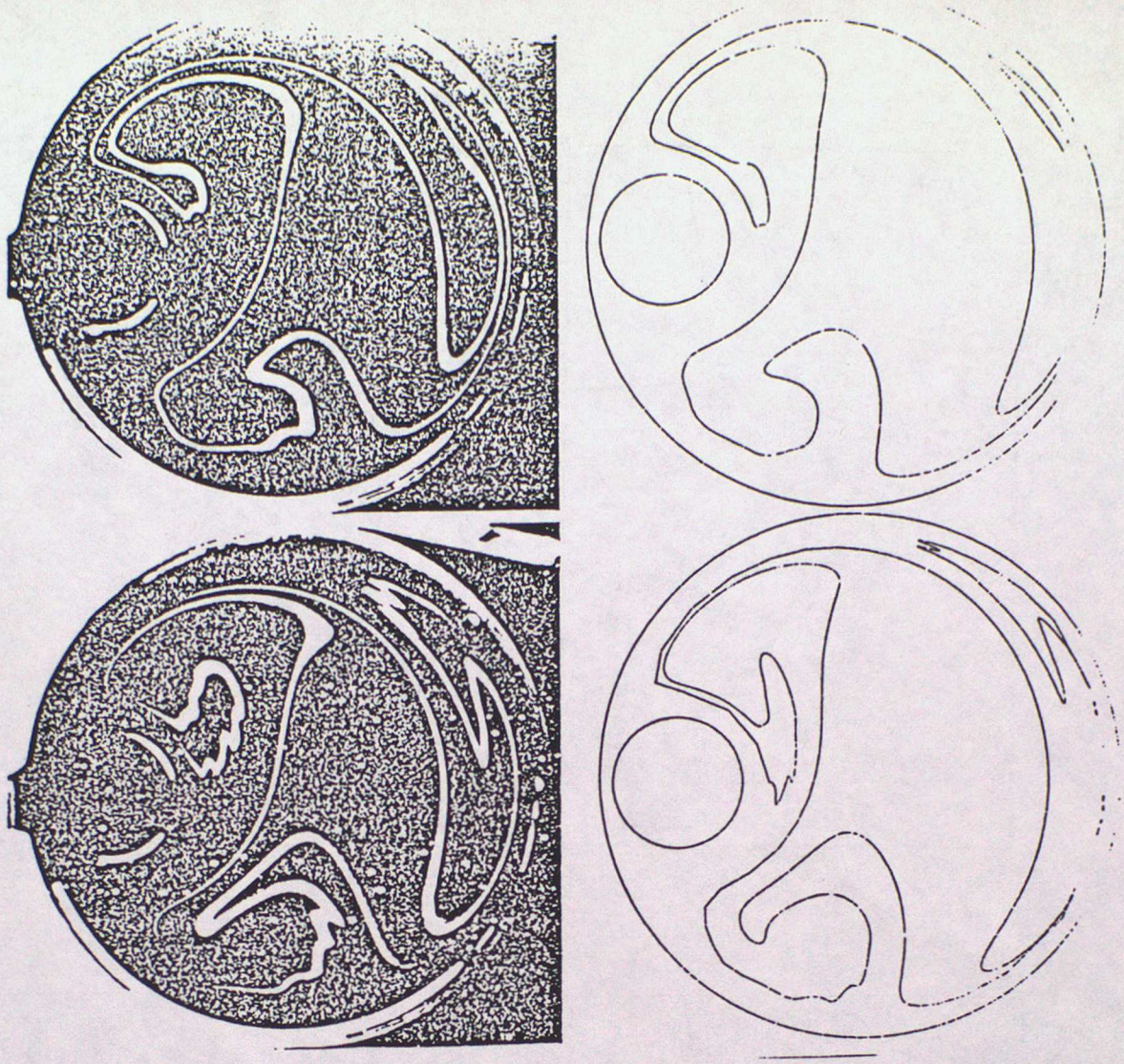

Fig 3(b)

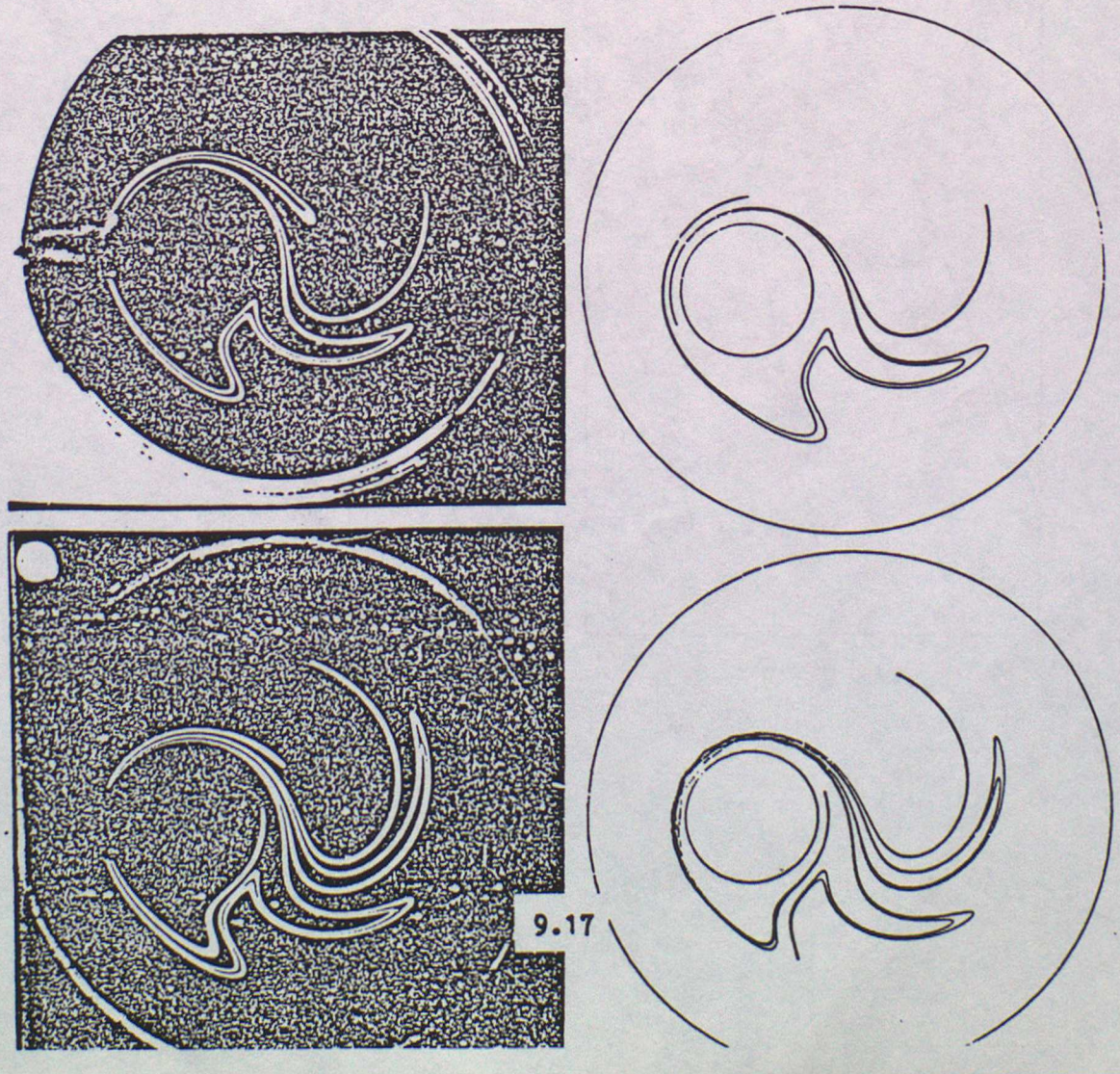

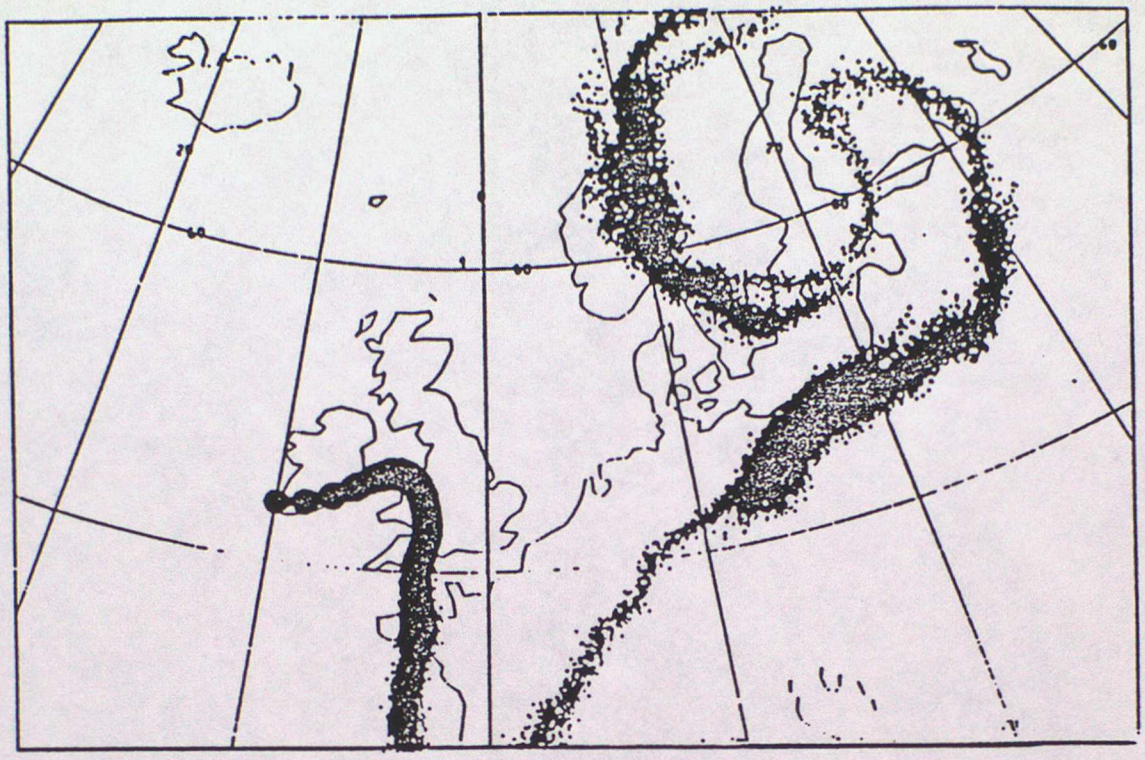

Fig 4(a)

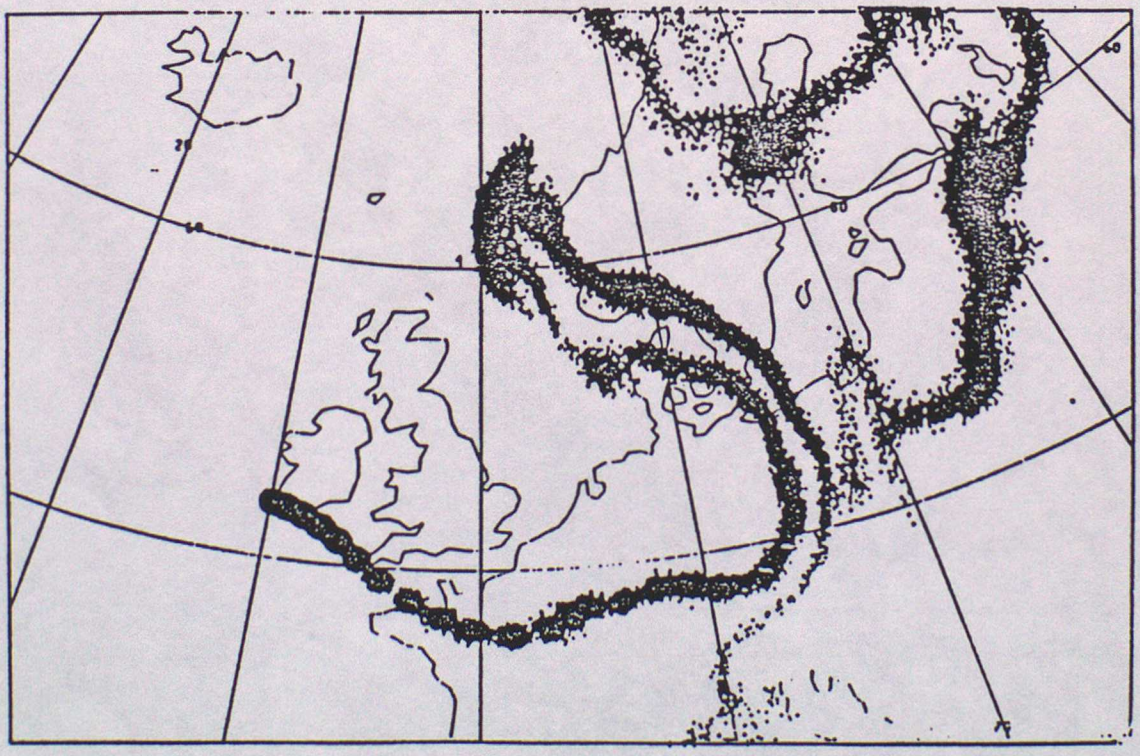

Fig 4(b)

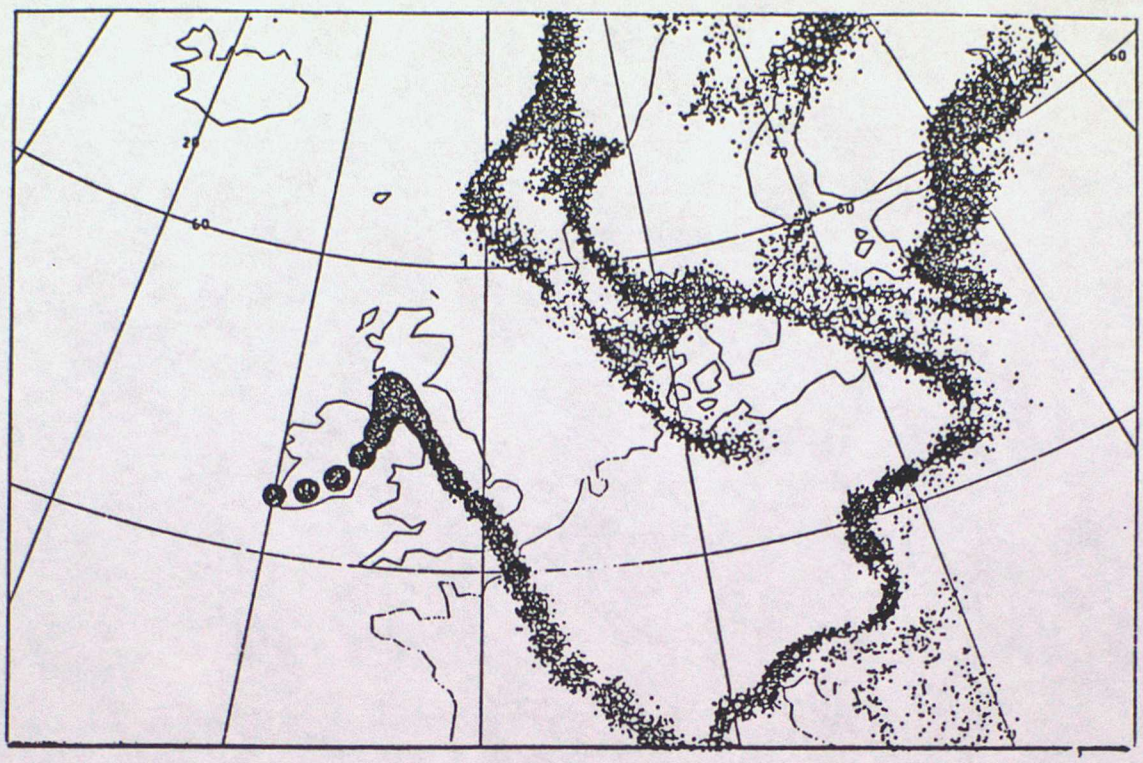

Fig. 4(c)

Fig. 4(d)

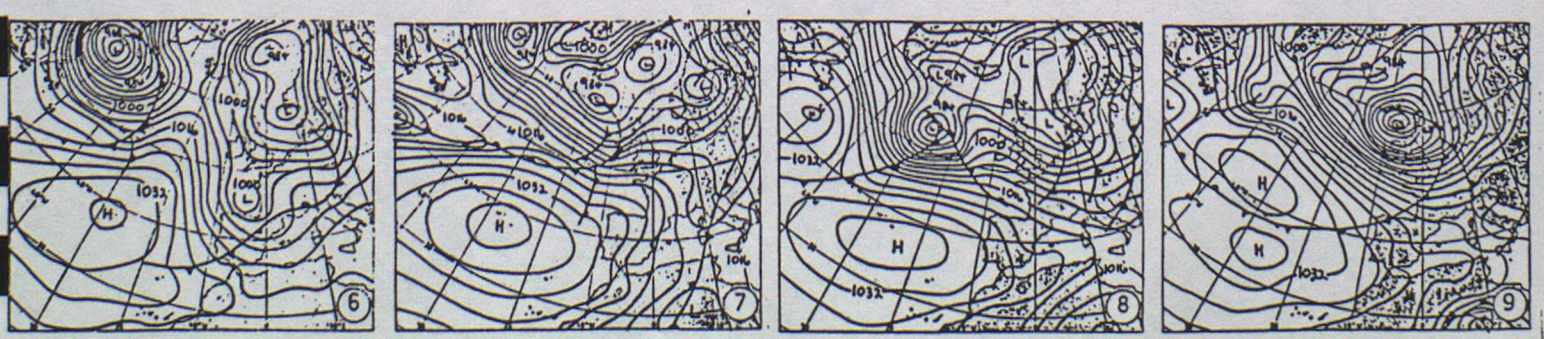

Fig. 4(e)

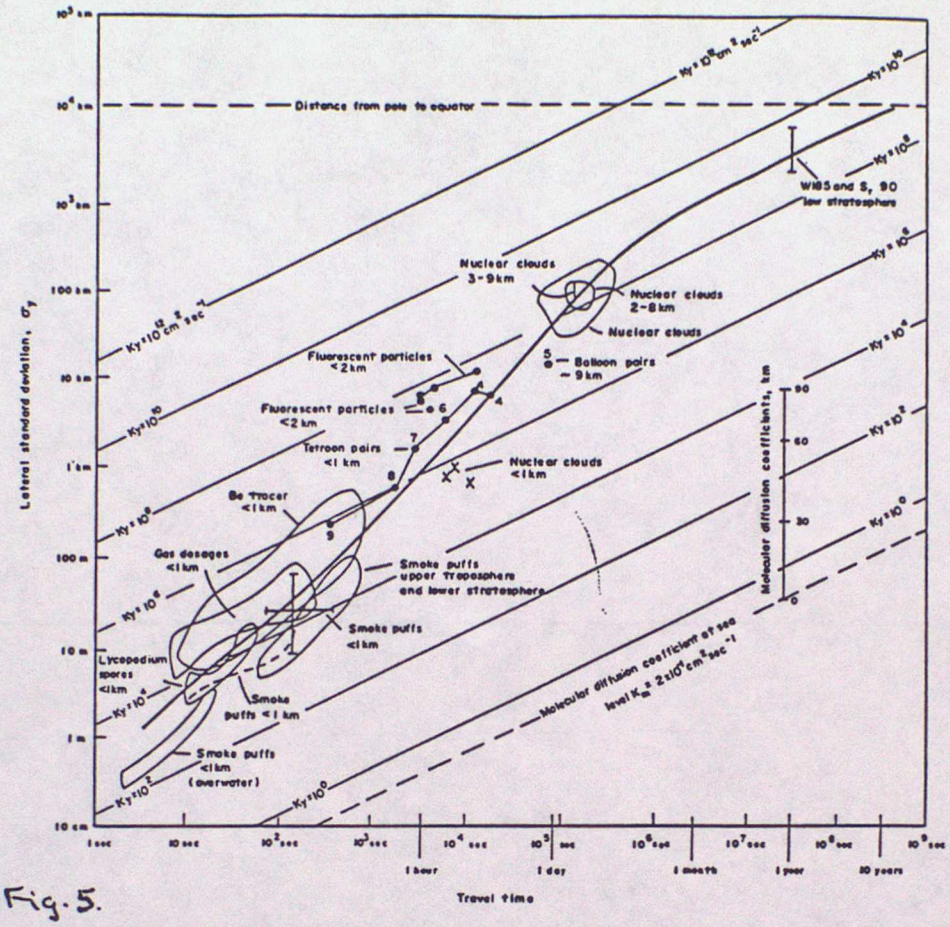

Fig. 5.

Summary of data on horizontal atmospheric diffusion, from Hage and Church (1967).

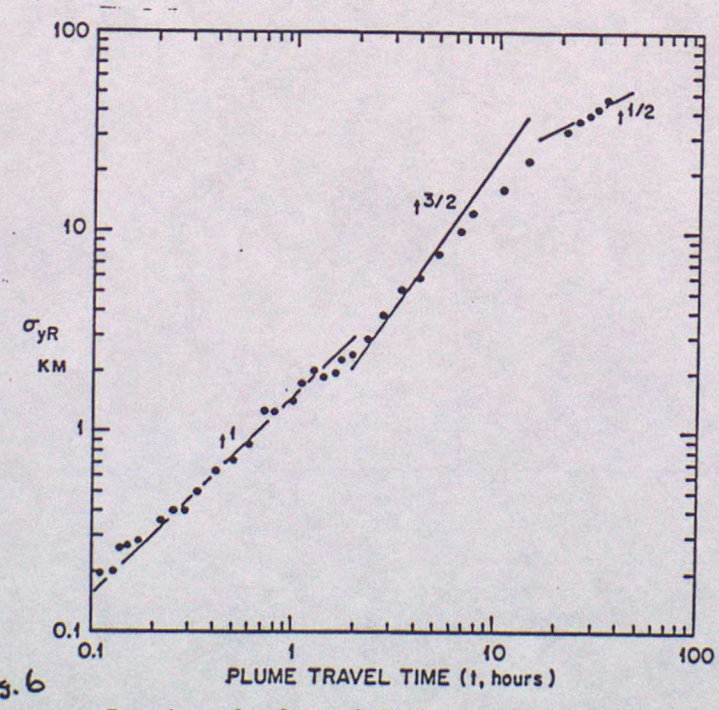

Fig. 6

Experimental values of σ_{yR} based on Australian smelter plume-width measurements by Carras and Williams (1981). Each point is an average of 15 contiguous data points

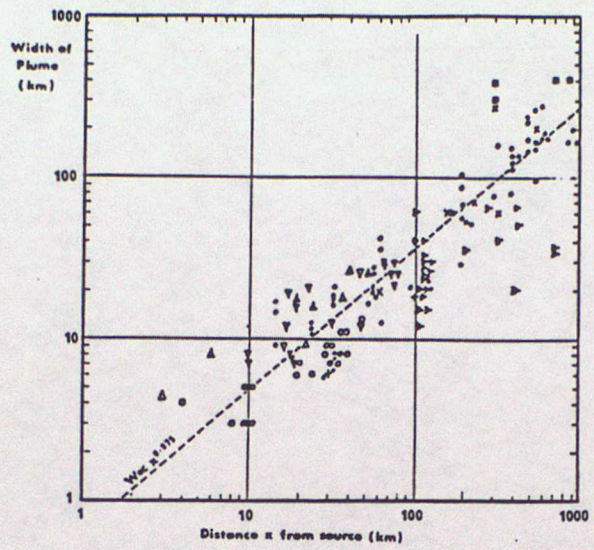

Fig. 7.

Data on the width of plumes as a function of distance from the source. × Richardson and Proctor (1925); ▽ Porton data (Pasquill, 1974); + Gifford (see Slade, 1968); □ Classified project (see Slade, 1968); △ Braham *et al.* (1952); ○ Smith and Heffernan (1956); ● Mt. Isa data (Bigg *et al.*, 1978; Carras and Williams, 1981); ⊱ Crabtree (1982): data collected over the sea.

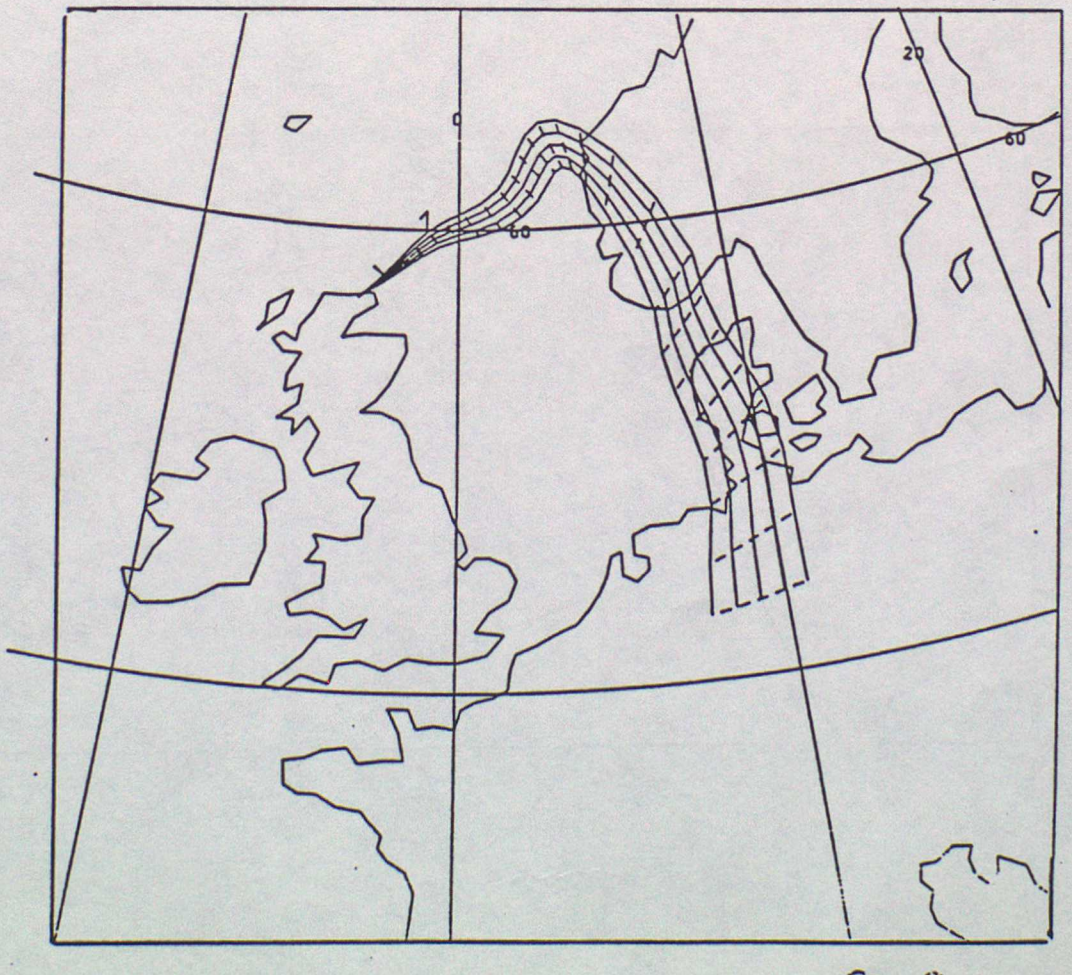

Fig. 8

RELEASE FROM 0000GMT 15/07/1988 - CONTINUING

AT SELLAFIELD 54 25N 3 30W

0 Z SUN 17/07/1988

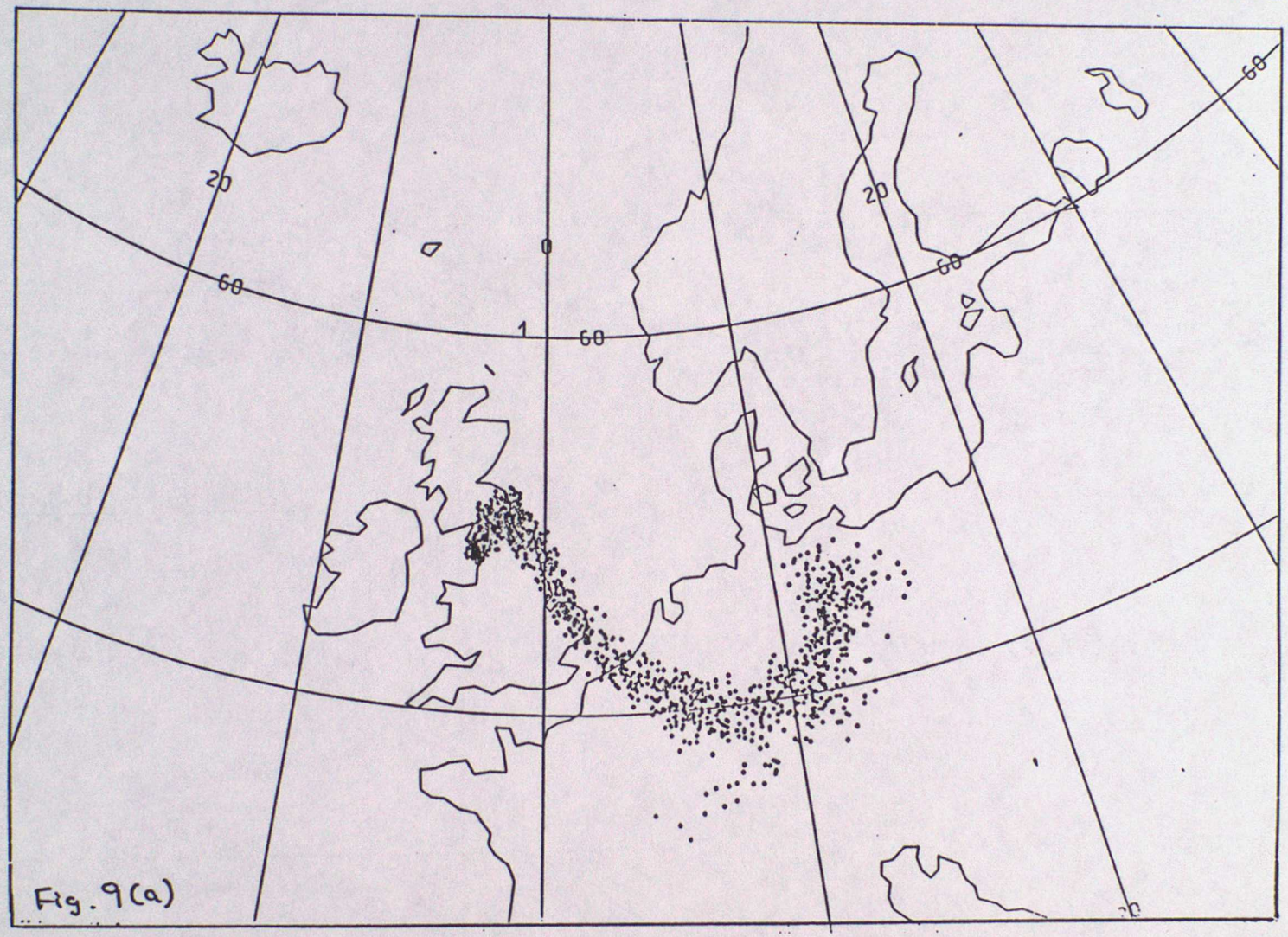

Fig. 9(a)

RELEASE FROM 0000GMT 15/07/1988 - CONTINUING

AT SELLAFIELD 54 25N 3 30W

0 Z SUN 17/07/1988

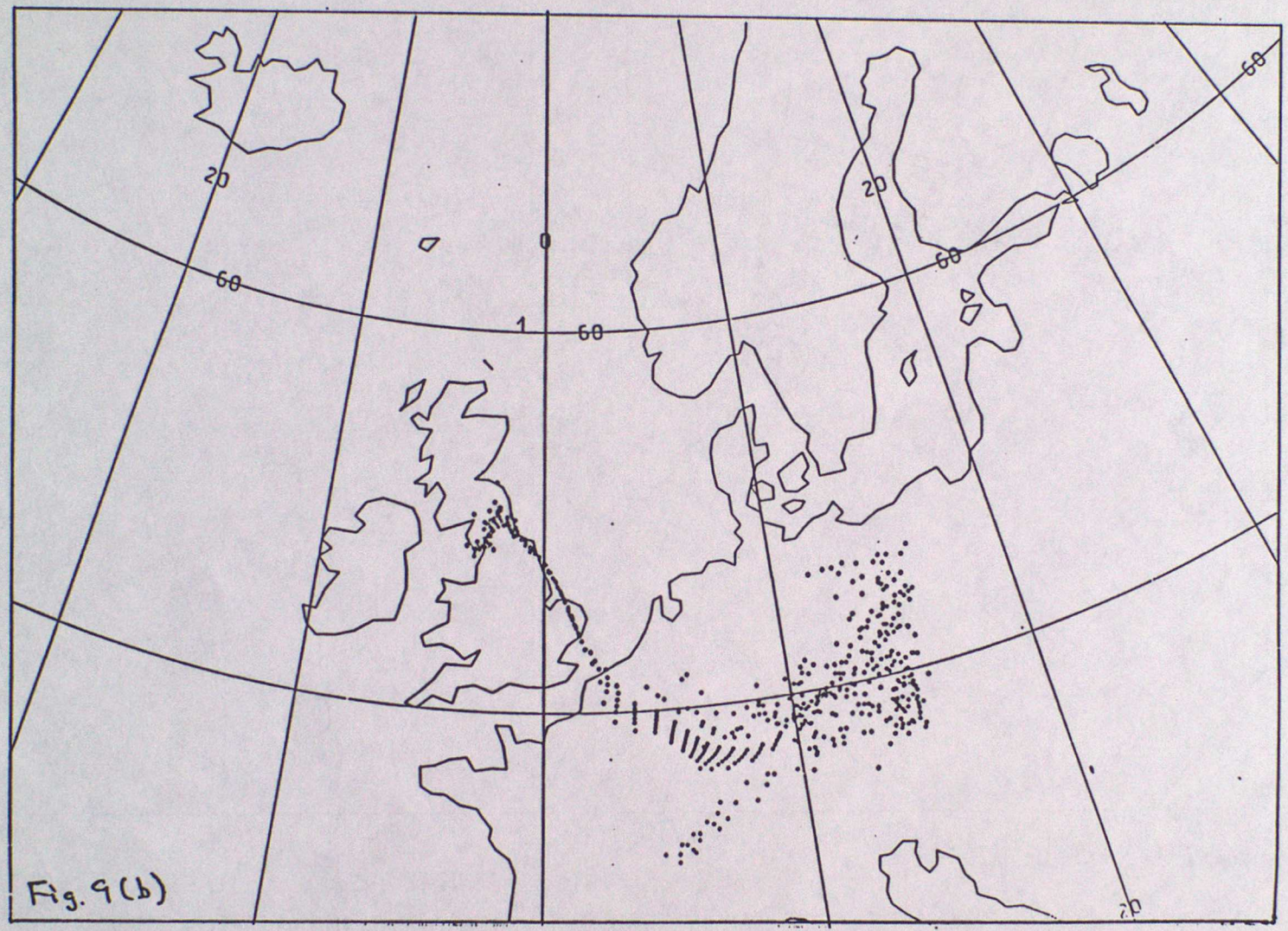

Fig. 9(b)

1 - 4

5 - 8

9 - 12

13 - 16

17 - 20

21 - 24

RELEASE FROM 0000GMT 15/07/1988 - CONTINUING

AT SELLAFIELD 54 25N 3 30W

12 Z TUES 19/07/1988

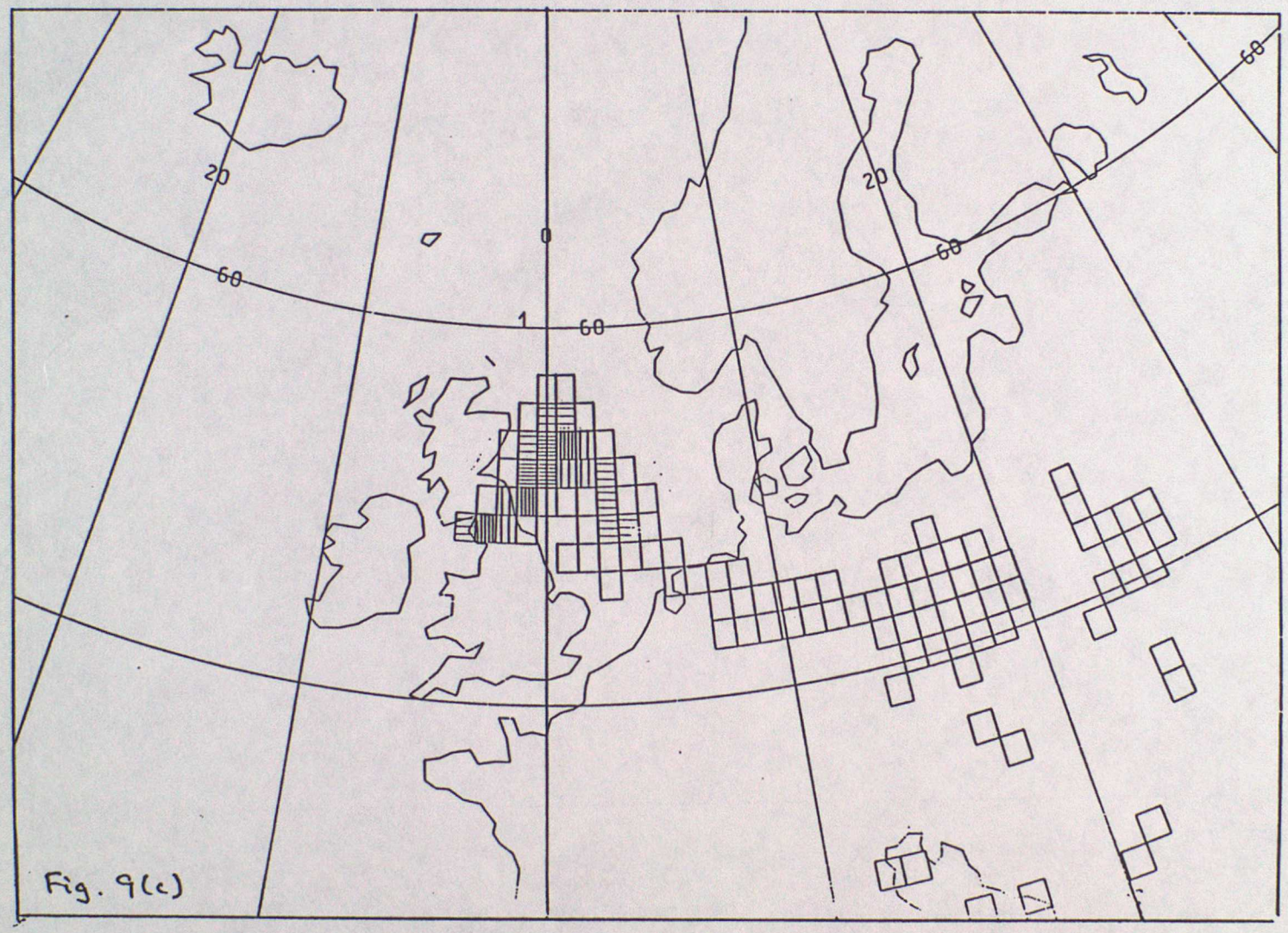

Fig. 9(c)

9.24

Lessons from the dispersion and deposition of debris from Chernobyl

F.B. Smith

Meteorological Office, Bracknell

Summary

Activity escaped from the wrecked reactor at Chernobyl for 10 days and spread over most of Europe. Part of the debris crossed Britain a week after it was emitted. Heavy thunderstorms and a northward-moving cold front washed out much of the radoactive iodine and caesium, especially on to the upland areas of North Wales, northern England, south-west Scotland, and Ulster. Several lessons have been learnt, including information on the dry and wet removal rates. These lessons are discussed in this paper.

1. The accident

The release of radioactive debris into the atmosphere from Reactor 4 at the nuclear power plant at Chernobyl in the Ukraine was the most serious in the history of the civil nuclear industry.

The disaster started in the early morning of 26 April 1986 during a rather special experiment. The aim was to test the safety of the reactor should two breakdowns occur simultaneously: firstly should the steam from the reactor suddenly fail to reach the great turbine generators and secondly should the supply of electricity from the national grid to the turbines be cut off. The question then was: would the mechanical inertia of rotation of the turbines be sufficient to generate enough electricity to keep such vital components as the pumps working within the reactor for up to 50 seconds before stand-by diesel generators could be started and take over the necessary supply.

In fulfilment of this experiment the power of the reactor was brought to well below 20% of normal power in spite of the fact that the particular design of the reactor at Chernobyl was known to become potentially unstable at such low levels. At 0123 local time this instability was realized and the reactor accelerated from a small fraction of full power to 100 times full power in just 4 seconds, causing an explosive generation of steam and the rupturing of pipes and protective shielding. The core was now exposed to the air and rapid chemical reactions resulted causing a second explosion. The reactor building was destroyed and burning graphite and core debris were spewed out over the site and into the atmosphere.

The loss of radioactive material to the atmosphere persisted for nearly 10 days in spite of valiant efforts to seal the reactor with about 5000 tonnes of material dropped from helicopters. Roughly 2×10^{18} becquerels of activity were released into the air during this period, about a third of which went out in the first few hours. (A becquerel (Bq) represents one atomic disintegration per second.) Debris released in this early period was very hot and rose 1 or 2 kilometres into the atmosphere. Later emissions were much cooler and travelled largely within the boundary layer over long distances except when advected upwards at fronts or in large convective clouds.

2. The spread of debris over Europe

At the time of the explosion a ridge of high pressure was centred over north-west USSR (see Fig. 1). The wind circulation associated with this ridge carried the upper part of the plume away towards the Baltic Sea and Scandinavia. Nearer the ground, the nocturnal clear skies had resulted in the development of a 500 m deep surface-based inversion. This inversion, whilst not preventing the sedimentation of the larger particles in the airborne debris, helped to insulate the local population from the downward diffusion of the inhalable small particles which could have caused a great deal of damage within people's lungs.

Once the plume reached Scandinavia, it split into three 'fingers'. One moved away to the east across northern parts of the USSR into Japan and China. A second finger, caused by a jet ahead of the cold front of an active depression, crossed central Norway and the Norwegian Sea and moved towards North America. Heavy rain which affected this finger on 28 April resulted in very large depositions of activity in central Scandinavia which contaminated the lichens and mosses, the main diet of the Lapp reindeer. A third finger moved south-westwards in response to a transient ridge of high pressure which followed the depression across north-west Europe. The finger moved across central Europe and the Alpine areas into France and then turned northwards, entering the United Kingdom in the early hours of Friday, 2 May.

3. Passage over the United Kingdom

The passage of the debris over Britain makes an interesting story which can only be summarized here. A fuller description is given in Smith and Clarke (n.d.). Beautiful warm spring weather on Friday, 2 May experienced over much of Britain was soon replaced by wet and stormy conditions on the Saturday and Sunday as a depression to the south-west of Cornwall deepened and an associated cold front moved into the country. Additionally, the warm air moving in from France ahead of the front became increasingly unstable and thunderstorms developed over the south-east of England in the early hours of Saturday, moved fitfully north-westwards and caught up the main body of the cloud of debris over North Wales and northern England. These storms drew great quantities of contaminated low-level air into their systems causing considerable rainfall and heavy depositions, particularly in Snowdonia, the Skipton area of Yorkshire, Cumbria, the Isle of Man, Ulster and south-west Scotland. Parts of the radioactive cloud were drawn off to the west across Ireland by the circulation of the depression, but most of the debris continued to move northwards, the tail of the cloud eventually leaving the northernmost parts of Scotland by the end of Sunday. However, small traces of activity were detected later in the subsequent week as parts of the debris drawn off by the depression recrossed the country. Some of these features can be seen in Fig. 2.

4. Deposition of hazardous nuclides

The cloud of debris contained a host of different radio-nuclides originating from the reactor. From a health point of view the most important of these were iodine-131, a short-lived isotope which gets into milk and then into human thyroids, caseium-134 with a half-life of about 2 years, and caesium-137 with a half-life of 30 years. The caesium isotopes can accumulate in the human body and, like the iodine-131, can cause cancer. Nevertheless, the risk of this is very small indeed and, except in the most heavily contaminated areas around Chernobyl itself, increases in cancer incidence within the population are likely to prove undetectable. The main pathway for these isotopes into the body is through foodstuffs and not by direct inhalation. Consequently the activity has to be deposited first on the ground. This deposition arises not just from the 'cleansing' action of rain, a process generally termed 'wet deposition', but also from dry deposition — the combined effect of sedimentation of large particles under gravity, of impaction of particulates and aerosols on leaves (etc.) and absorption of reactive gases by the soil and vegetation.

Dry deposition depends on the product of the concentration, C, of the material close to the surface and a so-called 'deposition velocity' v_d:

$$\text{Dry deposition} = v_d C.$$

By comparison with wet deposition, dry deposition is rather slow; just 1 mm of rain can remove more material than can dry deposition operating over 24 hours. However, dry deposition is an almost continuous processes whereas wet deposition is usually very intermittent. Consequently in the deposition of acidifying species (in the acid rain problem) dry deposition is more important than wet deposition except in a few very wet areas of Europe like the Norwegian mountains.

In the Chernobyl debris, iodine-131 was partly gaseous in form and partly particulate. The gaseous component dry-deposited some eight times more rapidly than the particulate component. This can be inferred from the relative concentrations and depositions of both particulate caesium-137 and iodine in areas where no rain occurred (on the assumption that particulate iodine deposited as efficiently as the caesium).

The wet removal is assumed to follow the simplified expression:

$$\text{Wet deposition} = wCR.$$

where C is the average concentration in the air during the rain, C is the rainfall expressed in millimetres and w is an empirically determined coefficient. Units of concentration are becquerels per cubic metre; units of deposition are becquerels per square metre. Based on measured depositions and air concentrations the following values of v_d and w have been inferred:

Iondine-131, gaseous: $v_d = 0.4$ cm s^{-1}, $w = 490$
particulate: $v_d = 0.05$ cm s^{-1}, $w = 650$
Caesium-137, particulate: $v_d = 0.05$ cm s^{-1}, $w = 650$.

5. Rainfall over the United Kingdom

In the first few days and weeks following the passage of the Chernobyl debris over the United Kingdom the only rainfall data available in sufficient detail were from the weather radar output. Although the radar coverage at that time only covered England, Wales and the most southern parts of Scotland the picture provided was extremely useful and sufficiently accurate to pinpoint the areas most likely to have been significantly contaminated by deposition. By July 1986 enough surface rain-gauge data had become available for a reasonable rainfall map for the whole of the United Kingdom to be drawn up, although it was not until late September that a complete quality-controlled map could be prepared. Fig. 3 shows this final rainfall picture. The values represent the rainfall which actually intercepted the radioactive cloud. Two points are of particular interest: firstly the convective storms resulted in narrow but very elongated 'footprints' of rainfall; secondly it is clear that the strength of the storms responded in a quite dramatic way to the nature of the terrain over which they were passing. Level uniform countryside tended to weaken the storms whereas large cities like London, mountains, and stretches of sea like the Solway Firth, rapidly strengthened them.

6. Total depositions

Fig. 4 gives the estimated deposition map for caesium-137 over the United Kingdom using the deposition parameters given above in conjunction with the rainfall data implicit in Fig. 3 and the assessed concentrations of caesium-137 in the air. The levels of deposition vary enormously over the country and the highest reflect the areas of heaviest rainfall. The maximum estimated deposition is in excess of 30 000 Bq m^{-2} near Whithorn in Dumfries and Galloway. These depositions and the corresponding ones of iodine-131 can be integrated over the whole of the United Kingdom and compared with the estimated emissions from Chernobyl:

Iodine-131: Total deposition on the United Kingdom = 2×10^{15} Bq,
Deposition as a fraction of total emission = 0.7%,
Deposition as a fraction of first day's emission = 2%

Caesium-137: Total deposition on the United Kingdom = 3×10^{14} Bq,
Deposition as a fraction of total emission = 0.8%,
Deposition as a fraction of first day's emission = 3 %.

The depositions are compared with the emissions on the first day of the accident because trajectory analyses indicate that the debris that crossed the United Kingdom was emitted in a roughly 2-hour slot in the late morning of 26 April. It is interesting that a higher percentage of the caesium emission than of the iodine emission on that day was deposited on the United Kingdom; this can only be because the iodine, being partly gaseous, had lost more *en route* by dry deposition before reaching this country.

Caesium-134 is believed to have behaved in a very similar manner to caesium-137, and in fact was used to distinguish deposited caesium-137 arising from Chernobyl from that previously in the ground which had its origins in the weapons tests of the 1950s and 1960s. During the passage of the Chernobyl debris the concentration of caesium-134 was typically just over half that of the caesium-137. Consequently the total caesium-134 deposition on the United Kingdom is inferred to be about 1.5×10^{14} Bq.

7. Agricultural effects

The consequences for agriculture in the United Kingdom were only of real significance in sheep farming. In all other areas levels of activity were well below the emergency reference levels set by the Government (except for some game birds and freshwater fish in limited parts of south-west Scotland). Unfortunately many upland sheep-farming areas were affected by relatively heavy depositions of caesium-137, and this has led to restrictions on the movement and slaughter of sheep on farms where levels in excess of 1000 Bq kg have been recorded. To make matters worse, levels have changed only very slowly on some of these farms in contrast to the more rapid decline observed in many lowland areas. The important element appears to be the nature of the soil. Soils rich in clay minerals rapidly lock in the free caesium so that it becomes unavailable to the vegetation. Poor acidic soils typical of many upland areas are unable to do this and the caesium cycles through the uppermost humic layers of the soil and the vegetation so that its availability to grazing sheep falls off only very slowly.

8. Summary of the lessons of Chernobyl

A new perspective has been gained from the terrible accident at Chernobyl. This will be invaluable in the preparation of new models now under way in the Meteorological Office and elsewhere, and in the design and operation of monitoring networks and other procedures for use should another major accident every occur in the future. This perspective can be summarized through a listing of so-called 'lessons'. Limiting these to those with some meteorological interest, they may be subdivided into three categories: lessons regarding transport in the atmosphere, lessons regarding deposition and lessons for agriculture.

8.1 *Transport and dispersion*

(a) Synoptic-scale deformation: Close to the source, the plume probably behaved very much like a conventional plume from a factory chimney, growing under the action of three-dimensional turbulence in a quasi-conical manner. When the width of the plume exceeded 100 or 200 kilometres, the synoptic variations of velocity became dominant and the plume then grew through deformation as decribed by Gifford (1987).

(b) Wind shear in the vertical: Changes of wind speed and direction with height through the plume were principal factors, in diluting the concentration within the plume, especially when deformation became dominant. Dilution occurs when shear is coupled with vertical mixing, either concurrently or successively through a diurnal cycle.

(c) Correction of trajectories using radiological data: Although it appears that most trajectory analyses carried out on the Chernobyl release have been reasonably successful in predicting the spread of the debris over Europe, it is almost certain that individual trajectories starting from Chernobyl at the same time differed significantly at long range and the apparent overall success simply reflects the very variable meteorological situation during the whole release. In other circumstances, differences might be more obvious. Radiological reports of activity would then be invaluable in optimizing the information that models are capable of giving. Fig. 5 shows the output of the Meteorological Office's basic Monte Carlo model simulation of the Chernobyl accident at four different times in apparent good accord with the known movement of the debris. This agreement has been optimized to some extent by judiciously selecting the best wind level in the light of radiological data.

8.2 *Deposition*

(a) Atmospheric stability at the source: Large releases will usually be hot releases and much of the airborne debris will rise away from the surface. How far is rises will depend critically on the stability of the air, and this will have consequences for the subsequent transport and deposition of the material. As seen earlier, a stable surface layer can protect the local population from much of the small inhalable particles and radioactive gases.

(b) Deposition rates for differing species: Washout rates and dry deposition velocities will differ significantly from one species to another, and these need to be well known in advance of any accident if model output is to be of real value.

(c) Convective rainfall and deposition shows banded structure: As evident in Figs 3 and 4, rainfall and deposition resulting from the thunderstorms during the passage of the Chernobyl debris over the United Kingdom were banded in narrow elongated 'footprints'. Interpolation between measurements of caesium-137 (for example) on grass or in soil should therefore be carried out with strong along-wind weighting and not with simple circular weighting.

8.3 *Agriculture*

(a) The importance of wet deposition: The Chernobyl accident has emphasized how much more efficient wet deposition is compared with dry deposition whenever rain occurs. Agriculturists wishing to monitor levels of deposition rapidly should therefore concentrate initially on areas where significant rain intercepted the debris. Quick help for this can be obtained from operational weather radar as long as the debris' movement is roughly known from models or from monitors in the field.

(b) Retention on vegetation: In areas where little or no rain occurred most of the deposition was through dry deposition and a high percentage was retained on the vegetation available to grazing animals. In areas of significant rain the total deposition may have been much higher but retention on the vegetation appeared to have been only some 10–25% of the deposited particulates, and very small indeed for the gases. This effect was very evident in the levels of iodine-131 in milk: levels in comparatively dry areas were not dramatically smaller than in wet areas for these reasons (Clark and Smith 1988).

(c) The influence of soil type on long-term effects: As seen from the aftermath of Chernobyl, soil type can critically influence the duration of the continued contamination of foodstuffs and grazing animals.

References

Clark, M.J. and Smith, F.B. 1988 Wet and dry deposition of Chernobyl releases. *Nature*, 332, 245–249.

Gifford, F.A. 1987 The time-scale of atmospheric diffusion considered in relation to the universal diffusion function, f_1. *Atmos Environ*, 21, 1315–1320.

Smith, F.B. and Clark, M.J. n.d. The transport and deposition of airborne debris from the Chernobyl nuclear power plant accident, with special emphasis on the consequences to the United Kingdom. *Sci Pap*, Meteorol Off, No. 42. (To be published.)

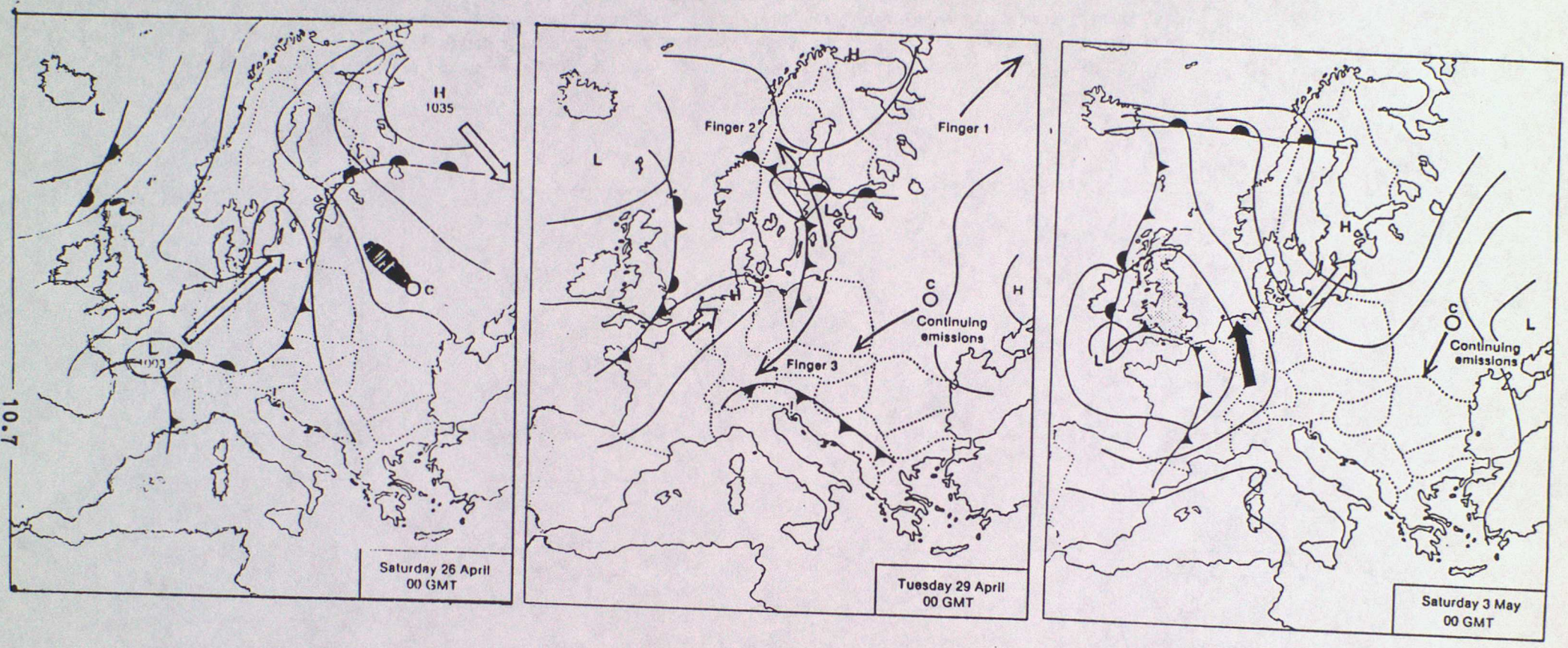

10.7

Figure 1. The three maps show how synoptic developments influenced the spread of the radioactive debris from Chernobyl in the days following the accident on April 26th, 1986.

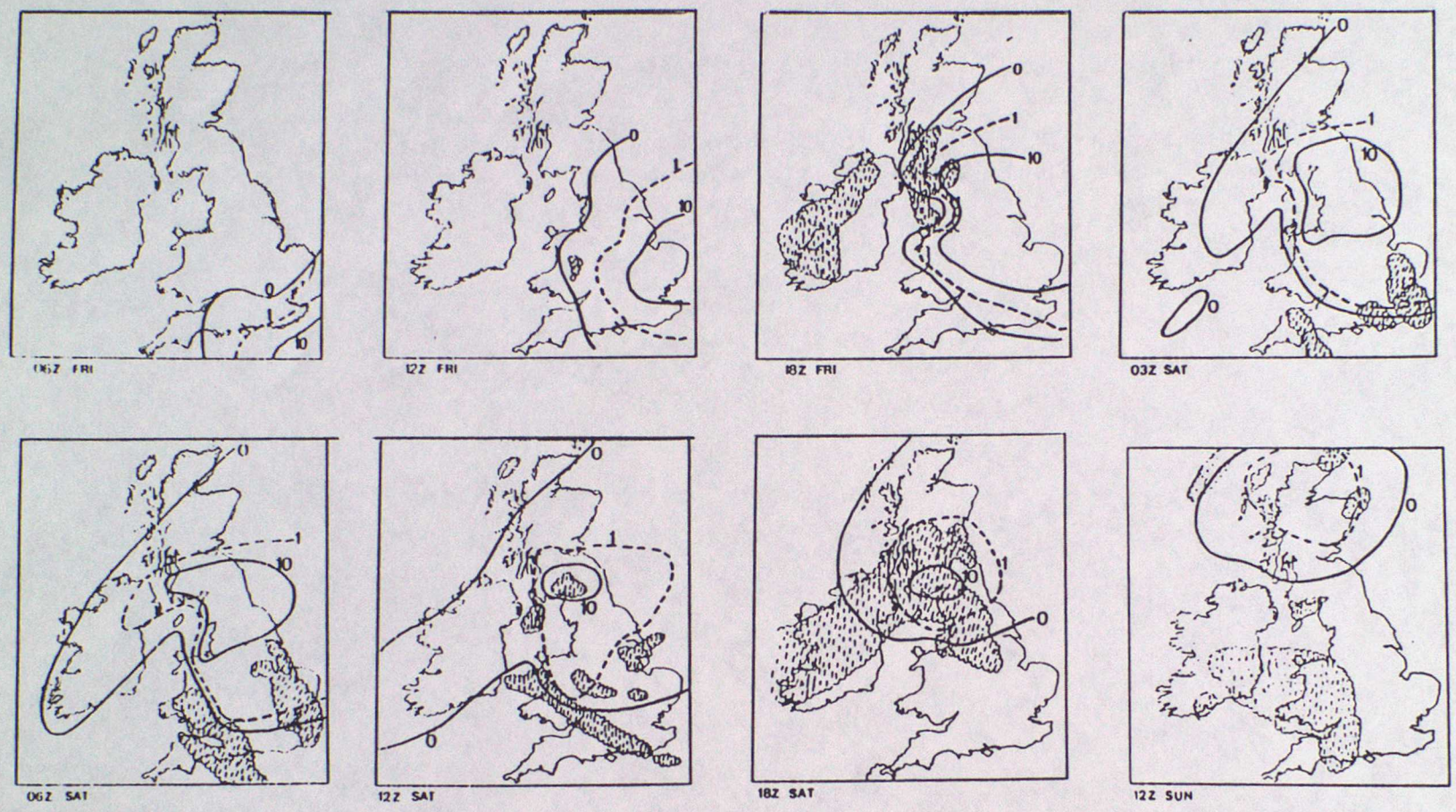

Figure 2. Position of the radioactive cloud over the British Isles at various times between Friday, May 2nd and Sunday, May 4th, 1986. Hatched areas are areas where some rainfall was reported, and hence where significant wet deposition of radioactivity may have been occurring.

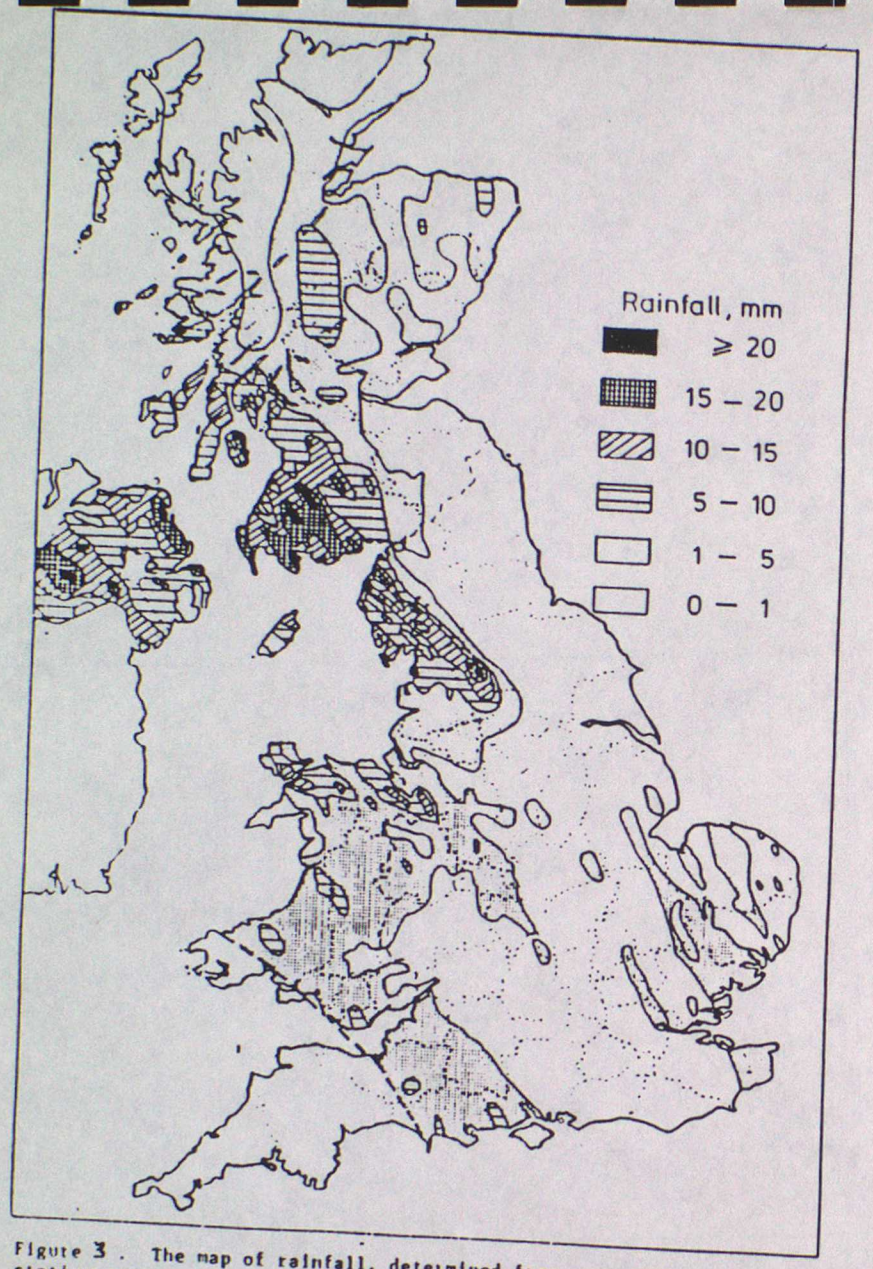

Figure 3 . The map of rainfall, determined from over 4000 raingauge station measurements, which intercepted radioactivity in the Chernobyl plume. Rain which did not fall during the time when the plume was overhead is excluded.

Figure 4 . Contours of empirically-derived total depositions of caesium-137, from Chernobyl, over the UK. Units are 4000 Bq m^{-2}.

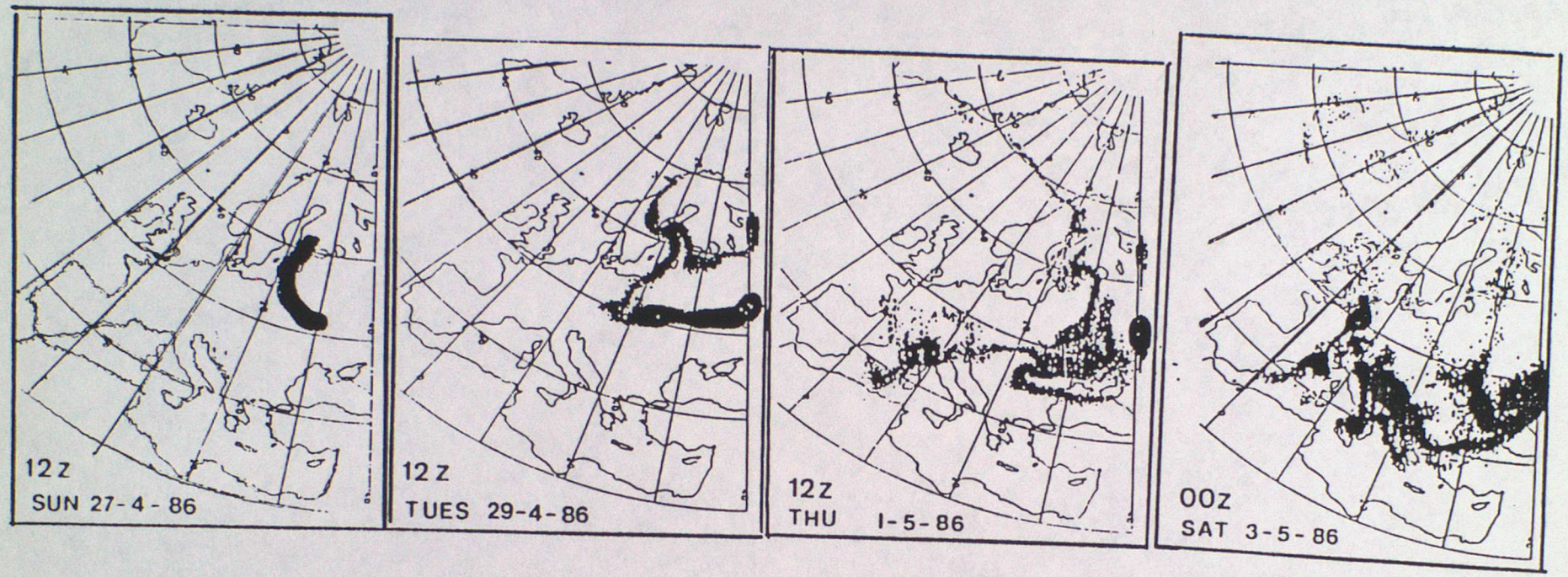

Figure 5. Simulation of the movement of debris from Chernobyl following the accident using a two-dimensional Monte-Carlo model (see text). The results show the fibrous and rather convoluted nature of the plume under the action of synoptic-scale distortion.